# THERMOPHYSICAL AND CONDUCTOMETRIC STUDIES OF APROTIC LITHIUM ELECTROLYTES IN APROTIC ORGANIC SOLVENTS FOR ENERGY STORAGE APPLICATIONS

Thesis Submitted for the Award of the Degree of

#### **DOCTOR OF PHILOSOPHY**

in

Chemistry

By

Chitra Sharma

**Registration Number: 41900185** 

**Supervised By** 

Dr. Harmanjit Singh Dosanjh (13688)

**Professor** 

**Department of Chemistry** 

**Lovely Professional University.** 

**Co-Supervised By** 

Dr. Ramesh Chand Thakur

**Associate Professor** 

**Department of Chemistry** 

**Himachal Pradesh University** 



LOVELY PROFESSIONAL UNIVERSITY, PUNJAB

#### **DECLARATION**

I hereby declare that the thesis entitled "Thermophysical and Conductometric studies of Aprotic Lithium electrolytes in aprotic organic solvents for Energy storage applications" submitted under the guidance of Dr Harmanjit Singh Dosanjh, Professor, Department of Chemistry, Lovely Professional University, Phagwara, Punjab and Dr. Ramesh Chand Thakur, Associate Professor, Department of Chemistry, Himachal Pradesh University, Summer Hill Shimla and as per the requirement for the award of the degree of Doctor of Philosophy (Ph.D.) in Chemistry is entirely a genuine record of my own research work. All sources and references used have been properly acknowledged. The work presented herein has not been submitted for the award of any other degree or diploma in any institution.

#### Chitra Sharma

Reg. No. - 41900185

Department of Chemistry,

Lovely Professional University,

Phagwara, Punjab, India.

#### **CERTIFICATE**

This to certify that Ms. Chitra Sharma has completed Doctor of Philosophy (Ph.D.) in Chemistry thesis entitled "Thermophysical and Conductometric studies of Aprotic Lithium electrolytes in aprotic organic solvents for Energy storage applications" is a bonafide work carried out by her under my supervision and guidance. To the best of my knowledge, the present work is the result of her original investigation and study. No part of the thesis has ever been submitted to any other University or institute for the award of any degree or diploma.

#### Dr Harmanjit Singh Dosanjh

Professor,

Department of Chemistry,

Lovely Professional University,

Phagwara, Punjab,

India

Date: 9th October, 2025

#### Dr. Ramesh Chand Thakur

Associate Professor,

Department of Chemistry,

Himachal Pradesh University,

Summer Hill Shimla,

India

#### **ABSTRACT**

From decades, solution chemistry has been the most crucial domain of physical chemistry. In order to attain deep insight about the nature of the interactions existing in the specific solution, the ultrasonic technique is being utilized in several fields of science to discover the thermodynamic and acoustic parameters which offers rational outcomes. Through this the physicochemical behaviour of the various moieties of the solution can be determined by the ultrasonic wave propagating in the medium. Its non-destructive nature renders it to be employed for exploring the several binding forces occurring in between the atoms and molecules in the system.

The major focus of the current experiment is to evaluate and analyse several crucial parameters such as thermodynamic, acoustic, spectroscopic, and conductometric investigation that could assist in determining the behaviour and comparative nature of molecular interactions in the systems under study.

The aims and objectives of the present investigations are:

- 1. To determine various thermo physical properties such as density and conductance of aprotic lithium electrolytes in binary aqueous mixtures of aprotic organic solvents at different concentrations and temperatures.
- 2. To calculate various thermophysical and acoustic parameters of the above solutions at different concentrations and temperatures.
- 3. To calculate various conductance parameters (specific conductance, limiting molar conductance and activation energy) of above-mentioned solutions.
- 4. Interpretation of above systems using spectroscopic and cyclic voltammetry (CV) techniques.

Following techniques are used to interpret the intermolecular interactions present among aprotic lithium electrolytes in binary aqueous mixtures of aprotic organic solvents

- Density measurements
- Speed of sound measurements
- Spectroscopic studies

- Conductivity measurements
- Cyclic Voltammetry

The thesis is divided into five chapters as mentioned below:

#### **Chapter 1: Introduction**

Chapter 1 includes detailed discussion of the various types of batteries and their usage along with their limitations. Apart from this, the properties of Aprotic Lithium Electrolytes are also discussed. The role of Glycol dimethyl ethers as organic solvents in the batteries is also explained. Since these solvents have a number of qualities that make them more environmentally friendly than many other solvents so their properties like Lower Volatility and Toxicity, Chemical Stability, Versatility and Biodegradability are outlined here. Further, advantages of Glyme-based Electrolytes are explained. A discussion has been carried about the intermolecular interactions between lithium salts and glymes. The overview of thermodynamics, conductance, Cyclic voltammetry and, FT-IR spectroscopy is presented. In this chapter, various thermodynamic parameters like apparent molar volume  $(V_{\phi})$ , limiting apparent molar volume $(V_{\phi}^{0})$ , standard partial molar volumes of transfer  $(\Delta V_{\phi}^{0})$  of the ternary mixtures, apparent molar isentropic compression  $(K_{\phi,s})$ , limiting apparent molar adiabatic compressibility  $(K_{\phi,s}^{0})$  & partial molar isentropic compression of transfer  $(\Delta K_{\phi,s}^{0})$  and their equations have been discussed.

#### **Chapter 2: Review of Literature**

Chapter 2 includes intensive literature survey on the conductometric, volumetric, acoustic & spectroscopic studies of Lithium salts with water as well as various other solvents. The advances in Li-ion batteries are also discussed. The literature review focuses on different energy storage technologies and the research on various electrolytes used in the energy storage devices that is contributing in creating a sustainable future. The role of Li salts in the energy storage devices is represented.

#### **Chapter 3: Experimental**

Chapter 3 outlines the specifications of chemicals used to carry out the experimental work. An overview of Lithium salts used in study have been provided. The details of the instruments used i.e. Anton Paar Density and speed of sound analyser (Anton Paar DSA 5000 M), conductivity meter, electrochemical workstation and FT-IR spectrophotometer have been discussed in this chapter.

#### **Chapter 4: Result and discussion**

Chapter 4 includes results and discussion of the entire research work. This chapter is divided into three sections I to III. Section I investigates solute-solvent interactions in ternary systems consisting of lithium trifluoromethanesulfonate (LiOTf) as the solute and tetraethylene glycol dimethyl ether (TEGDME) and 1,2-dimethoxyethane (DME) as solvents over a range of temperatures (293.15 K – 313.15 K). A multidisciplinary approach involving computational modelling, thermodynamic analysis, and acoustic measurements was used to elucidate molecular-level dynamics. The positive  $V_\phi^0$  values in the thermodynamic analysis revealed the prevalence of solute-solvent interactions in the investigated ternary (LiOTf + H<sub>2</sub>O + DME/TEGDME) solutions. Hepler constant was determined to predict the structure maker/breaker behaviour. Cyclic voltammetry (CV) analysis showed that TEGDME offers a higher electrochemical window (EW) of 1.36 V in 0.01 TEGDME and 1.40 V in 0.05 TEGDME compared to that of 1.25 V in 0.01 DME and 1.38 V in 0.05 DME, yielding favourable and comparable working electrochemical windows. Further, the specific conductivity, molar conductivity, limiting molar conductance and activation energy of conductance have been determined to validate the interactions present in the given systems. Section II contains comparative evaluation of the thermophysical and acoustic characteristics of lithium tetrafluoroborate and lithium hexafluorophosphate in binary aqueous solutions of tetraethylene glycol dimethyl ether. Various thermophysical and acoustic variables including apparent molar volume, partial molar volume and transit volumes, apparent and partial molar isentropic compression are estimated using the values of density and speed of sound. These findings can be beneficial in developing different electrolytes for lithium-ion Section III depicts Thermophysical and acoustic measurements of LiFSI

and LiTFSI in (0.01, 0.03 and 0.05) mol kg<sup>-1</sup> tetraglyme (TEGDME) at different working temperatures. The thermophysical parameters like apparent molar volume, partial molar volume, apparent molar isentropic compression and, partial molar isentropic compression are determined. Additionally, infrared spectral analyses are conducted to evaluate the interactions that take place in the mixes under investigation. Furthermore, the activation energy of conductance, limiting molar conductance, specific conductivity, and molar conductivity have all been computed to deduce the interactions that exist in the systems.

#### **Chapter 5: Conclusion**

Chapter 5 consists of the main findings, conclusion as well as comparative analysis of volumetric, acoustic, conductometric and spectroscopic studies of the studied Lithium salts in DME and TEGDME. This chapter discusses the results derived from the various thermodynamic characteristics. Furthermore, this chapter also outlines the current work's future scope.

#### **ACKNOWLEDGEMENT**

I devote this space to acknowledge all those who have made this degree a reality. I was never alone in this endeavour. Completing my Ph.D. and writing this thesis has been an incredible journey—one that would not have been possible without the support and encouragement of many exceptional individuals.

First and foremost, I bow in gratitude to the Almighty, whose divine blessings, strength, and grace have guided me throughout this journey. His presence instilled in me patience, perseverance, and resilience during the most challenging phases of my research.

I express my heartfelt gratitude to my esteemed supervisor, **Dr. Harmanjit Singh Dosanjh**, and co-supervisor, **Dr. Ramesh Chand Thakur**, for their exceptional mentorship, constant encouragement, and invaluable guidance. Their profound knowledge, insightful suggestions, and unwavering support laid the foundation for this research. Their passion for academic excellence has been a continuous source of inspiration, and I shall always remain indebted to them for their faith in my capabilities and for motivating me to aim higher.

I am especially grateful to **Dr. Harpreet Kaur** and **Dr. Abhinay Thakur** for their thoughtful guidance and kind encouragement. Despite their demanding schedules, they always took the time to patiently address my queries and offer constructive insights that significantly enriched my work. I also extend my sincere thanks to **Dr. Vivek Pathania**, from DAV College, Sector 10, Chandigarh, for providing access to essential experimental facilities, which played a vital role in the progress of my research.

I would also like to acknowledge my lab mate, **Dr. Nidhi**, for her generous assistance and collaboration during experimental work, and **Mr. Manoj**, for his cooperation and consistent support in providing essential laboratory facilities throughout my research.

I express my heartfelt gratitude to my husband, **Dr. Vishal Sharma**, for his unwavering support, encouragement, and belief in my dreams. I am also thankful to my kids, **Geetansh** and **Hitul**, whose love and smiles brought strength and joy to my journey, inspiring me every day. My heartfelt thanks go to my **parents** and **parents-in-law** for

their blessings, moral support, and continuous encouragement throughout this journey. Their love, prayers, and belief in my potential have always been a source of strength and inspiration.

To all those who have contributed, directly or indirectly, to this research endeavour, I extend my deepest thanks and warmest regards.

CHITRA SHARMA

# TABLE OF CONTENTS

| Declaration          | II   |
|----------------------|------|
| Certificate          | III  |
| Abstract             | IV   |
| Acknowledgement      | VIII |
| Table of Contents    | X    |
| List of Figures      | XV   |
| List of Tables       | XVII |
| List of Abbreviation | XXI  |

# TABLE OF CONTENTS

| CHAPTER 1. INTRODUCTION |   |       |
|-------------------------|---|-------|
| 1.                      | Introduction                                | 2     |
| 1.1                     | Types of batteries                          | 3     |
| 1.1.1                   | Lead acid batteries                         | 3     |
| 1.1.2                   | Nickel-based batteries                      | 3     |
| 1.1.3                   | Sodium-sulphur battery                      | 3     |
| 1.1.4                   | Lithium-ion batteries                       | 3-4   |
| 1.2                     | Aprotic Lithium Electrolytes                | 4     |
| 1.2.1                   | High Ionic Conductivity                     | 5-6   |
| 1.2.2                   | Electrochemical Stability                   | 6     |
| 1.2.3                   | Low Volatility                              | 6     |
| 1.2.4                   | Low Viscosity                               | 6     |
| 1.2.5                   | Wide Liquid Range                           | 6     |
| 1.2.6                   | Compatibility with Lithium Metal            | 6     |
| 1.2.7                   | Minimal Side Reactions                      | 7     |
| 1.2.8                   | Tailorable Properties                       | 7     |
| 1.2.9                   | Thermal Stability                           | 7     |
| 1.2.10                  | Controlled Decomposition                    | 7-9   |
| 1.3                     | Introduction to Glycol dimethyl ethers      | 9     |
| 1.3.1                   | Properties to Glycol dimethyl ethers        | 9     |
| 1.3.1.1                 | Lower Volatility and Toxicity               | 9     |
| 1.3.1.2                 | Chemical stability                          | 10    |
| 1.3.1.3                 | Versatility and Biodegradability            | 10    |
| 1.3.1.4                 | Applications in Green Chemistry             | 10    |
| 1.3.1.5                 | Advantages of Glyme-based Electrolytes      | 10    |
| 1.3.1.6                 | Safety Improvements                         | 10-11 |
| 1.3.2                   | Tailored electrolyte Properties             | 11    |
| 1.3.3                   | Compatibility with Advanced Battery Systems | 11-12 |

| 1.3.4                           | Composition of potential electrolyte                | 12-13 |
|---------------------------------|---|-------|
| 1.4                             | Molecular interactions                              | 13    |
| 1.4.1                           | Thermodynamic properties                            | 13-14 |
| 1.4.2                           | Acoustical properties                               | 14    |
| 1.4.3                           | Conductance studies                                 | 14    |
| 1.4.4                           | FT-IR spectral studies                              | 14-15 |
| 1.4.5                           | Cyclic Voltammetry                                  | 15-16 |
| 1.5                             | Parameters derived from density measurements        | 16    |
| 1.5.1                           | Apparent molar volume                               | 16-18 |
| 1.5.2                           | Apparent molar volume at infinite dilution          | 18-19 |
| 1.5.3                           | Partial molar volume of transfer                    | 19    |
| 1.5.4                           | Co-spheres overlap model                            | 19-21 |
| 1.5.5                           | Effect of Temperature on partial molar volume       | 21-22 |
| 1.6                             | Parameters derived from speed of sound measurements | 22    |
| 1.6.1                           | Apparent molar isentropic compression               | 22-23 |
| 1.6.2                           | Partial molar isentropic compression                | 23    |
| 1.6.3                           | Partial molar isentropic compression of transfer    | 23    |
| 1.6.4                           | Pair and triplet interaction coefficients           | 23-24 |
| 1.7                             | Conductance Studies                                 | 24    |
| 1.7.1                           | Specific conductance                                | 24    |
| 1.8                             | Research Gap  | 25    |
|                                 | References  | 26-30 |
| CHAPTER 2. REVIEW OF LITERATURE |   |       |
| 2.                              | Review of Literature                                | 32-53 |
|                                 | References  | 54-62 |
| CHAPTER 3. EXPERIMENTAL         |   |       |
| 3                               | Experimental  | 64    |
| 3.1                             | Materials   | 64    |
| 3.2                             | Brief Overview of Lithium Salts used in study       | 65    |

| 3.2.1  | Lithium bis(trifluoromethanesulphonyl)imide         | 65     |
|--------|---|--------|
| 3.2.2  | Lithium trifluoromethanesulfonate                   | 65-66  |
| 3.2.3  | Lithium bis(fluorosulphonyl)imide                   | 66     |
| 3.2.4  | Lithium hexafluorophosphate                         | 66-67  |
| 3.2.5  | Lithium tetrafluoroborate                           | 67     |
| 3.3    | Experimental techniques                             | 67-68  |
| 3.3.1  | Density and speed of sound measurements             | 68-69  |
| 3.3.2  | Conductivity measurements                           | 70     |
| 3.3.3  | FT-IR Spectroscopic Studies                         | 71     |
| 3.3.4  | Cyclic Voltammetry                                  | 71-72  |
|        | References  | 73     |
|        | CHAPTER 4. RESULTS AND DISCUSSION                   |        |
|        | SECTION-I   |        |
| 4.1    | Section -I  | 75     |
| 4.1.1  | Density and Acoustic measurements                   | 76     |
| 4.1.2  | Thermophysical parameters derived from Density 76   |        |
| 4.1.2  | measurements  | 70     |
| 4.1.3  | Apparent molar volume                               | 76-81  |
| 4.1.4  | Partial molar volume                                | 82-84  |
| 4.1.5  | Temperature dependence of partial molar volume      | 85-86  |
| 4.1.6  | Acoustic parameters derived from the speed of sound | 87     |
| 4.1.0  | (acoustic) measurements                             | 67     |
| 4.1.7  | Apparent molar isentropic compressibility           | 87-92  |
| 4.1.8  | Partial molar isentropic compressibility            | 93-94  |
| 4.1.9  | Pair and triplet interaction coefficient            | 94-95  |
| 4.1.10 | Cyclic voltammetry Studies                          | 95-99  |
| 4.1.11 | Conductance studies                                 | 99-104 |
|        |   |        |
|        |   |        |

| SECTION-II     |  |                    |  |
|----------------|--|--------------------|--|
| 4.2<br>4.2.1   | Results Thermophysical parameters derived from Density measurements  | 106<br>106-115     |  |
| 4.2.2<br>4.2.3 | Acoustic parameters derived using the speed of sound measurements  Partial Molar Isentropic Compression  SECTION-III | 115-119<br>120-122 |  |
| 4.3            | Result and Discussion  | 124                |  |
| 4.3.1          | Density and acoustic measurements  | 124                |  |
| 4.3.2          | Thermophysical parameters derived from density measurements  | 124-128            |  |
| 4.3.3          | Apparent molar volume  | 129-130            |  |
| 4.3.4          | Partial molar volume   | 131-132            |  |
| 4.3.5          | Temperature dependence of partial molar volume   | 133-135            |  |
| 4.3.6          | Acoustic parameters derived using the speed of sound measurements  | 135-139            |  |
| 4.3.7          | Apparent molar isentropic compression  | 140-141            |  |
| 4.3.8          | Partial molar isentropic compression   | 142-143            |  |
| 4.3.9          | FT-IR spectral studies   | 144-146            |  |
| 4.3.10         | Conductance studies  | 147-153            |  |
|                | References   | 154-160            |  |
|                | CHAPTER 5. CONCLUSION  |                    |  |
|                | Conclusion   | 162-163            |  |
|                | Future scope of work   | 164-165            |  |
|                | LIST OF PUBLICATIONS   | 166-167            |  |
|                | LIST OF CONFERENCES/WEBINARS/SHORT<br>TERM COURSES ATTENDED  | 168-174            |  |

# **LIST OF FIGURES**

| CHAPTER 1. INTRODUCTION                          |   |    |  |
|--|---|----|--|
| Figure 1.1                                       | Ion hydration Co-spheres overlap  | 20 |  |
| Figure 1.2                                       | Figure 1.2 Interaction of two Co-spheres  |    |  |
|  | CHAPTER 3. EXPERIMENTAL   |    |  |
| Figure 3.1                                       | General structure of Lithium bis(trifluoromethanesulphonyl)imide                                      | 65 |  |
| Figure 3.2                                       | General structure of Lithium trifluoromethanesulfonate  | 66 |  |
| Figure 3.3                                       | General structure of Lithium bis(fluorosulphonyl)imide  | 66 |  |
| Figure 3.4                                       | General structure of Lithium hexafluorophosphate  | 67 |  |
| Figure 3.5                                       | General structure of Lithium tetrafluoroborate  | 67 |  |
| Figure 3.6                                       | Anton Paar DSA 5000M  | 69 |  |
| Figure 3.7                                       | Density and sound velocity cell of DSA 5000M  | 69 |  |
| Figure 3.8 Systronics Conductivity meter 308     |   | 70 |  |
| Figure 3.9 Shimadzu FTIR-8400S Spectrophotometer |   | 71 |  |
| Metrohm Autolab PGSTAT204 multi-channel          |   |    |  |
| Figure 3.10                                      | Potentiostat/galvanostat electrochemical workstation  | 72 |  |
|  | CHAPTER 4. RESULTS AND DISCUSSION   |    |  |
|  | SECTION-I   |    |  |
|  | Plots of variation of apparent molar volume $(V_{\phi})$ of LiOTf in 0.01                             |    |  |
| Figure 4.1                                       | mol.kg <sup>-1</sup> (labelled as Blue) and 0.05 mol.kg <sup>-1</sup> (labelled as red) in (a)        | 81 |  |
| riguit 4.1                                       | aqueous DME solution (b) aqueous TEGDME solution at T =   | 01 |  |
|  | (293.15 K, 298.15 K, 303.15 K, 308.15 K and 313.15 K).  |    |  |
| Figure 4.2                                       | Plots of variation of apparent molar isentropic compressibility                                       | 92 |  |
| 11guit 7,2                                       | $(K_{\phi,S})$ of LiOTf in 0.01 mol.kg <sup>-1</sup> (labelled as Blue) and 0.05 mol.kg <sup>-1</sup> | 12 |  |

| Figure 4.3 | 1 (labelled as red) in (a) aqueous DME solution (b) aqueous TEGDME solution at T = (293.15 K, 298.15 K, 303.15 K, 308.15 K and 313.15 K)  Depiction of the CV plots (V vs. A) for (a) 0.01 DME and 0.05 DME, (b) 0.05 LiOTf + 0.01 DME and 0.30 LiOTf + 0.01 DME, (c) 0.05 LiOTf + 0.05 DME and 0.30 LiOTf + 0.05 DME, (d) 0.05 TEGDME and 0.01 TEGDME, (e) 0.05 LiOTf + 0.01 TEGDME and 0.30 LiOTf + 0.01 TEGDME and 0.30 LiOTf + 0.05 TEGDME | 98  |
|------------|---|-----|
|            | SECTION-III   |     |
| Figure 4.4 | Plots of variation of apparent molar volume ( $V_{\phi}$ ) of LiTFSI in 0.01 mol·kg <sup>-1</sup> (Red) and 0.05 mol·kg <sup>-1</sup> (cyan) of aqueous media of TEGDME at T = (293.15, 298.15, 303.15, 308.15 and 313.15) K  | 130 |
| Figure 4.5 | Plots of variation of apparent molar volume $(V_{\phi})$ of, LiFSI in 0.01 mol·kg <sup>-1</sup> (Red) and 0.05 mol·kg <sup>-1</sup> (blue) of aqueous media of TEGDME at T = (293.15, 298.15, 303.15, 308.15 and 313.15) K.   | 130 |
| Figure 4.6 | Plots of variation of apparent molar volume $(K_{\phi,s})$ of, LiTFSI in 0.01 mol·kg <sup>-1</sup> (Red) and 0.05 mol·kg <sup>-1</sup> (cyan) of aqueous media of TEGDME at T = (293.15, 298.15, 303.15, 308.15 and 313.15) K.  | 141 |
| Figure 4.7 | Plots of variation of apparent molar volume ( $K_{\phi,s}$ ) of LiFSI in 0.01 mol·kg <sup>-1</sup> (Red) and 0.05 mol·kg <sup>-1</sup> (cyan) of aqueous media of TEGDME at T = (293.15, 298.15, 303.15, 308.15 and 313.15) K.  | 141 |
| Figure 4.8 | Plots of FT-IR spectra of (a) 0.05 mol/kg of LiTFSI and, (b) 0.30 mol/kg of LiTFSI in (0.01, 0.03 and 0.05) mol·kg <sup>-1</sup> of aqueous media of TEGDME.  | 145 |
| Figure 4.9 | Plots of FT-IR spectra of (a) 0.05 mol/kg of LiFSI and, (b) 0.30 mol/kg of LiFSI in (0.01, 0.03 and 0.05) mol·kg <sup>-1</sup> of aqueous media of TEGDME.  | 146 |

# **LIST OF TABLES**

| CHAPTER 3. EXPERIMENTAL           |  |       |
|-----------------------------------|--|-------|
| Table 3.1                         | Details of chemical utilized during research work  | 64    |
| CHAPTER 4. RESULTS AND DISCUSSION |  |       |
|                                   | SECTION-I  |       |
| T 11 44                           | The molality, densities $(\rho)$ , apparent molar volumes  | 77.00 |
| Table 4.1                         | $(V_{\phi})$ of LiOTf in aqueous DME and aqueous TEGDME  | 77-80 |
|                                   | solutions at various temperatures, $P = 0.1MPa$  |       |
| Table 4.2                         | Partial molar volumes, $(V_{\phi}^{0})$ of LiOTf in aqueous DME  | 83    |
|                                   | and aqueous TEGDME solutions at various temperatures   |       |
|                                   | Partial molar volume of transfer, $\Delta V_{\phi}^{0} \times 10^{6} / (\text{m}^{3}  \text{mol}^{-1})$ of |       |
| Table 4.3                         | LiOTf in aqueous DME and aqueous TEGDME  | 84    |
|                                   | solutions at various temperatures  |       |
|                                   | Values of empirical parameters determined from Eq.   |       |
| Table 4.4                         | (1.18) for LiOTf in aqueous DME and aqueous  | 85    |
|                                   | TEGDME   |       |
|                                   | Limiting apparent molar expansibilities $(\phi_E^0)$ of LiOTf  |       |
| Table 4.5                         | in aqueous solution of DME and aqueous TEGDME  | 86    |
|                                   | solutions at various temperatures  |       |
|                                   | Values of ultrasonic speed, (u) and apparent molar   |       |
| Table 4.6                         | isentropic compressibility, $(K_{\phi,s})$ of LiOTf in aqueous   | 88-91 |
| 1 abic 4.0                        | DME and aqueous TEGDME solution at various   | 00-71 |
|                                   | temperatures, $P = 0.1MPa$   |       |
|                                   | Partial molar isentropic compressibility, $(K_{\phi,s}^0)$ of  |       |
| Table 4.7                         | LiOTf in an aqueous solution of DME and aqueous  | 93-94 |
|                                   | TEGDME at various temperatures   |       |

| <b>Table 4.8</b>       | Pair interaction coefficients, $(V_{AB}, K_{AB})$ and triplet interaction coefficients, $(V_{ABB}, K_{ABB})$ of LiOTf in an aqueous solution of DME and aqueous TEGDME at various temperatures       |         |
|------------------------|--|---------|
| Table 4.9              | Several EW values attained from the CV analysis of LiOTf in an aqueous solution of DME and aqueous  TEGDME at ambient temperature  99  |         |
| Table 4.10             | Specific conductance ( $\kappa$ ) and molar conductance ( $\Lambda_m$ ) of LiOTf in aqueous DME and TEGDME solutions at different temperatures   | 100-102 |
| <b>Table 4.11</b>      | Limiting molar conductance $(\Lambda_m^0)$ of LiOTf in aqueous DME and TEGDME solutions at different temperatures.   | 103     |
| <b>Table 4.12</b>      | Activation energy of conductance $(E_{\lambda})$ of LiOTf in aqueous DME and TEGDME solutions.   |         |
| SECTION-II             |  |         |
| Table 4.13             | Temperature-dependent densities and $V_{\phi}$ of LiBF <sub>4</sub> and LiPF <sub>6</sub> in aqueous TEGDME medium, $P = 0.1$ MPa  | 107-110 |
|                        |  |         |
| <b>Table 4.14</b>      | Temperature-dependent $V_{\phi}^{0}$ and $S_{v}^{*}$ of LiBF <sub>4</sub> and LiPF <sub>6</sub> in aqueous media of TEGDME   | 111     |
| Table 4.14  Table 4.15 | •  | 111     |
|                        | aqueous media of TEGDME  Temperature-dependent $\Delta V_{\phi}^{0}$ of LiBF <sub>4</sub> and LiPF <sub>6</sub> in   |         |
| Table 4.15             | aqueous media of TEGDME  Temperature-dependent $\Delta V_{\phi}^{0}$ of LiBF <sub>4</sub> and LiPF <sub>6</sub> in aqueous media of TEGDME media  Empirical variables computed using Eqn. (1.18) for | 113     |

| <b>Table 4.19</b> | $K_{\phi,s}^0$ and $S_K^*$ of LiBF <sub>4</sub> and LiPF <sub>6</sub> in aqueous media of TEGDME at various temp   | 121     |
|-------------------|--|---------|
| <b>Table 4.20</b> | $\Delta K_{\phi,s}^0$ of LiBF <sub>4</sub> and LiPF <sub>6</sub> in aqueous media of TEGDME medium   | 122     |
|                   | SECTION-III  |         |
| Table 4.21        | The molality, densities ( $\rho$ ), apparent molar volumes ( $V_{\phi}$ ) of LiFSI and LiTFSI in aqueous TEGDME media at various temperatures, P = 0.1MPa                        | 125-128 |
| <b>Table 4.22</b> | Partial molar volumes, $(V_{\phi}^{0})$ and experimental slopes, $(S_{v}^{*})$ of LiFSI and LiTFSI in aqueous media of TEGDME at various temperatures                            | 132     |
| <b>Table 4.23</b> | Values of empirical parameters determined from Eq. (1.18) for LiFSI and LiTFSI in aqueous media of TEGDME  | 133     |
| <b>Table 4.24</b> | Limiting apparent molar expansibilities ( $\phi_E^0$ ) of LiFSI and LiTFSI in aqueous media of TEGDME at various temperatures  | 134-135 |
| <b>Table 4.25</b> | Values of ultrasonic speed, $(u)$ and apparent molar isentropic compression, $(K_{\phi,s})$ of LiFSI and LiTFSI in aqueous media of TEGDME at various temperatures, $P = 0.1MPa$ | 136-139 |
| <b>Table 4.26</b> | Partial molar isentropic compression, $(K_{\phi,s}^0)$ and empirical slopes, $(S_K^*)$ of LiFSI and LiTFSI in aqueous media of TEGDME at various temperatures                    | 143     |
| <b>Table 4.27</b> | Specific conductance ( $\kappa$ ), and molar conductance ( $\Lambda_m$ ) of LiTFSI and LiFSI in aqueous TEGDME solutions at different temperatures.                              | 148-151 |

| <b>Table 4.28</b> | Limiting molar conductance $(\Lambda_m^0)$ of LiTFSI and LiFSI in | 152 |
|-------------------|---|-----|
|                   | aqueous DME solutions at different temperatures.                  | 132 |
|                   | Activation energy of conductance ( $E_{\lambda}$ ) of LiTFSI and  |     |
| <b>Table 4.29</b> | LiFSI in aqueous TEGDME solutions at different                    | 153 |
|                   | temperatures.   |     |

#### **LIST OF ABBREVIATIONS**

LiTFSI Lithium bis(trifluoromethanesulphonyl)imide

LiOTf Lithium trifluoromethanesulfonate

LiFSI Lithium bis(fluorosulphonyl)imide

LiPF<sub>6</sub> Lithium hexafluorophosphate
LiBF<sub>4</sub> Lithium tetrafluoroborate

TEGDME Tetraethylene glycol dimethyl ether

DME 1,2-dimethoxyethane

<sup>0</sup>C Temperature in degree Celsius

e.g. Example

T Temperature

P Pressure V Volume

ρ Density of solution

 $\rho_{o}$  Density of pure solvent

U Speed of Sound

g Gram

FT-IR Fourier transform infrared spectroscopy

mM Millimole
ml Milliliter
K Kelvin

ms<sup>-1</sup> Meter per second

c Molarity

cm/s Centimeter per second

∂ Partial differential

n<sub>1</sub>, n<sub>2</sub> Number of moles of constituent 1 and 2

kg.m<sup>-3</sup> Kilogram per cube meter

M Molality

MW Molecular weight

 $V_{\Phi}$  Apparent molar volume

| $V_{+}^{0}$ | Limiting value of apparent molar volume     |
|-------------|---|
| II * •      | ziming there at apparation material termina |

 $S_{V}^{*} S_{K}^{*}$  Experimental slope

 $\Delta V_{\Phi}^{0}$  Partial molar volume of transfer

a, b, c Empirical constants

ARD Average relative deviation
RSD Relative standard deviation

 $\Phi_E^0$ Limiting apparent molar expansivity

 $(\partial \varphi_E^0/\partial T)$  Hepler constant

 $K_{\phi,s}$  Apparent molar isentropic compression

 $\kappa_{S,0}$ ,  $\kappa_{S}$  Isentropic compressibilities of pure solvent and

solution

 $\Delta K_{\varphi,s}^0$  Partial molar isentropic compression of transfer

H Planck's constant

R Gas constant

N Avogadro's number

J Joule

d Derivative

 $\begin{array}{ccc} X & & \text{Mole fraction} \\ V_m & & \text{Molar volumes} \end{array}$ 

Na<sup>+</sup>, K<sup>+</sup> Sodium and potassium ion

mol kg<sup>-1</sup> Mole per kilogram

m³⋅mol⁻¹ Meter cube per mole

m<sub>A</sub> Molality of solute in solventm<sub>B</sub> Molality of stock solution

σ Standard deviation

m<sup>3</sup>·mol<sup>-1</sup>·K<sup>-2</sup> Cubic meter per mole per square kelvin

m³·mol⁻¹·GPa⁻¹ Cubic meter per mole giga per pascal

a,b,c Empirical parameters

κ Specific Conductivity

| $\Lambda_{ m m}$   | Molar conductivity               |
|--------------------|----------------------------------|
| $E_{\lambda}$      | Activation Energy of conductance |
| $\Lambda_{ m m}^0$ | Limiting Molar Conductance       |

# Chapter 1 Introduction

#### 1. Introduction

Among all the resources available across the globe, energy is the most important resource. Energy is needed to carry out life activities, to promote economic and social development in order to create a better quality of living. Nature being a big reservoir of energy provides a wide variety of resources, primarily described as renewable and non-renewable sources of energy. The non-exhaustible natural sources of energy that are always being replenished are known as renewable sources of energy. Examples of renewable sources include solar, hydroelectric, geothermal, tidal, wind, etc. The abundant natural sources of energy that cannot be naturally replenished are known as non-renewable sources of energy. They take thousands of years to replenish. Examples of non-renewable sources are oil, natural gas, coal etc. In general, renewable energy sources are widely considered as sustainable energy resources.

The concept of sustainability focuses on long-term survival of society. Their need lies in the equilibrium between the resources and sustainability. The natural resources are present in abundance, still the demand of energy is growing globally as a result of overpopulation, industrial development, urban development and economic development contributing to energy crises. Energy produced from natural resources should be stored and used as needed to meet the growing demand for power. Among the methods utilized to store energy worldwide are energy storage devices. Extensive researches and development efforts are being done to bring the technologies used in energy storage devices to commercial maturity (Kousksou et al., 2014). To meet with the increasing energy demands, researchers worldwide are trying to establish viable energy substitutes. Considering the modern breakthroughs in chemistry, the prevalent energy storage systems include, flow batteries, supercapacitors and rechargeable batteries. Among these means of energy storage, to cope up with the need of sustainable energy, the rechargeable battery is the best solution (Deng, 2015). The combination of electrochemical cells used to transform chemical energy into electrical energy is called as "battery". The batteries which can be recharged are termed as secondary batteries and those which cannot be recharged are classified as primary batteries (Mclarnon &

Cairns, 1989). Few of these types of batteries that are having industrial applications are discussed below:

#### 1.1 Types of batteries

#### 1.1.1. Lead acid batteries

Lead-acid batteries come in two main varieties: valve-regulated batteries and flooded batteries. Lead-acid batteries with valve regulation require less upkeep, emit fewer gases, and have low self-discharge rate. Due to sulfation, chances of premature failure are always there (Díaz-González *et al.*, 2012). Working of lead-acid batteries depend upon chemical reactions in the presence of PbO<sub>2</sub> (cathode electrode), Pb (anode electrode) and H<sub>2</sub>SO<sub>4</sub> (electrolyte).

#### 1.1.2. Nickel-based batteries

The electrolyte used in these types of batteries is nickel hydroxide and potassium hydroxide with some amount of lithium hydroxide (McDowall, 2006). NiCd batteries will begin to lose capacity if they are not completely depleted before being recharged (Morioka *et al.*, 2001).

#### 1.1.3. Sodium-sulphur battery (NaS)

A NaS battery comprises of sulphur and sodium both in molten state as positive anode and negative terminal respectively. The material which separates cathode and anode acts as electrolyte (beta alumina). Typical NaS battery cells are tubular in shape, with the sodium typically housed inside an electrolyte-formed inner chamber. The power output of sodium-sulphur battery is very small at room temperature. To keep the sulphur in molten form, the temperature must be maintained 350 °C.

#### 1.1.4. Lithium-ion batteries

Portable devices like smartphones, laptops etc. use lithium-ion batteries as a source of electric power. A typical Lithium-ion battery consists of anode made up of graphite and cathode made up of a complex of oxide of a transition metal with Li such as lithium manganese oxide (LiMn<sub>2</sub>O<sub>4</sub>), lithium iron phosphate (LiFePO<sub>4</sub>), lithium cobalt oxide (LiCoO<sub>2</sub>). Cathode and anode are placed in electrolyte solution (Lithium salts + mixture of solvents). Higher Production cost & Less power density are the main limitations of these type of batteries.

It is evident from the above data that all kind of batteries discussed here, have their own merits and demerits (Deng, 2015). Researchers have explored electrolytes such as lithium salts in solvents, ionic liquids, ceramics, and polymers, but these electrolytes are of high cost and shows low ionic conductivity, therefore limiting its industrial use (Anouti *et al.*, 2012), (Younesi *et al.*, 2015). Lithium-ion batteries (LIBs), on the other hand, are widely used in electronics, electric vehicles, and energy storage devices owing to their high energy density, long cycle life, and low self-discharge (Xu, 2004).

#### 1.2 Aprotic Lithium Electrolytes

The performance of the Lithium-ion batteries is dependent on the type of the electrolytes used. Aprotic lithium electrolytes, maintains the electrochemical stability while enabling the ion transport. (Barthel *et al.*, 1990). Aprotic lithium electrolytes are non-aqueous that do not donate protons and are used in lithium-ion batteries and hence are potential candidates for energy storage applications. (Ray *et al.*, 2017). Aprotic lithium electrolytes dissolve lithium salts and enable lithium-ion transport, a key process for electrochemical reactions that produce electric current. Their properties, such as thermal stability and conductivity, vary considerably with composition. They have ability to dissolve lithium salts and facilitate the movement of lithium ions during battery operation, that results in electrochemical reactions to generate electric current.

The compensated Arrhenius formalism (CAF) states that cyclic carbonates shows higher diffusion activation energies as compared to typical aprotic solvents as a result of strong inter molecular interactions. (Khan *et al.*, 2021). Non-fluorinated tri-lithium salts have been shown to offer potential cost savings and superior performance characteristics, including high conductivities and good thermostability. Additionally, the electrochemical stability of substrates like copper in Li-ion battery electrolytes can be influenced by the composition of the electrolytes and the presence of impurities.

Furthermore, it is noteworthy that the electrochemical stability of substrates like copper in Li-ion battery electrolytes is also affected by other factors like temperature, pressure, and other reactive substances in the electrolyte. Therefore, a comprehensive

understanding of the attributes that influence the electrochemical stability of substrates in Li-ion battery electrolytes is important for optimizing battery performance and preventing unwanted side reactions. In particular, the proton conductivity of aprotic lithium electrolytes and their ability to dissolve lithium salts without forming a liquid-like layer plays a significant role in their electrochemical stability (Ray *et al.*, 2017). Lithium hexafluorophosphate (LiPF<sub>6</sub>), lithium hexafluoro arsenate (LiAsF<sub>6</sub>), and lithium perchlorate (LiClO<sub>4</sub>) are the most often utilized lithium salts in these electrolytes.

These electrolytes' aprotic character aids in preventing interactions with lithium metal, which is essential for the functionality and safety of LIBs. The properties of aprotic lithium electrolytes have a great influence on the safety and working of lithium-ion batteries in a variety of ways (Laino & Curioni, 2013). Because of these qualities, aprotic lithium electrolytes are the focus of ongoing research and development efforts in battery technology because they work together to improve energy storage systems' dependability and efficiency. Aprotic lithium electrolytes have unique properties that not only improve energy density, cycle life, and charge rates but also greatly increase the safety of lithium-ion batteries when they are in use (Pigłowska *et al.*, 2021). Because of their superior performance and safety, aprotic lithium electrolytes are necessary for the creation of reliable energy storage systems which are highly efficient too. A variety of significant features make aprotic lithium electrolytes essential for energy storage applications, particularly lithium-ion batteries. A few of these attributes are as follows:

#### 1.2.1. High Ionic Conductivity

Aprotic solvents typically exhibit high ionic conductivity due to which efficient ion transport among the anode and cathode take place during charge/discharge cycles, enhancing charge and discharge rates (Davidson & Kebarle, 1976). It is evident that the ionic mobility of the electrolyte affects the working of batteries powered by lithiumion, and the entire functioning of the battery system may be enhanced by carefully choosing the electrolyte. Therefore, researchers must carefully consider the ionic

mobility of the electrolyte when designing and optimizing lithium-ion battery systems to ensure maximum efficiency and stability.

#### 1.2.2. Electrochemical Stability

Aprotic lithium electrolytes are stable over a wide range of voltages, reducing the risk of decomposition during battery operation. This stability allows for higher energy density and improved battery performance (Vraneš *et al.*, 2017) and allows for operation at higher voltages without electrolyte decomposition, leading to increased energy density. Ensures stable performance over extended cycles, contributing to longer battery life.

#### 1.2.3. Low Volatility

Many aprotic solvents have low volatility, which minimizes the risk of evaporation and enhances the safety and longevity of the battery. Low volatility minimizes the risk of electrolyte evaporation, which can lead to battery drying out and performance loss (Cox *et al.*, 1974). Low volatility reduces the likelihood of vapours that could ignite or explode under certain conditions.

#### 1.2.4. Low Viscosity

Reduces resistance to ion movement, allowing for better conductivity and faster response times during cycling. Enhances the overall rate capability of the battery (Cox *et al.*, 1974).

#### 1.2.5. Wide Liquid Range

Aprotic electrolytes function consistently under a variety of environmental situations because they frequently stay liquid across a wide temperature range (Kim, 1978).

#### 1.2.6. Compatibility with Lithium Metal

To enhance the efficiency and safety, these electrolytes may efficiently solvate lithium ions, therefore, allowing them to travel more freely and reducing the formation of dendrites on lithium metal anodes. This facilitates efficient lithium-ion solvation which is considered as an essential process for anodes with large capacities as it reduces the development of dendrites, which may cause short circuits (RC, 2018).

#### 1.2.7. Minimal Side Reactions

Because aprotic solvents are non-protic, there is a decreased chance of side reactions that could cause electrolyte degradation, extending the battery's cycle life. Because aprotic solvents are non-protic, there is a decreased chance of unintended reactions that could produce heat or gases, improving battery safety (Parker & Alexander, 1968). Also, it lowers the possibility of fire and explosion by limiting the production of combustible byproducts.

#### 1.2.8. Tailorable Properties

The chemical composition of aprotic lithium electrolytes can be modified to optimize properties such as viscosity and conductivity, allowing for customization based on specific application requirements.

#### 1.2.9. Thermal Stability

Many aprotic electrolytes exhibit good thermal stability, which is important for maintaining performance under high-temperature conditions. Maintains liquid state and performance across a broad temperature spectrum, ensuring reliable operation in various environmental conditions. Reduces the risk of performance degradation under extreme temperatures (Zhenzhen Wu, Yuhui Tian, Hao Chen, Liguang Wang, Shangshu Qian, Tianpin Wu, 2022). Good thermal stability prevents breakdown at elevated temperatures, which is crucial for preventing thermal runaway scenarios and maintain structural integrity under stress, reducing the risk of battery failure.

#### 1.2.10. Controlled Decomposition

In case of thermal or mechanical abuse, aprotic electrolytes may decompose in a controlled manner, producing less heat and fewer flammable gases compared to other types of electrolytes (Kim, 1978).

In summary, aprotic lithium electrolytes are essential to lithium-ion battery function, with their properties directly influencing battery performance. They are used in a variety of applications, from portable electronics to electric vehicles, and are integral to the development of systems for the storage of energy for both mobile and stationary applications (Feng *et al.*, 2019). A strong electrolyte that can tolerate high temperatures and current voltages, has a long shelf life, and makes the lithium ions

move fast, is necessary for a long-lasting and safe battery. Solid-state, polymer, and liquid electrolytes are among the varieties. Theoretical capacity, energy density, and electrochemical potential make lithium-ion cell chemistries among the top choices for electrical energy storage for high-power and high-energy applications, which includes stationary storage and transportation (Patil *et al.*, 2016). It is extremely light, electropositive, and non-toxic in addition to being generally accessible. The potential for energy storage in lithium-based batteries is greater due to this basic advantage over alternative chemistries. However, because lithium is very reactive, creating safe lithium-based battery cells is a technologically difficult task.

Till date, this difficulty has been met by employing substances that can donate lithium ions (Li<sup>+</sup>) rather than metallic lithium (Mozhzhukhina *et al.*, 2015). In a reversible chemical reaction, the ions are moved between two electrodes. From the literature review, it is observed that Li-ion batteries yield less environmental hazards than all other types of batteries that contain lead /cadmium (Divya & Østergaard, 2009), In spite of having numerous positive attributes, Lithium ion batteries slack in the attributes i.e., power and energy densities, cycle life and its production cost. Thus, the term "metal-free lithium battery" is frequently used to refer to the Li-ion battery. The ongoing research and development in this field aim to optimize these electrolytes for better battery performance, including higher voltage operation and improved safety (Sharma & Thakur, 2022) along with other organic solvents. For a lithium-ion cell to be both safe and effective, the right electrolyte must be chosen.

A combination of organic solvents and lithium salt makes up the electrolyte. Thus, it is the need of hour to explore thermophysical and conductometric studies of various Lithium electrolytes with the solvents (Di Lecce *et al.*, 2022). Aprotic lithium electrolytes don't react with lithium, they are frequently used in Li-ion batteries. Typically, the components of these electrolytes are lithium salts dissolved in an aprotic (non-aqueous) solvent. Ethyl methyl carbonate (EMC), dimethyl carbonate (DMC), propylene carbonate (PC) and Diethyl carbonate (DEC) are a few examples of aprotic solvents used in Li-ion batteries. These solvents are appropriate for lithium-ion batteries due to their high dielectric constants, low viscosity, and strong chemical stability. One

of the main organic solvents used with these kinds of electrolytes is glycol dimethyl ethers (Glyme).

#### 1.3 Introduction to Glycol dimethyl ethers (Solvents)

An important component of the battery's operation, the organic solvent is essential for promoting the flow of lithium ions. Among the common organic solvents are ethylene carbonate, propylene carbonate, diethyl carbonate, ethyl carbonate and dimethyl carbonate. Glymes, also known as glycol dimethyl ethers, are a class of aprotic solvents that have drawn high interest in energy storage systems and electrochemistry (Di Lecce *et al.*, 2022). Their distinct characteristics render them appropriate for employment as solvents in electrolytes based on lithium. Glyme solvents are considered more environmentally friendly than typical organic solvents because of their decreased volatility and toxicity, chemical stability, possibility for biodegradability, and diversity in application. In lithium batteries, glyme-based electrolytes present a viable substitute for traditional solvents, offering greater conductivity, safety, and stability as well as the possibility of better performance in next-generation energy storage devices (Chrétien *et al.*, 2014). These solvents have a number of qualities that make them more environmentally friendly than many other solvents. A few of these qualities are as follows:

#### 1.3.1 Properties of Glycol dimethyl ethers (Glymes)

#### 1.3.1.1 Lower Volatility and Toxicity

Generally, glymes (Glycol dimethyl ethers) are less volatile than traditional organic solvents, which lowers the possibility of inhalation exposure and air pollution while using them. This feature reduces the number of hazardous fumes released into the atmosphere, making the workplace safer. Additionally, a lot of glymes are less hazardous than typical lab solvents (Horwitz *et al.*, 2018). Although some glymes have lower acute toxicity, they are a safer option for a variety of applications even though they may have long-term reproductive and developmental harm.

#### 1.3.1.2. Chemical Stability

They are less likely to break down or react with other compounds under typical circumstances because they are chemically and thermally stable. Because of their stability, glymes are a more environmentally responsible choice for industrial and laboratory procedures as they lower the possibility of producing dangerous consequences.

#### 1.3.1.3. Versatility and Biodegradability

Glymes are environmentally compatible since they may be made from renewable materials and have been studied for their biodegradability (Lombardo *et al.*, 2013). Their capacity to combine with ions to create complexes increases their usefulness in a variety of applications, like catalysis and energy storage, without having the negative environmental effects of more hazardous solvents.

#### 1.3.1.4 Applications in Green Chemistry

Because of their potential to result in more environmentally friendly procedures, glymes are being used more and more in green chemistry applications including electrochemistry and organic synthesis (Lombardo *et al.*, 2013). For example, its application in battery technology supports the drive for more environmentally friendly energy storage options.

#### 1.3.1.5 Advantages of Glyme-based Electrolytes

Glyme based electrolytes offer several advantages over conventional alkylcarbonate solvents for lithium batteries.

#### 1.3.1.6 Safety Improvements

Glymes generally boost the safety of lithium batteries since they are less combustible than alkyl-carbonate solutions. Glyme-based electrolytes are less dangerous and better for the environment than standard solvents. Many organic solvents are less flammable than traditional solvents when paired with aprotic electrolytes, improving the safety profile of the battery system (Di Lecce *et al.*, 2022). This is especially necessary for applications in portable electronics and electric cars.

Long-chain glymes exhibit exceptionally high safety, very low toxicity, and remarkable stability. Glyme-based electrolytes have greater stability, particularly in the polymer state and in a variety of circumstances, such as the presence of sulphur, oxygen, and high-energy lithium metal. The right choice of organic solvent can improve the electrochemical stability of the electrolyte (Wei *et al.*, 2020). Dimethyl sulfoxide (DMSO) and ethylene carbonate (EC) are two examples of solvents that can produce stable solid electrolyte interphases (SEI) on anode, which is an essential process for the longevity and functionality of batteries.

Glyme solvents can be used at higher concentrations of salt to provide improved conductivity since they dissolve more readily in lithium salts. Compared to alkylcarbonate solvents, glute solutions exhibit higher lithium-ion transport and ionic conductivity (Horwitz *et al.*, 2018). Ionic conductivity is increased by the easier solubility of lithium salts in organic solvents, particularly those with high dielectric constants. This is necessary for efficient lithium-ion transfer to take place during battery operation.

Different cathodes that are more cost-effective, have a higher energy density, or are clearly more environmentally friendly can be employed with electrolytes based on grease. Glyme-based electrolytes are capable to get better cell performance in terms of cycle life, safety and energy density, when used in place of currently available electrolyte (Di Lecce *et al.*, 2022). Lithium-ion batteries' performance and stability can be improved to a great extent by adding organic solvents to aprotic lithium electrolytes. The following are some important factors and advantages of this combination:

#### 1.3.2 Tailored electrolyte Properties

The viscosity, boiling point, and solvation dynamics can all be adjusted with the addition of organic solvents. By doing this, the electrolyte can be optimized for particular battery chemistries and operating circumstances (Watanabe *et al.*, 2017).

#### 1.3.3 Compatibility with Advanced Battery systems

Lithium-oxygen (Li-O<sub>2</sub>) and lithium-sulphur (Li-S) batteries are examples of advanced battery technologies that require the coupling of aprotic lithium electrolytes

with organic solvents. Solvents that are stable and effective in extreme electrochemical conditions are frequently needed for these systems (Shi *et al.*, 2013).

#### 1.3.4 Composition of potential Electrolyte

In summary, aprotic lithium electrolytes are essential to the advancement of lithiumion battery technology. Their unique characteristics enable higher performance, safety, and efficiency which pave the way for next-generation energy storage solutions. It will take more research to optimize these electrolytes to fulfil the growing demand for sustainable, high-capacity energy storage options. When discussing battery operation, it is important to note that the interactions between the electrodes, charged molecules, and applied electric potential are highly complex, and they are particularly important in the production of well-designed electrolyte. We may examine each parameter and component alone as well as in combinations thanks to methodology and modeling. The mostly used batteries now-a-days are Li-ion batteries and the electrolyte for LIB is composed of two components mixture that are ethylene carbonate and dimethyl carbonate and LiPF<sub>6</sub> salt (Patil et al., 2016). The use of this mixture in batteries is found out to be quite dangerous and self-destructive, also a few incidents of self-destructive laptops and mobile phones were witnessed. Also, the salt used gets hydrolyzed during the reaction in storage devices which further leads to the formation of a poisonous chemical HF which has very adverse effects on environment and is also unsafe.

To overcome these limitations of the composition used in Li-ion batteries different composition has been tried as the electrolytes which fulfil the requirement needed for a good battery including high electrochemical and thermal stability, potential and capacitance (Chrétien et al., 2014). While talking about the functioning of the batteries, the interaction between the electrodes, the charged molecules and applied electric potential are quite difficult to handle and these interactions plays a specific role in the manufacturing of good, designed electrolyte. For energy storage applications, we give a comprehensive analysis of the thermophysical and conductometric characteristics of aprotic lithium electrolytes in aprotic organic solvents in this work. We study how different organic solvents, and lithium salts affect the electrolytes' density, ionic conductivity, and electrochemical stability. The findings offer important new

information about how to create effective and safe electrolytes for next-generation LIBs and other energy storage devices. Methodology/modelling allow us to study each of the parameter and components separately as well as in the combinations too. And to investigate the combination, we also do thermal, transport, conductance and spectroscopic studies which will help us to measure the constants which are essential for the consideration of the suitable electrode material to be used in energy storage devices.

#### 1.4 Molecular interactions

The performance of glyme-based electrolytes, which may find application in energy storage technologies, is primarily determined by the interactions that exist between the molecules that make up the electrolyte. The interactions between lithium salts and glymes are primarily coordination interactions, where the lithium cation coordinates with the ether oxygen atoms of glymes. Both electrostatic and magnetic forces play a role for the interaction between Li<sup>+</sup> ions and glycme molecules, which include mono-, di-, tri-, and tetra-glyme. By nature of their negative charge, the oxygen atoms that make up the glyme molecules are able to attract the positively charged Li<sup>+</sup> ions. The energy required to stabilize the Li<sup>+</sup> complex rises in proportion to the number of oxygen atoms in glyme molecule. However, the amount of energy required to stabilize each oxygen atom decreases. This is due to the fact that the negative charge present on the oxygen atom which is in contact with the Li<sup>+</sup> causes the electrostatic and electromagnetic interaction that are attractive between other oxygen atoms and the Li<sup>+</sup> to be reduced (Saito et al., 2017). The physicochemical features of glyme-based electrolytes, such as ionic conductivity and electrochemical window are determined by the molecular interactions. In order to build electrolytes that have higher performance for lithium batteries, it is helpful to understand these interactions.

#### 1.4.1. Thermodynamic properties

Aspects of thermodynamics that are connected to heat and other types of energy. The flow of heat is implied by the term thermodynamics. This study examines how energy changes in conjunction with chemical and physical processes. One can explain

a substance's state using a variety of thermodynamic parameters, including its mass, temperature, pressure, thermal conductivity, etc. Thermodynamic properties can be widespread or intensive. While a system's intensive characteristics, like pressure, density, viscosity, etc., are unaffected by the amount of a substance present, its extended qualities, like mass, volume, and energy, are reliant on the amount of a material being introduced (Nidhi & Kaur, 2022).

# 1.4.2. Acoustical properties

Acoustical properties are the properties controlling the respond of materials to sound waves, which we further perceive as sound. The acoustic property also indicates the interactions among molecules providing the exact data for molecular interactions, specifically when conductometric data fails to provide the exact in cases interpretation of the interactions.

### 1.4.3. Conductance studies

The ionic conductivity of these electrolytes, a crucial factor affecting battery efficiency, can be better understood by conductometric investigations. This knowledge is supported by thermophysical investigations that look at the thermal characteristics of aprotic lithium electrolytes, such as density and viscosity, which are essential for improving electrolyte formulations. The design of more effective electrolytes can be guided by the interaction between thermophysical characteristics and ionic conductivity, which can disclose the mechanisms controlling ion transport. The main objective of this study is to investigate the conductometric and thermophysical characteristics of aprotic lithium electrolytes in different organic solvents. Ions can travel through cracks in the crystal lattice of a solid or an aqueous solution through a process known as ionic conduction. Electrolytic solutions have a particular feature called conductance that controls the type of solvent-solvent, ion-solvent and ion-ion synergies in mixed solvents. This research provides thermodynamic data in the shape of association constants, as well as kinetic data in the type of ionic conductivities.

### 1.4.4. FT-IR spectral studies

FT-IR spectrum analysis can be used to assess the interactions within a system. The infrared spectrum peak is caused by variations in the net dipole moment resulting

from the vibrations of distinct atoms inside a molecule. The bond length change is predicted by these spectral studies. To confirm the thermodynamic properties of the synergies, present in the systems at varying concentrations of lithium salts and glymes, FT-IR spectroscopy has been performed.

# 1.4.5. Cyclic Voltammetry

The technique used to detect the current that appears in an electrochemical cell when the voltage is too high is called cyclic voltammetry. This method is primarily used to forecast the electrode's electrochemical characteristics, which aids in determining if the electrode has the potential to be effectively electrochemically and, if so, helps verify the electrode's viability for usage in energy storage devices. Furthermore, useful in explaining the reduction peaks to the component reduction are the cyclic voltammograms. These constituents mostly consist of oxygen and water, which are preexisting in the ionic liquids. In addition to measuring various electrochemical stabilities, voltammetry techniques like cyclic voltammetry (CV) & linear sweep voltammetry (LSV) are primarily used to determine critical data of electrochemical reactions, such as the location of the electroactive species redox potential. To put it briefly, making attractive ionic liquids and optimizing their use require a grasp of the physicochemical characteristics of ionic liquids. Having a solid understanding of the different physical and chemical properties is necessary before beginning any industrial application. The densities, acoustic, viscosity, and conductance values of the various systems can be used to forecast the diverse characteristics that show the varied interactions, structure maker, and structure breaker behaviour of solute in solvents. It is possible to combine classical and thermodynamic methods to find the mixes' equilibrium properties.

In the investigated system, using various thermodynamic parameters (Apparent molar volume, partial molar volume, partial molar isentropic compression, partial molar isentropic compression of transfer, partial molar volume of transfer, pair & triplet interaction coefficients) are calculated using density & sound speed values at different temperatures. Conductivity data is used to look at the nature of a solute's ability to form/break structures in a specific solvent. Additionally, FT-IR spectrum analyses of

the ternary mixes (Li salt + aqueous glyme) at various concentrations have been carried out to validate the type of interactions (intermolecular and intramolecular) among the solute and solvent system expected from thermodynamic parameters determined. Furthermore, experiments using cyclic voltammetry have been conducted to examine the electrochemical characteristics of the ternary systems.

# 1.5. Parameters derived from density measurements

Volumetric properties are helpful in determining the interactions present in the solution. The density values obtained are employed to calculate the parameters at various temperatures and concentrations of solute and that of a solvent. Below is a discussion of the different parameters.

# 1.5.1. Apparent molar volume (AMV)

The AMV  $(V_{\phi})$  of a solute is determined by adding one mole of solute to the solution in such a way that it has no profound effect on the solution concentration. When the pressure, temperature, and concentration of the constituents in the solution are kept constant and one mole of the solute is added to a large volume of solution, the volume of the solution changes; this is referred to as the partial molar volume  $(V_{\phi}^{0})$  on a specific concentration. It is calculated using the equation:

$$\bar{V}_2 = V_{\phi}^0 = \left(\frac{\partial V}{\partial n_2}\right)_{\text{T.P.n.}} \tag{1.1}$$

where,  $n_i$  represents to the number of moles of all other constituents excluding i<sup>th</sup> constituents. During the formation of a solution with two constituents equation (1.1) can be written as

$$\overline{V}_2 = \left(\frac{\partial V}{\partial n_2}\right)_{\text{T.P.}n_1} \tag{1.2}$$

Where, subscript 1 stands for solvent whereas 2 symbolizes solute.

Further, in a solution, the volume is dependent on pressure, temperature and amount of every component present.

Considering a binary system, when its temperature and pressure is kept constant, the differential volume on adding or eliminating any of the components can be presented as

$$dV = \left(\frac{\partial V}{\partial n_1}\right)_{\text{T,P,}n_1} dn_1 + \left(\frac{\partial V}{\partial n_2}\right)_{\text{T,P,}n_2} dn_2 \tag{1.3}$$

Differential volume can be stated as

$$dV = \bar{V}_1 \, dn_1 + \bar{V}_2 \, dn_2 \tag{1.4}$$

Upon integration of equation (1.4), an expression is found from which we can obtain the volume of the solute from the partial molar volume as stated below

$$V = n_1 \, \bar{V}_1 + n_2 \, \bar{V}_2 \tag{1.5}$$

Where  $\bar{V}_1$  and  $\bar{V}_2$  are partial molar volume of solvent as well as solute respectively,  $n_1$  stands number of moles of constituent 1 whereas  $n_2$  is for a number of moles of constituent 2.

In a system with a fixed number of moles of solvent ( $n_1$ ),  $n_2$  moles of solute are added. Here change in the volume of the solution can be expected. This change in volume obtained due to added volume is known as apparent molar volume ( $V_{\phi}$ ).

$$V_{\phi} = \frac{V - n_1 V_1^0}{n_2} \text{(at constant T and P)}$$
 (1.6)

On rearrangement of equation (1.6),

$$V = n_2 V_{\phi} + n_1 V_1^0 \tag{1.7}$$

At a particular temperature, V is the volume of the mixture,  $n_1$  as well as  $n_2$  are the number of moles of solvent and solute correspondingly.  $V_1^0$  refers to the molar volume of the solvent (pure).

On differentiating equation (1.7) with respect to  $n_2$  at a constant T, P and  $n_1$ , the following equation can be obtained:

$$\left(\frac{\partial V}{\partial n_2}\right)_{\text{T,P},n_i} = \bar{V}_2 = V_{\phi} + n_2 \left(\frac{\partial V_{\phi}}{\partial n_2}\right)_{\text{T,P},n_i}$$
(1.8)

On rearrangement of equation (1.5), the following equation can be obtained,

$$\bar{V}_1 = \left(\frac{V - n_2 \, \bar{V}_2}{n_1}\right) \tag{1.9}$$

Substituting equation (1.8) in equation (1.9),

$$\bar{V}_1 = 1/n_1 \left[ n_1 V_1^0 - n_2^2 (\partial V_{\phi} / \partial n_2)_{T,P,n_1} \right]$$
 (1.10)

From the obtained values of densities and the Molecular weight of solvent & solute i.e.  $M_1$  and  $M_2$ , the apparent molar volume can be expressed as:

$$V_{\phi} = 1/m \left[ (n_1 M_1 + n_2 M_2) / (\rho - n_1 V_1^0) \right]$$
 (1.11)

At concentration moles per unit volume, substituting  $n_2 = m$  infers that the molality m of the mixture equals the number of moles of water in 1000g, and hence the equation (1.11) becomes

$$V_{\phi} = 1/m \left[ (1000 + mM_2)/\rho - (1000/\rho_0) \right]$$
Or  $V_{\phi} = M_2/\rho + \left[ 1000(\rho_0 - \rho) / m\rho\rho_0 \right]$  (1.12)

Where  $\rho$  and  $\rho_0$  represents the densities of solution & solvent in pure form, m is the molality while  $M_2$  stands for the molar mass of the solute. When the densities are represented in g cm<sup>-3</sup> factor 1000 appears. On rearrangement of the above equation, an expression for AMV can be obtained that can be employed in ternary mixtures studied

$$V_{\phi} = (M/\rho) - \{(\rho_0 - \rho)/m_A \rho \rho_0\}$$
 (1.13)

Where M denotes molar mass of the solute (kg mol<sup>-1</sup>),  $m_A$  denotes the molality of solute in mol kg<sup>-1</sup> and  $\rho$  id density of solution and  $\rho_0$  is density of pure solvent.

When molar concentration is used, then we use  $(n_2 = C)$ ,

$$V_{\phi} = (M/\rho) - \{(\rho_0 - \rho)/C\rho_0\}$$
 (1.14)

# 1.5.2. Apparent molar volume at infinite dilution

Various interactions can be determined using apparent molar volume as well as molality and information relevant to the dominant interactions in the dilute solutions

can be interpreted. There is a linear functional relationship given by Masson between the molality and apparent molar volume that is applicable even at elevated concentrations.

$$V_{\phi} = V_{\phi}^{0} + S_{V}^{*} m_{A} \tag{1.15}$$

where  $V_{\phi}^{0}$  is the partial molar volume at infinite dilution  $V_{\phi} = V_{\phi}^{0}$ ,  $S_{V}^{*}$  is the slope, and  $m_{A}$  is the solute molality. The plot of  $V_{\phi}$  and  $m_{V}^{0}$  is undeviating and by least squares fitting of the values  $V_{\phi}^{0}$  is collected from equation (1.15). In case of ionic solutes, the apparent molar volume is obtained from the following equation

$$V_{\phi} = V_{\phi}^{0} + S_{V}^{*} C^{1/2} \tag{1.16}$$

Further, the slope is altered by the charge and type of the ions. According to Debye-Huckell limiting law, coined by Redlich and Rosenfeld at a given ionic charge, a constant limiting slope must be achieved, and on that basis the following extrapolation function was obtained

$$V_{\phi} = V_{\phi}^{0} + S_{V}^{*} C^{1/2} + b_{v}C$$
 (1.17)

Where  $S_V^*$  is limiting slope calculated from Debye –Huckel limiting law and  $b_v$  is the empirical constant premediated through experimental results.

### 1.5.3. Partial molar volume of transfer

The transfer volume of solute from water to aqueous glyme at infinite dilution was calculated from the following equation

$$\Delta V_{\phi}^{0} = V_{\phi}^{0}$$
 (in aqueous glyme solution) -  $V_{\phi}^{0}$  (in water) (1.18)

The partial molar volume of transfer can be studied based on the co-sphere overlap model.

# 1.5.4. Co-spheres overlap model

The environment of the solute or the nature of ions besides the concentrations of ion influences the overlap of hydration Co-spheres and release of water molecules. The overlap of ion-hydration Co-spheres has been represented in **Figure 1.1.** 

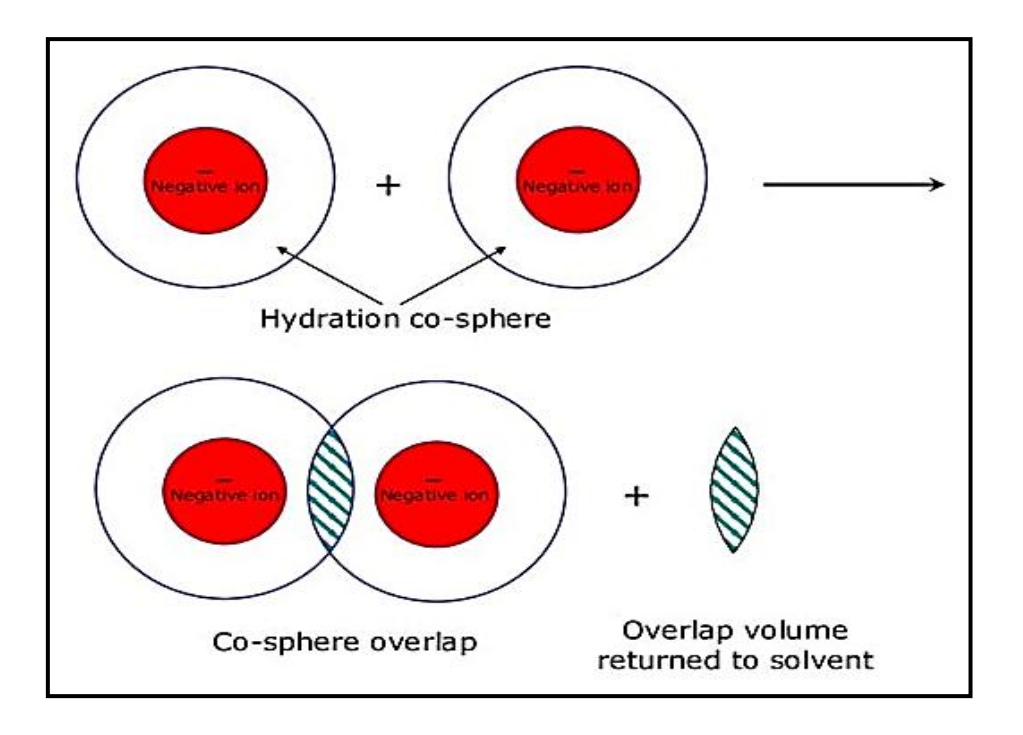


Figure 1.1: Ion hydration Co-spheres overlap adapted (Krishnan et al., 2007).

When there is displacement in the co-sphere materials then two solute particles can come effectively close together such that there is co-sphere overlap that results in a change in the thermodynamic parameters. Co-sphere model suggests that when two hydrophobic hydration co-spheres overlap the negative change in volume is observed because of release of few water molecules to the bulk from the hydration sphere. The reason for this is that the polar species have lower water molecule volumes in the solvate sphere as shown in figure 1.2. On the other hand, electrostriction and a reduction in the hydrogen-bonded network cause the water molecules in the solvate sphere to move to the bulk. (Krishnan et al., 2007). Hence, ion-hydrophobic and hydrophobic hydrophobic interactions give rise to negative values whereas ion charged/hydrophilic group interactions results in positive values (Streng & Wen, 1974). At infinite dilution, the interactions among the solute molecules are lacking; consequently, the observed transfer volumes are results from solute-solvent interactions. In terms of solute-co-solute interactions, dehydration is caused by the highly hydrated ions that interact strongly with polar groups while weakly hydrated ions have weaker interactions.

The volume changes due to various types of interactions are summarized as

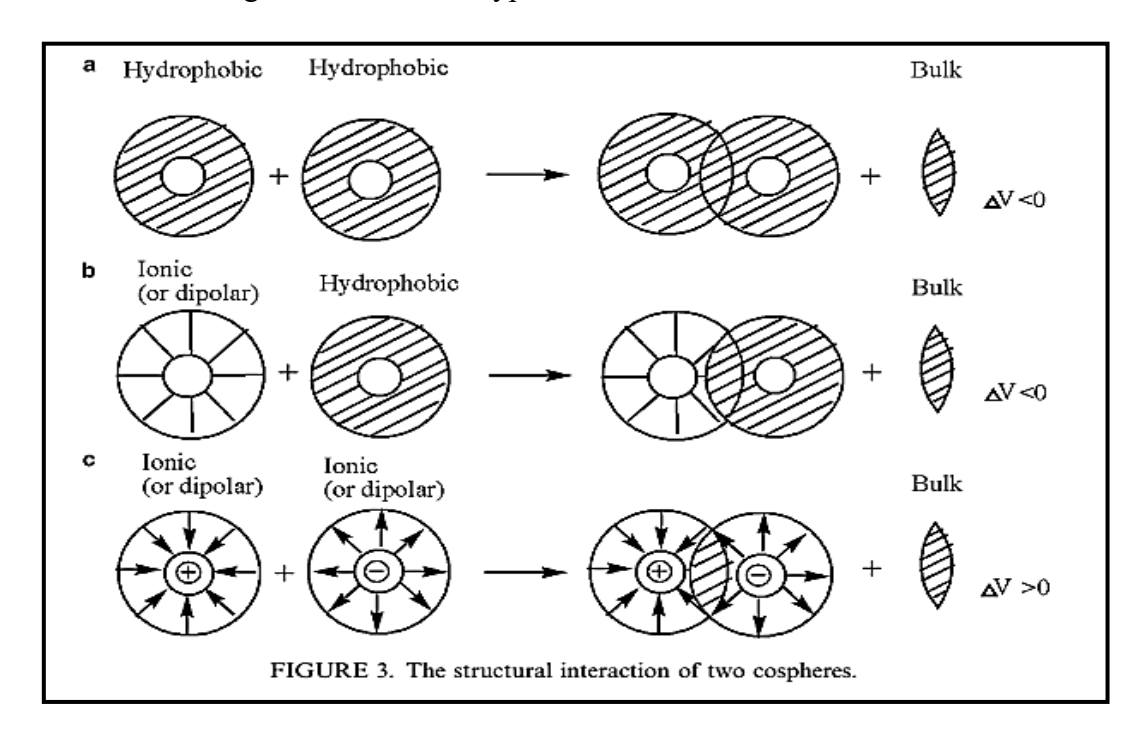


Figure 1.2: Interaction of two Co-spheres adapted from (Lin et al., 2006).

# 1.5.5. Effect of Temperature on partial molar volume

The effect of apparent molar volume with temperature and at infinite dilution  $(V_{\phi}^{0})$  can be calculated using following equation

$$V_{\phi}^{0} = a + b (T - T_{\text{ref}}) + c (T - T_{\text{ref}})^{2}$$
 (1.19)

Where a, b, and c stand for the empirical constants. T is in Kelvin and  $T_{\rm ref}$  is 298.15 K. The deviations are observed in the theoretical and experimental values of  $V_{\phi}^{0}$ . To calculate the deviations ARD ( $\sigma$ ) the following equation can be used:

$$\sigma = (1/n) \sum \left[ abs \left( \left( Y_{exp.} - Y_{calc.} \right) / Y_{exp.} \right) \right]$$
 (1.20)

Where,  $(Y = V_{\phi}^{0})$  i.e partial molar volume at infinite dilution.

Moreover, insights regarding the interactions present in the solution can be achieved using partial molar expansibilities  $\phi_E^0$  obtained using the following equation:

$$\phi_E^0 = (\partial V_{\phi}^0 / \partial T)_p = b + 2 c (T - T_{\text{ref}})$$
 (1.21)

The positive  $\phi_E^0$  values suggest the existence of solute-solvent interactions. Hepler determined the solute ability to behave as a structure promoter or structure breaker in a mixed solvent system, (Hepler, 1969):

$$(\partial \phi_E^0 / \partial T)_p = (\partial^2 V_{\phi}^0 / \partial T^2)_p = 2C \tag{1.22}$$

The sign of  $(\partial \phi_E^0/\partial T)_p$  determines the ability of a solute to act as a structure promoter or structure breaker in the solvent.

### 1.6. Parameters derived from speed of sound measurements

Acoustic studies deduce information about the various interactions (intermolecular and intramolecular), complex formation, and associated structural changes of Li salts in aqueous solution of various additives (Widegren & Magee, 2007). It supports the results obtained by the partial molar volume. The parameters derived from the speed of sound help in getting information about molecular interactions. The apparent molar compressibility of one mole of a solute at infinite dilution is represented by the partial molar adiabatic compressibility of the solute. Speed of sound gives information regarding the thermo physical properties of solutions (Bahadur & Deenadayalu, 2011; Thakur, Juglan, Kumar, & Kaur, 2019).

### 1.6.1. Apparent molar isentropic compression

The experimental density and speed of sound data of solute in glyme-based aqueous solutions may be used to compute the apparent molar isentropic compression by employing the following equation:

$$K_{\phi,s} = \left[ (M\kappa_S/\rho) - \left\{ (\kappa_{S,0}\rho - \kappa_S\rho_0) / (m_A\rho\rho_0) \right\} \right]$$
 (1.23)

Here  $m_A$  denotes molality, M is the solute's molar mass,  $\rho$  is the density of solute and  $\rho_0$  is the density of solvent.  $\kappa_S$  is the isentropic compressibility of solution &  $\kappa_{S,0}$  is the isentropic compressibility of pure solvent. For the calculation of coefficient of isentropic compressibility ( $\kappa_S$ ), Laplace Newton's equation given below is used

$$\kappa_{\rm S} = 1 / (u^2 \rho) \tag{1.24}$$

where u refers to the speed of sound and  $\rho$  refers to solution's density.

### 1.6.2. Partial molar isentropic compression

The variation in the values of the apparent molar isentropic compression  $K_{\phi,s}$  due to molal concentration can be calculated by below-stated equation:

$$K_{\phi,s} = K_{\phi,s}^0 + S_K^* m_A \tag{1.25}$$

 $K_{\phi,s}^0$  is limiting molar isentropic compression,  $S_K^*$  refers to experimental slope representing (solute-solute) interactions,  $m_A$  is the molality of solute in solution. The negative values of  $K_{\phi,s}^0$  for a solute represents strong solute-solvent interactions while small  $S_K^*$  values states weaker solute-solute interactions.

# 1.6.3. Partial molar isentropic compression of transfer

To calculate partial molar isentropic compression of transfer  $\Delta K_{\phi,s}^0$  of lithium from water to solutions at infinite dilution following equation has been used:

$$\Delta K_{\phi,s}^0 = K_{\phi,s}$$
 (in aqueous glyme solution) -  $K_{\phi,s}^0$  (in water) (1.26)

The values of  $\Delta K_{\phi,s}^0$  deduces the association of solvent molecules with solute molecules, which enhances the interactions among the ions.

### 1.6.4. Pair and triplet interaction coefficients

Friedman and Krishanan reviewed and refined a theory proposed by McMillan and Mayer to determine the interaction coefficients that indicate interactions among two and more than two solute molecules, respectively. (McMillan & Mayer, 1945) (Millero, Surdo, & Shin, 1978). Hence, partial molar volume of transfer can be represented as:

 $\Delta V_{\phi}^{0}$  (water to aqueous (DME/TEGDME) solution) = 2  $V_{AB} m_B + 3 V_{ABB} m_B^2$  (1.27) And partial molar isentropic compression of transfer is expressed as  $\Delta K_{\phi,s}^{0}$  (water to aqueous DME/TEGDME solution) = 2  $K_{AB} m_B + 3 K_{ABB} m_B^2$  (1.28) Where, A denotes solute, B denotes IL,  $m_B$  is molality of aqueous IL.  $V_{AB}$  and  $V_{ABB}$  for volume whereas  $K_{AB}$  and  $K_{ABB}$  for isentropic compression symbolizes pair and triplet interaction coefficients. Calculation of these constants were done using by fitting the  $\Delta V_{\phi}^0$  and  $\Delta K_{\phi,s}^0$  values to equation (1.25) and (1.26). The positive values of  $V_{AB}$  show the presence of pair wise interactions between solute and solvent.

### 1.7. Conductance Studies

The efficiency with which an electrolyte conducts electricity in solution is measured by its molar conductivity, which is the conducting power of all the ions created by dissolving one mole of the electrolyte in solution. It is denoted by symbol  $\Lambda_m$ 

$$\Lambda_m = \text{specific conductance} \times 1/c$$
 (1.29)

# 1.7.1. Specific conductance

The reciprocal of specific resistance which is defined as the resistance of the specimen having 1 m length and 1 m<sup>2</sup> cross-section is known as specific conductance. It can also be called as conductance of one metre cube of material. It is denoted by  $\kappa$ .

$$\kappa = 1/\rho = (1/a) \times \text{conductance}$$
 (1.30)

Here,  $\rho$  is specific resistance and (1/a) is called cell constant.

The relationship between molar conductivity and specific conductivity is given by

$$\Lambda_m = \kappa \times 1000 \text{ N} \tag{1.31}$$

Here, N is the normality of the solution.

Limiting molar conductivity can be calculated from Onsager relation

$$\Lambda_m = \Lambda_m^0 - S\sqrt{c} \tag{1.32}$$

# 1.8. Research Gap

From the survey of literature, it is evident that a lot of work has been conducted on thermophysical studies of several Lithium based electrolytes in number of organic solvents, but a little attention has been paid on glymes ie. Monoglyme and tetraglyme to explore their applications in Lithium- ion batteries. In the proposed study, Thermophysical and conductometric studies of various Lithium electrolytes with glymes will be done at various concentrations and results will be analyzed to propose the optimized parameters required to enhance the cell cyclabilities and efficiency of Lithium-ion batteries. In the proposed study we will try to determine the thermophysical and conductometric studies of aprotic Lithium electrolytes in aprotic organic solvents, glymes. A variety of salts have been used in rechargeable batteries. Owing to small size of Lithium ion, the energy density of Lithium-ion battery is higher. The intercalation of Lithium ions is also fast, so the Lithium-ion batteries are preferred over other rechargeable batteries. Glymes as solvents have a wide electrochemical window, excellent thermal and chemical stability, low toxicity, and low volatility.

In addition to the above stated properties, glymes have both hydrophilic and hydrophobic properties that other organic solvents do not exhibit.

The aims and objectives of the present investigations are:

- 1. To determine various thermo physical properties such as density and conductance of aprotic lithium electrolytes in binary aqueous mixtures of aprotic organic solvents at different concentrations and temperatures.
- 2. To calculate various thermophysical and acoustic parameters of the above solutions at different concentrations and temperatures.
- 3. To calculate various conductance parameters (specific conductance, limiting molar conductance and activation energy) of above-mentioned solutions.
- 4. Interpretation of above systems using spectroscopic and cyclic voltammetry (CV) techniques.

# **References:**

Anouti, M., Dougassa, Y. R., Tessier, C., El Ouatani, L., & Jacquemin, J. (2012). Low pressure carbon dioxide solubility in pure electrolyte solvents for lithium-ion batteries as a function of temperature. Measurement and prediction. *Journal of Chemical Thermodynamics*, 50, 71–79. https://doi.org/10.1016/j.jct.2012.01.027

Barthel, J., Bachhuber, K., Buchner, R., Gill, J. B., & Kleebauer, M. (1990). Dielectric spectra of some common solvents in the microwave region. Dipolar aprotic solvents and amides. *Chemical Physics Letters*, *167*(1–2), 62–66. https://doi.org/10.1016/0009-2614(90)85071-J

Chrétien, F., Jones, J., Damas, C., Lemordant, D., Willmann, P., & Anouti, M. (2014). Impact of Solid Electrolyte Interphase lithium salts on cycling ability of Li-ion battery: Beneficial effect of glymes additives. *Journal of Power Sources*, 248, 969–977. https://doi.org/10.1016/j.jpowsour.2013.09.092

Cox, B. G., Hedwig, G. R., Parker, A. J., & Watts, D. W. (1974). Solvation of ions. XIX. Thermodynamic properties for transfer of single ions between protic and dipolar aprotic solvents. *Australian Journal of Chemistry*, 27(3), 477–501. https://doi.org/10.1071/CH9740477

Davidson, W. R., & Kebarle, P. (1976). Ionic Solvation by Aprotic Solvents. Gas Phase Solvation of the Alkali Ions by Acetonitrile. *Journal of the American Chemical Society*, 98(20), 6125–6133. https://doi.org/10.1021/ja00436a010

Deng, D. (2015). Li-ion batteries: Basics, progress, and challenges. *Energy Science and Engineering*, *3*(5), 385–418. https://doi.org/10.1002/ese3.95

Di Lecce, D., Marangon, V., Jung, H. G., Tominaga, Y., Greenbaum, S., & Hassoun, J. (2022). Glyme-based electrolytes: Suitable solutions for next-generation lithium batteries. *Green Chemistry*, 24(3), 1021–1048. https://doi.org/10.1039/d1gc03996b

Díaz-González, F., Sumper, A., Gomis-Bellmunt, O., & Villafáfila-Robles, R. (2012). A review of energy storage technologies for wind power applications. *Renewable and Sustainable Energy Reviews*, *16*(4), 2154–2171.

https://doi.org/10.1016/j.rser.2012.01.029

Divya, K. C., & Østergaard, J. (2009). Battery energy storage technology for power systems-An overview. *Electric Power Systems Research*, 79(4), 511–520. https://doi.org/10.1016/j.epsr.2008.09.017

Feng, S., Huang, M., Lamb, J. R., Zhang, W., Tatara, R., Zhang, Y., Guang Zhu, Y., Perkinson, C. F., Johnson, J. A., & Shao-Horn, Y. (2019). Molecular Design of Stable Sulfamide- and Sulfonamide-Based Electrolytes for Aprotic Li-O2 Batteries. *Chem*, 5(10), 2630–2641. https://doi.org/10.1016/j.chempr.2019.07.003

Horwitz, G., Factorovich, M., Rodriguez, J., Laria, D., & Corti, H. R. (2018). Ionic Transport and Speciation of Lithium Salts in Glymes: Experimental and Theoretical Results for Electrolytes of Interest for Lithium-Air Batteries. *ACS Omega*, *3*(9), 11205–11215. https://doi.org/10.1021/acsomega.8b01443

Khan, I. A., Gnezdilov, O. I., Filippov, A., & Shah, F. U. (2021). Ion Transport and Electrochemical Properties of Fluorine-Free Lithium-Ion Battery Electrolytes Derived from Biomass. *ACS Sustainable Chemistry and Engineering*, *9*(23), 7769–7780. https://doi.org/10.1021/acssuschemeng.1c00939

Kim, J. I. (1978). Preferential solvation of single ions. A critical study of the Ph4AsPh4B assumption for single ion thermodynamics in amphiprotic and dipolar-aprotic solvents. *Journal of Physical Chemistry*, 82(2), 191–199. https://doi.org/10.1021/j100491a013

Kousksou, T., Bruel, P., Jamil, A., El Rhafiki, T., & Zeraouli, Y. (2014). Energy storage: Applications and challenges. *Solar Energy Materials and Solar Cells*, *120*(PART A), 59–80. https://doi.org/10.1016/j.solmat.2013.08.015

Laino, T., & Curioni, A. (2013). Chemical reactivity of aprotic electrolytes on a solid Li2O 2 surface: Screening solvents for Li-air batteries. *New Journal of Physics*, *15*. https://doi.org/10.1088/1367-2630/15/9/095009

Lombardo, L., Brutti, S., Navarra, M. A., Panero, S., & Reale, P. (2013). Mixtures of ionic liquid-Alkylcarbonates as electrolytes for safe lithium-ion batteries. *Journal of* 

Power Sources, 227, 8–14. https://doi.org/10.1016/j.jpowsour.2012.11.017

McDowall, J. (2006). Integrating energy storage with wind power in weak electricity grids. *Journal of Power Sources*, 162(2 SPEC. ISS.), 959–964. https://doi.org/10.1016/j.jpowsour.2005.06.034

Mclarnon, F. R., & Cairns, E. J. (1989). Lawrence Berkeley National Laboratory LBL Publications Title Energy Storage Permalink

https://escholarship.org/uc/item/7dt8q203 Publication Date.

https://escholarship.org/uc/item/7dt8q203

Morioka, Y., Narukawa, S., & Itou, T. (2001). State-of-the-art of alkaline rechargeable batteries. *Journal of Power Sources*, 100(1–2), 107–116. https://doi.org/10.1016/S0378-7753(01)00888-6

Mozhzhukhina, N., Longinotti, M. P., Corti, H. R., & Calvo, E. J. (2015). A conductivity study of preferential solvation of lithium ion in acetonitrile-dimethyl sulfoxide mixtures. *Electrochimica Acta*, *154*, 456–461.

https://doi.org/10.1016/j.electacta.2014.12.022

Nidhi, & Kaur, H. (2022). Advancement in field of Energy storage applications by using Ionic Liquids. *Journal of Physics: Conference Series*, 2267(1). https://doi.org/10.1088/1742-6596/2267/1/012043

Parker, A. J., & Alexander, R. (1968). Solvation of Ions. XIII. Solvent Activity Coefficients of Ions in Protic and Dipolar Aprotic Solvents. A Comparison of Extrathermodynamic Assumptions. *Journal of the American Chemical Society*, 90(13), 3313–3319. https://doi.org/10.1021/ja01015a003

Patil, R. A., Talebi, M., Xu, C., Bhawal, S. S., & Armstrong, D. W. (2016). Synthesis of Thermally Stable Geminal Dicationic Ionic Liquids and Related Ionic Compounds: An Examination of Physicochemical Properties by Structural Modification. *Chemistry of Materials*, 28(12), 4315–4323. https://doi.org/10.1021/acs.chemmater.6b01247

Pigłowska, M., Kurc, B., Galiński, M., Fuć, P., Kamińska, M., Szymlet, N., & Daszkiewicz, P. (2021). Challenges for safe electrolytes applied in lithium-ion cells—

a review. *Materials*, 14(22), 1–52. https://doi.org/10.3390/ma14226783

Ray, P., Vogl, T., Balducci, A., & Kirchner, B. (2017). Structural Investigations on Lithium-Doped Protic and Aprotic Ionic Liquids. *Journal of Physical Chemistry B*, 121(20), 5279–5292. https://doi.org/10.1021/acs.jpcb.7b02636

RC, N. T. A. K. H.; F. I. K. A. T. (2018). Recent progress in the application of electrochemically rechargeable metal-air batteries: A focus review. *AIP Conf. Proc.*, 41(5), 28–34. http://rykj.cbpt.cnki.net

Sharma, C., & Thakur, R. C. (2022). Potential solvents and electrolytes for energy storage applications: A Review. *Journal of Physics: Conference Series*, 2267(1). https://doi.org/10.1088/1742-6596/2267/1/012051

Shi, C., Quiroz-Guzman, M., DeSilva, A., & Brennecke, J. F. (2013). Physicochemical and Electrochemical Properties of Ionic Liquids Containing Aprotic Heterocyclic Anions Doped With Lithium Salts. *Journal of The Electrochemical Society*, *160*(9), A1604–A1610. https://doi.org/10.1149/2.116309jes

Vraneš, M., Cvjetićanin, N., Papović, S., Šarac, B., Prislan, I., Megušar, P., Gadžurić, S., & Bešter-Rogač, M. (2017). Electrical, electrochemical and thermal properties of the ionic liquid + lactone binary mixtures as the potential electrolytes for lithium-ion batteries. *Journal of Molecular Liquids*, 243, 52–60.

https://doi.org/10.1016/j.molliq.2017.07.129

Watanabe, M., Thomas, M. L., Zhang, S., Ueno, K., Yasuda, T., & Dokko, K. (2017). Application of Ionic Liquids to Energy Storage and Conversion Materials and Devices. *Chemical Reviews*, *117*(10), 7190–7239.

https://doi.org/10.1021/acs.chemrev.6b00504

Wei, S., Inoue, S., Di Lecce, D., Li, Z., Tominaga, Y., & Hassoun, J. (2020). Towards a High-Performance Lithium-Metal Battery with Glyme Solution and an Olivine Cathode. *ChemElectroChem*, 7(11), 2344. https://doi.org/10.1002/celc.202000554

Xu, K. (2004). Nonaqueous liquid electrolytes for lithium-based rechargeable batteries. *Chemical Reviews*, *104*(10), 4303–4417. https://doi.org/10.1021/cr030203g

Younesi, R., Veith, G. M., Johansson, P., Edström, K., & Vegge, T. (2015). Lithium salts for advanced lithium batteries: Li-metal, Li-O2, and Li-S. *Energy and Environmental Science*, 8(7), 1905–1922. https://doi.org/10.1039/c5ee01215e

Zhenzhen Wu, Yuhui Tian, Hao Chen, Liguang Wang, Shangshu Qian, Tianpin Wu, S. Z. and J. L. (2022). Evolving aprotic Li–air batteries. *Chemical Society Reviews*, *51*, 8045–8101. https://doi.org/https://doi.org/10.1039/D2CS00003B

# Chapter 2 Review of Literature

### 2. Review of Literature

Globally, wind and solar energy are expanding rapidly, but when applied extensively, their evolving characteristics provide technological and financial difficulties. Energy storage devices would solve these issues. (Beaudin et al., 2010) examined the installation challenges, technological advancements, and condition of electrical energy storage (EES) systems for the integration of variable renewable energy resources (VRES) on a wide scale. It shows that each task from VRES needs different features in EES, and no single EES technology always works better than the others for different uses. Outside factors, like the supply of minerals and geography, can impact the successful wide use of EES technologies. Flywheels, capacitors, and batteries are the best options for handling changes in variable renewable energy sources, ensuring good power quality and keeping the grid stable. Capacitors, vanadium redox batteries, superconducting magnetic energy storage, flywheels and sodium-sulfur batteries are suitable for managing distributed VRES. The influence of supply constraints on the long-term growth of some EES may be either good or detrimental. (McDowall, 2006) describes the application of battery-based energy storage with a runtime of several minutes for wind generation stabilization in fragile electrical grids is covered in this study. This enables wind power to be widely used, replacing other generation methods and bridging to other power sources as needed. Thus, recommending lithium-ion batteries for the long run and nickel-cadmium batteries for the short to medium term.

The lithium-sulfur battery (Li-S) is a future-forward energy storage technology with high energy density, but its aprotic electrochemistry faces difficulties due to the complex solid-liquid-solid conversion process. (Hu *et al.*, 2020) have aimed to strengthen the electrochemical reaction in Li-S batteries by carefully designing the materials and structures used in the cathodes. It is still fully not understood that how these processes work and how they affect performance. Improvements in Li-S batteries focus on designing better materials, improving the layout of the cathode, and enhancing the electrolyte. It's important to understand how soluble Li-S species behave at reactive surfaces. There is a need to create new models and methods to study this in real-time,

which will help in figuring out how Li-S reacts and how lithium polysulfides (LiPSs) interact with the materials.

In view to this, the University of Ferrara and Tokyo University of Agriculture and Technology have created a small reusable battery that uses powerful metallic lithium (Wei et al., 2020). The solution, which uses glyme and LiNO<sub>3</sub> allows for good movement of ions, has a wide range of stability for electrical use, supports protective layers on the anode, and shows compatible behaviour between LiFePO<sub>4</sub> and the electrolyte. The Li/LiFePO<sub>4</sub> cells demonstrated a capacity of 140-150 mAh for the cathode. They work well with currents between 5 C and 1 C, keeping more than 70% of their capacity after 500 cycles, and they have a coulombic efficiency close to 100%. Similarly, (Ghalami-Choobar & Fallahkar, 2019) demonstrate how ethylene carbonate (EC) affects the optical, thermodynamic and transport properties of water-based 1ethyl-3-methylimidazolium bromide (EMImBr) solutions at various temperatures and pressures. They measured electrical conductance, activity coefficients & refractive indices of the ionic liquid [EMIm]Br in various mass fractions of EC in water-EC mixes. The changes in the refractive index from mixing were calculated using data and linked together with the Redlich-Kister and Cibulka formulae. The findings indicated that the ion-pairing process happens on its own, absorbs heat, and is driven by changes in disorder.

Likewise, (Chrétien *et al.*, 2014) focused on how these salts influence the cycle performance of graphite & LiNi<sub>1/3</sub>Mn<sub>1/3</sub>Co<sub>1/3</sub>O<sub>2</sub> (NMC) electrodes in both half-cell and full-cell battery setups and could be used to enhance the battery system. The results indicate that both LiOH and Li<sub>2</sub>O have a detrimental effect on the formation of the SEI layer, and that NMC reacts more strongly to added salt than graphite. Li<sub>2</sub>CO<sub>3</sub>, LiOCH<sub>3</sub>, and LiOC<sub>2</sub>H<sub>5</sub> help create a polymer layer on the SEI, which is useful. The amount of LiF in the SEI mostly relies on how much of it is present. They have also used methods like cyclic voltammetry, charge-discharge tests, & electrochemical impedance spectroscopy to study this. The results indicated that the length of the glyme (useful additives for electrolytes) chain is important in how it forms complexes, and this process is influenced by the type and amount of lithium salt used. Similarly, (Vraneš *et* 

al., 2017) investigated four mixes of 1-butyl-3-methylimidazolium bis(trifluoromethylsulfonyl)imide ionic liquid ([bmim][NTf2]) and certain lactones conduct electricity. The study found that the electrical conductivity of two-component mixtures decreases in the following order: {[bmim][NTf<sub>2</sub>] + GBL}, {[bmim][NTf<sub>2</sub>] + BBL $\}$ , {[bmim][NTf<sub>2</sub>] + GVL $\}$ , {[bmim][NTf<sub>2</sub>] + DVL $\}$ , and {[bmim][NTf<sub>2</sub>] + ECL $\}$ . This corelates with the trend of increasing thickening (viscosity) of the mixtures. The systems with 6 or 7-member lactone rings showed the best safety features. The electrochemical stability window for the most stable mixture i.e. for {[bmim][NTf<sub>2</sub>] + GBL} when exposed to normal air conditions is about 4.5 V (Sharma & Thakur, 2022). A recent smart and systematic approach by (X. Chen & Zhang, 2020) to design electrolytes, based on a strong understanding of how different ingredients combine and how they affect battery performance, is likely to speed up the progress of new lithium batteries. Their recent efforts have focused on studying the basic interactions in lithium battery solutions at the atomic level. This includes looking at how cations interact with solvents, anions, and other solvents.

There is also the crucial role of protic ionic liquids (PILs) which demonstrates exceptional qualities for use in lithium-ion batteries (LIBs), with some performing even better than aprotic ionic liquids (AILs). This study by (Nasrabadi & Ganesan, 2019) investigated the use of molecular dynamics simulations to examine how well PIL and AIL electrolytes performed in LIBs. In this study, the PIL and AIL electrolytes were doped with LiTFSI. Three main changes were seen when Li salt was added to IL solutions: (1) hard Li-TFSI complexes formed, (2) coordination between cations and anions increased, and (3) Li aggregates were created. As the amount of lithium salt rose, the density and thickness of the electrolytes grew. At the same time, the movement of ions, the ability to conduct electricity, and the level of ionic character decreased. The conductivity of lithium (Li) reaches its highest point when the lithium salt content is at 0.2. This is because the increase in lithium salt is balanced by higher viscosity. The PIL electrolyte has better lithium conductivity and transport qualities compared to the AIL electrolyte. In support to this phenomenon, a study by (Horwitz et al., 2020) tested lithium-air batteries using gold electrodes with two types of glyme-based electrolytes: diglyme (DG) and tetraglyme (TEGDME). The results showed that TEGDME is not

stable and breaks down at voltages between 3.6 and 3.9 V compared to lithium, even in the absence of oxygen and lithium ions. DG is more stable and only breaks down at 4.0 V compared to Li<sup>+</sup>/Li when oxygen is present. Adding water to the DG-based solution makes it break down more quickly, likely because it creates a type of oxygen called singlet oxygen. (Rivki *et al.*, n.d.) discussed the different type of electrolyte solution for lithium batteries, which is made by mixing LiX salts with glyme solvents. These fluids have benefits like being safe from catching fire, stable, non-toxic, good for the environment, effective in cells, and cost-efficient. They are especially important for long-chain glymes that are very safe and have low toxicity. They looked at the possibilities, benefits, and uses of glyme-based fluids in new energy storage systems, especially in high-energy batteries and other types of batteries.

It has been observed from the discussed literature that the different lithium salts for glyme-based fluids have shown good properties in cell designs that use insertion or conversion methods. The qualities of the electrolyte can differ in a Solid-state Ionic Liquid (SIL) compared to a regular electrolyte. This depends on the salt's concentration and type, as well as the length of the glyme chain. The stability of the [Li(Gn)]<sup>+</sup> complex can be understood by looking at the ratio of the self-diffusion rates of glyme and the Li<sup>+</sup> ion (DG/DLi). For instance, adding LiNO<sub>3</sub> to the glyme-based electrolyte helps protect the lithium-metal anode from problematic reactions caused by the breakdown of polysulfides. The electrolyte mixture affects how Li-O<sub>2</sub> works and the shape of the Li<sub>2</sub>O<sub>2</sub> product formed, which in turn impacts how well the cell performs. Similarly, glycol ethers and diglyme could be good solvents for lithium-air batteries because they stay stable in the presence of superoxide radicals. Diglyme has a low donor number, but it helps create Li<sub>2</sub>O<sub>2</sub> during discharge reactions, resulting in big deposits and high capacities. It's important to understand how lithium salts behave and move in these solvents to improve battery performance. This study looked at lithium trifluoromethanesulfonate (LiTf) and lithium bis(trifluoromethanesulfonyl)imide (LiTFSI) in two solvents: 1,2-dimethoxyethane (DME) and diglyme. In a research, (Horwitz et al., 2018) found consistent results for how ion pairs and triplet ions form. The LiTf/DME system was identified as the best option for encouraging the formation of large Li<sub>2</sub>O<sub>2</sub> masses. Molecular dynamics simulations helped explain these differences. The measured Li<sup>+</sup> movement, based on the fractional Walden rule, matched well with results from the simulations. The study showed that having lower conductivity in concentrated solutions doesn't always mean there is a better connection between particles, because the thickness of the solvent affects conductivity in these concentrated areas. The another review which looks at how high-temperature, intermediate-temperature, and room-temperature sodium-sulfur (Na/S) batteries work. (Li et al., 2019) talks about the important parts (positive electrodes, chemicals, separators) that affect the working of Na/S batteries. The goal was to enhance sulfur conductivity and stop shuttle effects. Although they can increase sulfur usage, carbonbased mesoporous positive electrode hosts are not cycle stable. Future studies should look into using carbon materials combined with metal chemicals to stop capacity loss. Materials similar to sulfur, like MoS<sub>3</sub>, can also be used for sodium-sulfur (Na/S) batteries. (Syali et al., 2020) also discussed some improvements in the mixtures used for room temperature sodium-sulfur (RT Na-S) batteries. It emphasizes how these batteries could be useful for storing energy in power grids and in electric cars. It explains how ionic solutions and additives can enhance electrochemical performance, the problems with solid electrolytes, and the benefits of gel polymer electrolytes. The review also points out the need for cheap, eco-friendly materials that carry sodium well, have strong stability in electricity, and do not allow for shuttle effects. Solid state electrolytes have been created to improve safety, provide good ionic exchange, and resist high temperatures. Future study should aim to create better polymer and gelpolymer electrolytes to enhance discharge capacity and performance.

(Anouti *et al.*, 2012) investigates the solubility of CO<sub>2</sub> in pure electrolyte solvents for Li-ion batteries, including methyl propionate, propylene carbonate, ethyl methyl carbonate, c-butyrolactone, diethyl carbonate, dimethyl carbonate, ethyl acetate, and ethylene carbonate. The solubility data was compared with literature, COSMO-RS methods, and the Peng–Robinson equation of state. The results indicate that linear carbonates dissolve more CO<sub>2</sub> than cyclic ones, with the best solubility found in MP and EA solvents. The study also measures important thermodynamic properties related to dissolving, such as enthalpy, Gibbs free energy, entropy, as well as the mixing energy of the solvent with CO<sub>2</sub> when it is in a theoretical liquid form. The results show that

these tools can help check how well substances dissolve in pure electrolyte solutions for Li-ion batteries, showing both salting-out and salting-in effects. The study's results can help create better ways to predict how well substances dissolve in pure electrolyte solutions for Li-ion batteries. (Aravindan *et al.*, 2011) discussed the utilization of lithium salts in electrolyte solutions for lithium rechargeable batteries. It shows how lithium salts are important for conducting electricity, forming solid-electrolyte surfaces, and how they affect aluminium current collectors. New lithium salts like fluoroalkylphosphate (LiFAP), oxalyldifluoroborate (LiODFB), and bis(oxalato)borate (LiBOB) are discussed. The text includes how they are made and their possible uses in future lithium-ion batteries. The paper emphasizes the need to further study Li-ion cells and high-voltage cathode materials. The paper also points out that mixed salt solutions like LiFAP/LiPF<sub>6</sub>, LiBOB/LiPF<sub>6</sub>, and LiBF<sub>4</sub>/LiODFB could be good choices for environmentally friendly electrolytes.

Lithium-ion batteries are a potential way to store energy for phones and electric cars. They have made consistent progress in energy and power density, and prices have gone down. There are still questions about how to improve performance and make energy storage more practical. To improve the negative electrode, (Armand et al., 2020) describes the way to increase the amount of silicon in mixtures with carbon materials and make the design of the electrode better. To improve the positive electrode, it is crucial to increase the nickel content in typical layered Li-transition metal oxides and to focus on safety and stability. Better ways to prepare electrodes will help increase energy and power output. Recycling efficiency is different for various parts of a lithiumion battery. Lithium is difficult to recover, while about 80% of cobalt can be recycled. There is a need to make sustainability better in several areas: using materials that can and cannot act electrochemically, how these materials are made and processed, covering the electrodes, and increasing their lifespan. To investigate more, (Arya & Sharma, 2017) presented the history, benefits, and uses of polymer electrolyte systems in storing and converting energy. They discussed liquid, gel, and solid polymer electrolyte systems, looking at their pros and disadvantages. The piece looks at how the host polymer matrix works, how to choose the right host polymer, and the use of salt, inorganic fillers or clay, and aprotic solvents. It also discusses different methods for making polymer electrolyte films. (Barthel et al., 1990) discussed the permittivity characteristics of amides, dipolar aprotic liquids, and dimethylacetamides between frequencies of 0.95 and 89 GHz. Amides show non-simple dielectric relaxation, which involves two or three types of relaxation processes similar to Debye behavior. The differences in permittivity values for dipolar aprotic liquids like DMF and DMA are less than 0.5%. The study indicates that using one uneven relaxation time distribution (CD) is a better fit than two Debye processes for propylene carbonate. The work also explores the influence of hydrogen bonding on amide structure and dynamics. Farinfrared data down to 5 cm-' (150 GHz) is provided for NMF and DMF, enabling a thorough analysis of their dielectric properties across a wide range of frequencies. All liquids show non-Debye dielectric behavior, with departures from Debye behavior on the high-frequency side. (Boisset et al., 2013) looks at three novel Deep Eutectic Solvents (DESs) derived from N-methyl acetamide and a Li-salt (LiX) in terms of their physical and electrochemical characteristics. DESs are liquids at room temperature when the amount of lithium salt is between 10% and 35%. Their electrochemical stability windows on Pt are wide, ranging from 4.7 to 5 V and they show passivating behaviour towards the aluminium collector. Using each selected DES as an electrolyte and LiFePO<sub>4</sub> (LFP) material as a cathode, a test cell was built and tested at 25°C, 60°C, and 80°C. With a capacity of up to 160 mAh g<sup>-1</sup> and 99% efficiency at 60°C, the results show that both DES and LFP electrode materials are compatible. Using DESs may help make LIBs safer and better for the earth.

(Coadou *et al.*, 2013) looks at how well two types of ionic liquids, one called protic (PIL) and the other aprotic (AIL), work as electrolytes for supercapacitors. The specific liquids compared are [HN<sub>111</sub>][TFSI] for the protic type and [S<sub>111</sub>][TFSI] for the aprotic type. The electrolytes were tried at 25 and -30°C using activated carbon as the electrode material. No major changes were observed in electrochemical performance whether a labile proton was present or not.  $\gamma$ -BL-based electrolytes performed well, providing specific capacitances of up to 131 and 80 F·g<sup>-1</sup>, even in low temperatures. They could make eco-friendly electrolytes for energy storage that work well even in cold conditions. The study also examined the electrochemical performance of six electrolytes based on [S<sub>111</sub>][TFSI] and [HN<sub>111</sub>][TFSI] mixed with ACN, PC, and  $\gamma$ -BL.

Similarly, (Zhao et al., 2021) developed zinc-nickel batteries (ZNB) which are intrinsically safe too with 20 Ah and 75 Ah capacities. The ZNB stacks performed better and had more energy stored in both mass and volume compared to Lead acid battery stacks. They were used to provide power in electric bikes, hybrid cars, solar power setups, and 10 kWh ZNB energy storage systems. These ZNB stacks were discovered to be more cost-effective for building and running energy storage systems when used at high discharge rates. The 24 V ZNB battery can be used in business. It worked steadily for 25 days, even after being charged and discharged multiple times. The ZNB stacks can be used for energy storage. They work well in solar power systems and can keep running in a 10 kWh energy storage setup. Although ZNBs are expensive to build, they have great potential as advanced devices for energy storage, particularly for uses that require high energy output. (Cox et al., 1974) looks at the energy, heat, and disorder of certain chemicals in different liquids, starting with water. It explains that changes in heat energy affect how anions behave when they move from protic to dipolar aprotic liquids. When anions and cations move from water to non-water media, there is a significant decrease in entropy. When cations move from water to liquids, it releases heat (exothermic). But for many anions, this process absorbs heat (endothermic). Factors influencing the enthalpy of solvation (AHtr(ion)) include born-type ion-dipole electrostatic interactions, specific interactions between ions and solvents, breaking of solvent-solvent hydrogen bonds, mutual polarizability or dispersion forces, formation of hydrogen bonds between waters, & strengthening hydrogen bonds in a surface around a hydrophobic ion (Daniel, 2008).

(Davidson & Kebarle, 1976) focused on the ion equilibria in the gas phase for  $Na^+$ ,  $K^+$ ,  $Rb^+$ , and  $Cs^+$  for n=1 to 5. The way temperature affects the equilibrium values K,  $\Gamma$  was used to assess the systems mentioned above. Compared to negative ions, positive ions have substantially larger initial interactions (low n). Acetonitrile's poor interaction with negative ions results from the dipole's positive pole being dispersed widely throughout the molecule's C and H atoms. As the value of n increases, the difference in how positive and negative ions interact with acetonitrile becomes smaller. The study measures the total energy needed to stabilize an ion, including the energy from the fixed dipole of the solvent molecule and the energy from the induced dipole

interaction with the ion. Acetonitrile binds more strongly to alkali ions than water does because it has a much higher dipole moment. The study looks at how acetonitrile (A) interacts compared to water (W) molecules. The results indicate that as n increases, the interactions will become similar. The interactions between positive and negative ions of the same size will be the same (Deng, 2015).

(Díaz-González et al., 2012) looks at different energy storage technologies used for wind power. It explains how they work, their features, and where they can be used. It talks about how fast energy changes can help systems like SMES, flywheels, and supercapacitors make wind farms work better and reduce changes in voltage and frequency. Choosing the right position and size for short-term storage technologies is important for them to work well. The layout of the wind farm, the types of wind turbines, and the control methods used all effect how the system works and is designed. Energy storage support improves system stability under perturbations, such as oscillation damping issues and LVRT capability. Isolated and hybrid systems with a lot of wind power can work better now because their output can be predicted more accurately and provide a steady flow of energy. The success of energy storage system (ESS) projects depends on their economic feasibility. Hydrogen storage technologies show promise but struggle with high prices and low energy efficiency. To make sure long-term storage technologies are used properly, ESS providers need effective management strategies and financial support. The goal is to make energy storage systems affordable for use in fixed installations, which will help increase the use of green energy in the power grid. Thus, understanding reaction processes and creating effective materials for aprotic Li-O<sub>2</sub> batteries at the atomic scale have been made possible by using DFT and molecular dynamic (MD) simulations. Li<sub>2</sub>O<sub>2</sub> is the best product that comes from charging and discharging in non-water-based Li-O<sub>2</sub> batteries. However, its insulation and insoluble properties can lower the battery's performance.

To change how Li<sub>2</sub>O<sub>2</sub> insulates, (Ding *et al.*, 2021) added defects like empty spaces (vacancies), impurities (dopants), charged particles (polarons), surface conductance, grain borders, and a non-crystalline form (amorphous Li<sub>2</sub>O<sub>2</sub>). The growth of Li<sub>2</sub>O<sub>2</sub> in Li–O<sub>2</sub> batteries can happen in two ways: on the surface of the cathode or in

the solution. This depends on how LiO<sub>2</sub> interacts with the cathode surface and the electrolyte. Electrolyte has a critical function in influencing cycle performance and discharge capacity. To understand the development process of Li<sub>2</sub>O<sub>2</sub> and create effective electrolytes for Li–O<sub>2</sub> batteries, the solvation free energy and ionic association strength of Li–O species in electrolytes have been calculated using DFT calculations and MD simulations. Future research should focus on investigating mass transport kinetics of O<sub>2</sub> and Li<sup>+</sup> in the battery system, constructing an actual environmental model, studying Li<sub>2</sub>O<sub>2</sub> growth in more detail, and conducting more experiments to verify theoretical simulations and develop predictive tools.

Because Li-ion batteries offer better energy and power densities and a longer lifespan, they might be the main energy storage component of off-grid renewable energy. For full adoption, prices will probably need to drop because of large-scale production. The growth of the electric car industry might encourage the use of Li-ion batteries in renewable energy, making these batteries cheaper. Li-ion batteries are better for the earth than lead-acid batteries because they need more common materials and can be recycled. Changing more than 1 billion cars to electric vehicles or plug-in hybrids that use 15-kWh batteries. Li-ion batteries could use as much as 30% of the world's known lithium supplies. Lithium can also come from other sources like sea water, and some of it can be produced by recycling. Lithium battery technology needs to reduce its carbon impact, which is currently around 70 kg of CO<sub>2</sub> for every kilowatthour. (Diouf & Pode, 2015)

The Peukert relationship explained by (Omar *et al.*, 2013), was created in 1897 for lead-acid batteries, doesn't work well for lithium-ion batteries because they have a narrow range of current and a consistent operating temperature. A new way has been created to clearly explain how much energy lithium-ion batteries can provide when conditions change. This new relationship, based on thorough experiments, can be used in battery math models. (Zhang *et al.*, 2023). Due to the large number of correlations and the intricacy of the calculation, the modified Peukert relationship is more challenging to apply since the Peukert constant depends on several relationships (Farret & Simões, 2006).

(Feng et al., 2019) looks into creating small molecules made from sulfamide and sulfonamide that can dissolve a lot of lithium salts and stay stable even in tough chemical and electrical conditions found in non-water Li-O<sub>2</sub> batteries. Three chemicals N-butyl-N, $N_0$ , $N_0$ -trimethylsulfamide (BTMSA), N,N-dimethyltrifluoromethanesulfonamide (DMCF3SA), and N-butyl-N-methyltrifluoromethanesulfonamide (BMCF<sub>3</sub>SA) - are promising for use in aprotic Li-O<sub>2</sub> batteries. These electrolyte components were made without weak C–H bonds, parts that can easily react with nucleophiles, and strong electron-donating groups that can be easily oxidized in electrochemical reactions. The study also explores the chemical and electrochemical stability of electrolytes containing 0.2 M LiTFSI in BTMSA, DMCF<sub>3</sub>SA, and BMCF<sub>3</sub>SA. The electrolytes were tested like they would be in lithiumoxygen batteries. It was discovered that the amounts of BTMSA, BMCF<sub>3</sub>SA, and DMCF<sub>3</sub>SA remained steady when exposed to 10 times the amount of Li<sub>2</sub>O<sub>2</sub> and KO<sub>2</sub> powders during chemical stability tests. The electrolytes showed superior stability under prolonged galvanostatic cycling tests. In short, these molecules are more stable in chemical and electrical terms in non-water-based Li-O2 batteries. This is probably because they limit how easily the byproducts from reactions dissolve, thanks to low electrolyte DNs. (Fletcher et al., 2018) demonstrated the use of ternary mixtures of sulfolane, 3-methyl sulfolane, and quaternary ammonium salts as low-cost alternatives for supercapacitor electrolytes. Sulfolane is selected because it has a strong ability to dissolve substances and a significant dipole moment, but its high freezing point is an issue. Researchers used a special mixture to lower the freezing point and improve the electrical conductivity of the liquid. The study showed that mixing a 60/40 combination with BTM-TFSI raised the solution's conductivity from 2.1 mS cm<sup>-1</sup> to 5.0 mS cm<sup>-1</sup>. The experts explain that the increase in capacitance with temperature is due to a variety of RC time constants in activated carbon electrodes.

As investigated, lithium oxygen batteries have the potential to revolutionize energy storage technology, but face hurdles like low efficiency and poor cycling stability. The catalytic cathode is a breakthrough point, but the electrolyte stability needs improvement (Guo *et al.*, 2017). Lithium metal electrodes have issues that make it hard to use them commercially. This is because they create lithium dendrites and have

low efficiency in storing charge. Future efforts should aim at creating catalysts that can perform two functions, improving the design of porous cathodes, and finding affordable materials. Carbon-based products are also appealing because they are stable (Hall & Bain, 2008). In an experiment, Lithium bis(fluorosulfonyl)imide (LiFSI) has been researched as a salt that helps conduct electricity in lithium-ion batteries. It melts at 145°C and stays solid up to 200°C. LiFSI is more stable against breaking down in water compared to LiPF<sub>6</sub>. It outperforms LiPF<sub>6</sub> in both Li/LiCoO<sub>2</sub> & graphite/LiCoO<sub>2</sub> cells with high purity (Han et al., 2011). LiFSI-based electrolytes don't dissolve aluminium at high potential, but adding small amounts of LiCl can cause aluminium to corrode. LiFSI beats LiPF<sub>6</sub> in Li/LiCoO<sub>2</sub> & graphite/LiCoO<sub>2</sub> cells under similar conditions. For the last 30 years, research on electrolytes has been working on creating and studying new Lithium salts. LiPF<sub>6</sub> is the main salt used in lithium battery electrolytes explained by (Henderson, 2014), but new electrodes and battery types have created a demand for new electrolyte mixtures. Selective fluorination decreases anion-Li<sup>+</sup> cation interactions, improving conductivity and anodic stability. Sometimes, stable salt can be a problem, so salt chemicals are used to enhance battery performance (Kalhoff et al., 2015).

(Kawakami *et al.*, 2010) discusses the creation of the biggest system for steady output using 34 MW sodium sulfur batteries at a 51 MW wind farm in Futamata, Japan. The system uses constant-output control to control the output power of the common coupling point to a planned number. Verification tests took place from 2008 to 2009, with a control error of ±2% for the agreed production capacity of 40MW. The 34MW NAS battery can provide steady power control. Similarly, (Khan *et al.*, 2021) introduces a new way to create electrolytes without fluorine for Li-ion batteries. By mixing lithium furan-2-carboxylate salt with tetra(n-butyl)-phosphonium furan-2-carboxylate IL in different molar ratios, the electrolytes are created. These electrolytes' anion is derived from plant and agricultural waste, which is a big step towards creating renewable electrolytes for batteries. The solutions have good thermal stability, decent ionic conductivity, and stable electrochemical performance at temperatures between 293 and 353 K. The study emphasizes the need to create safe, affordable, environmentally friendly, and long-lasting electrolytes for Li-ion batteries that do not contain fluorine. These electrolytes should be steady in heat and electricity to solve issues related to

safety, recycling, and cost. A study by (J. I. Kim, 1978) has confirmed that the Ph<sub>4</sub>AsPh<sub>4</sub>B electrolyte equally shares standard free energies of transfer between the cation and anion. The study applies Buckingham theory to determine the electrostatic components of standard free energies. It also uses experimental values for AfGo(Ph<sub>4</sub>Ge) and AfGo(Ph<sub>4</sub>C) to substitute for the non-electrostatic parts. The findings show that the energy input and the experimental values of Af Go(Ph<sub>4</sub>AsPh<sub>4</sub>B) in various organic solvents coincide rather well (T. Kim *et al.*, 2019). The study also investigates the molecular size of Ph<sub>4</sub>Ge, Ph<sub>4</sub>As<sup>+</sup>, and Ph<sub>4</sub>C in organic solvents, finding that the standard cation and anion are not equal in their molecular volumes (Kousksou *et al.*, 2014).

An efficient method for screening various solvents according to their chemical stability against Li<sub>2</sub>O<sub>2</sub> solid particles is presented in this work. Acetonitrile, pivalonitrile, dimethyl sulphoxide, N-methyl2-pyrrolidone, penta-ethylene glycol (PEG-5), and a fluorinated derivative are among the aprotic solvents whose minimal energy paths for several reactions with solid Li<sub>2</sub>O<sub>2</sub> are calculated and published by (Laino & Curioni, 2013). These data are used to derive reaction energy barriers, which show good agreement with experimental data and provide a practical method for testing and developing Li-air battery solvents based on first-principal calculations. Our knowledge of solvent stability in Li-air batteries was improved by the study, which also suggested a few chemical structures that might alter some chemical and physical characteristics while precisely adjusting other ones (May *et al.*, 2018).

With an emphasis on the aprotic electrolyte, which is frequently weak and has poor thermal stability, this study investigates the fire safety of lithium-ion batteries. (Adolph, 2016) employed graphite as a negative electrode and sulfolane as an aprotic solvent to examine the stability, cyclability, and performance of the aprotic electrolyte. A suitable negative electrode material for LiB was discovered to be lithium titanate oxide (LTO). The graphite material lost most of its potential capacity, according to the results, whereas the LTO material with the spinel intercalation structure did not decompose. Similarly, to boost energy efficiency and lower the use of non-renewable liquid fuel, novel materials and chemistry for LIBs have been created by (Väyrynen &

Salminen, 2012). Using an ionic liquid (IL), a lithium salt, and alkylcarbonate electrolytes, researchers have created novel electrolytes for Li-ion batteries. N-butyl-N-methylpyrrolidinium bis(trifluoromethanesulfonyl)imide (Py<sub>14</sub>TFSI) has been added to commercial carbonate-based electrolytes to enhance their electrochemical characteristics. After preparing and characterizing four new electrolyte compositions, LP<sub>30</sub>/Py14TFSI 70/30 wt/wt was found to be the best-performing electrolyte (Lombardo *et al.*, 2013). When exposed to a free flame, these electrolytes exhibit enhanced electrochemical stability windows, a significant decrease in self-extinguish time, and conductivity values that are comparable to those of pure carbonate-based electrolyte solutions (Manthiram, 2017).

The safety of LIBs in electric cars is covered in this paper by (Pigłowska et al., 2021), with particular attention to the different electrolytes that are employed. The authors talk on the global trend toward green chemistry and the usage of hydrogen as a fuel cell source. Emergency response, detection and reliability, standards and regulations, ignition and propagation, transportation, and end-of-life are the five primary safety issues with LIBs. Safety can be increased by non-flammable electrolytes such tetrafluoroborate, bis(trifluoromethylsulfonyl)imide anion, and bis(oxalate)borate cation. Likewise, the demand for alkaline rechargeable batteries, like Ni-Cd and Ni-MH, is growing because of their excellent power and affordability. Ni-Cd batteries have become more and more common as power sources for portable information and communication devices since they were first made available for purchase in 1990. In this article, (Morioka et al., 2001) explained the energy density of electrodes, which has increased to 91 Wh/kg and 340 Wh/l due to advancements in electrode materials and components. The environmental benefits of Ni-Cd batteries are their high-power output, quick charging, affordability, and long lifespan. Despite the introduction of Li-ion and rechargeable batteries, they are anticipated to hold onto their market share. Both common and specialized applications are the focus of R&D, with impressive advancements anticipated.

LiPF<sub>6</sub>'s electrical mobility in acetonitrile–dimethyl sulfoxide (CAN–DMSO) mixtures; a possible electrolyte in lithium-air batteries was investigated in this work by

(Mozhzhukhina et al., 2015). To find the salt's association constant and infinite dilution molar conductivity, the researchers employed a precise conductance technique. Tetrabutylammonium hexafluorophosphate's (TBAPF<sub>6</sub>) electrical conductivity was also measured. The results show that the curvature of LiPF6's molar conductivity composition dependency for ACN molar fraction (Xacn) 0.95 is qualitatively different from that of TBAPF<sub>6</sub>. In order to comprehensively evaluate the effects of lithium salts on Li-O<sub>2</sub> battery performance and the stability of salt anions in the O<sub>2</sub> environment during discharge/charge cycles, seven common lithium salts in tetraglyme were studied as battery electrolytes by (Nasybulin et al., 2013). Nuclear magnetic resonance spectroscopy, X-ray photoelectron spectroscopy, & X-ray diffraction were used to examine the discharge products. The findings demonstrated that the electrolyte's salt content had a significant impact on Li-O<sub>2</sub> batteries' performance. When lithium bis(oxalato)borate (LiBOB) and lithium tetrafluoroborate (LiBF<sub>4</sub>) broke down during discharge, they produced Li oxalate and LiF respectively, along with lithium borates. Optimal stability during the discharge procedure was demonstrated by other salts, including LiTf, LiClO<sub>4</sub>, LiPF<sub>6</sub>, LiBr, and LiTFSI. When it came to cycling performance, LiTFSI and LiTf excelled. According to the study, a completely reversible Li-O<sub>2</sub> battery requires a more stable nonaqueous electrolyte that contains lithium salt and organic solvent.

When evaluating the activity coefficients of single-ion solvents in various solvents, such as dimethylformamide, hexamethylphosphoramide, dimethylacetamide, water, dimethyl sulfoxide, acetonitrile, nitromethane, N-methyl-2-pyrrolidone, formamide, 80% v/v DMSO-methanol at 25 °C, and sulfolane at 30 °C, the study compares extrathermodynamic assumptions. One of the simplest extra thermodynamic assumptions applied to novel solvent systems explained by (Parker & Alexander, 1968) is the iodine-triiodide assumption. Although atomic spectrum data served as the basis for the initial way of estimating atomic parameters in the Complete Neglect of Differential Overlap theory, the research found that, molecular orbitals are more susceptible to changes in the diagonal-to-off-diagonal parameter ratio. Better dipole moments are obtained from the updated calculations, but theoretical bond angles are

somewhat worsened. According to the study, the most effective method for determining solvent activity coefficients may be to use experimental data, such as dipole moments.

As possible electrolytes for Li-ion batteries, the study by (Ray et al., 2017) examines the solvation of lithium bis(trifluoromethanesulfonyl)imide (LiNTf<sub>2</sub>) in four distinct [NTf<sub>2</sub>] based ionic liquids. The ionic liquids were systematically altered to evaluate the effects of structural changes, such as bigger rings, the impact of an alkyl chain and the lack of an acidic proton on the [Li]<sup>+</sup> cations' mobility and solvation cations. Clarifying the interactions between the [Li]<sup>+</sup> and [NTf<sub>2</sub>] <sup>-</sup> ions is another goal of the study, which shows that the aprotic solvent has somewhat larger coordination numbers. [Li]<sup>+</sup> autocorrelation functions are analyzed to investigate the quick motion of the [Li]<sup>+</sup> cations within cages generated by the neighbouring [NTf<sub>2</sub>]<sup>-</sup> anions. The detailed description of the solvation process of [Li]<sup>+</sup> salt inside the hydrogen-bonded network of the ionic liquids is based on classical and ab initio molecular dynamics simulations. Although considerable effort is required to corroborate these assertions, the study shows that the solvation of [Li]<sup>+</sup> in ILs occurs via an inhomogeneous structural mechanism regarded as a "universal" kind of ion solvation. (Bai et al., 2020) explained that due to the rise in wasted batteries brought on by the growing need for lithium-ion batteries in electric cars, & renewable energy storage, recycling systems that are both economical and environmentally friendly must be developed. For recycling LIBs, three recycling techniques—pyrometallurgical, hydrometallurgical, and direct recycling—are being created and enhanced. It is preferable to automate sorting and disassembly to save expenses and safeguard human workers. Solid-state batteries and other cutting-edge recycling technologies are required to enhance LIB performance and promote the circular economy.

Limitations of lithium metal batteries include limited lithium supplies, high cost, and poor safety performance are described by (Wang *et al.*, 2021). Because of its high voltage, low cost, and rich content, sodium is a perfect lithium alternative. Materials based on sulfur are easily oxidized and have a high energy density and potential specific capacity. At 300 °C, conventional sodium-sulfur batteries are utilized. In order to address the issues like energy loss, flammability and explosions caused by

high-temperature usage conditions, research is focused on developing room temperature sodium-sulfur batteries. Enhancing sulfur conductivity, efficient sulfur fixing, and sodium-inhibiting dendrites are the main goals of cathode research. To prevent capacity deterioration, carbon-based materials combined with metal compounds, such as metal nitrides and metal oxides, can be investigated. It is also a good idea to have a separate cathode that is free of binder. One important element influencing sodium-sulfur batteries is electrolyte performance. It has been demonstrated that combining carbonate-based and ionic liquid-based electrolytes is a superior option. These objectives can be met, and digest volume expansion can be accomplished with a carbon nanofoam sandwich. By effectively preventing sodium dendrite growth, an Al<sub>2</sub>O<sub>3</sub> layer can be deposited on sodium to increase its service life. Na<sub>2</sub>S and metal sulfides can be combined to create composite anodes, which enhance storage efficiency.

A lot of study has been done on room-temperature sodium-sulfur (RT-Na/S) batteries because of their high specific capacity and plentiful raw ingredients. However, performance has been subpar due to problems such dendritic development, volume change, decreased electrical conductivity, and the polysulfide shuttle effect (P. Chen et al., 2022). For RT-Na/S batteries, recent studies have concentrated on anode protection, separator modification, electrolyte optimization, and cathode material improvement. Although 3D carbon materials were used in the sulfur cathode of the first RT-Na/S batteries, their adsorption and confinement capacities were restricted. To enhance the adsorption and catalytic conversion properties of NaPSs, researchers have added heteroatoms for recombination. The primary area of study for enhancing electrochemical performance has been liquid electrolytes, like ether and ester electrolytes. Future studies should focus on enhancing the wettability of the separator and electrolyte, employing carbon-based polar adsorbents, and incorporating catalysts to convert NaPSs.

(Chawla & Safa, 2019) explained the Sodium-Sulfur and Sodium-Air Batteries, because of their lightweight, reliable, and flexible characteristics, lithium-ion batteries are crucial for electric cars and portable gadgets. But because lithium is expensive and

scarce, scientists are looking into alternatives like sodium batteries. Although they have limitations in terms of cyclability, sodium-sulfur and sodium-air batteries show promise. More research is required to address problems including low conductivity and polysulfide production, while current efforts are concentrated on increasing capacity retention and cycle life. Better batteries for electronic gadgets may be developed with the use of more recent separators and catalysts.

Enhancing Li/S battery performance requires electrolyte optimization. The latest developments for various electrolytes, concepts, designs, and materials is examined in this paper by (Scheers et al., 2014), along with how their physical and chemical characteristics impact overall performance. The most advanced Li/S battery electrolyte available today, 1M LiTFSI DIOX:DME (1:1 v/v) (LiNO<sub>3</sub>), was created to balance battery needs in the face of extreme PS release circumstances. This breakthrough has been contested, though, by the reversed liquid Li/S idea, which depends on large concentrations of dissolved PS. With ternary solvent mixes and the growing number of ILs, binary DIOX:DME solvent-based electrolytes have potential for improvement. However, the additional expense of IL/organic based electrolytes must be weighed against the usage of more costly "designer solvents". Few new lithium salts are being used in the field, and little is known about the separator's function in Li/S electrolytes. The ultimate Li/S cell performance must be the main emphasis in order to logically enhance electrolytes for Li/S batteries. It is essential to properly identify scientifically the processes in which electrolyte performance and characteristics are limiting variables. In situ observations or model experiments employing ex-situ methods are frequently the foundation of electrolyte analysis.

The most common Li-salt found in commercial LIBs that can be recharged having graphite anode and 3–4 V cathode material is lithium hexafluorophosphate (LiPF<sub>6</sub>). LiPF<sub>6</sub> might not be the best Li-salt for lithium-metal, lithium-oxygen, and lithium-sulfur batteries, among other Li-based batteries. New electrolyte chemistries explained by (Younesi *et al.*, 2015) that maintain their integrity during cell cycling and offer high coulombic efficiency with a Li-metal anode are necessary for the development of advanced batteries. For LIBs with graphite anodes and moderate

voltage cathodes (3–4 V), LiPF<sub>6</sub> offers a set of suitable characteristics. Studies haven't been able to create a reliable electrode without dendritic development and with a high enough Coulombic efficiency, though. Research on metal-oxygen batteries will facilitate the growth of new chemistries for electrochemical energy storage and conversion systems, while Li-O<sub>2</sub> batteries experience electrolyte degradation. LiTf may be the ideal Li-salt for Li-S cells, however further research is required to determine its compatibility with Li-metal anodes and stability when exposed to reactive species.

Energy storage systems are essential for energy conservation because the industrial sector mostly depends on fossil fuels to supply its energy needs (Sharma & Thakur, 2022). With an emphasis on eco-friendly solvents and electrolytes, this paper examines a variety of materials and solvents utilized in energy storage applications throughout the previous 20 years. For a variety of energy storage technologies, including flow batteries, supercapacitors, and rechargeable batteries, solvents with large electrochemical windows, high thermal and chemical stability, low toxicity, and volatility are crucial. The type of solvents and electrolytes used in battery production are very important, and employing eco-friendly solvents and electrolytes is key to enhancing energy performance and producing long-lasting, safe, and effective gadgets. Glymes are the best solvents for lithium-ion batteries because of their hydrophilic and hydrophobic characteristics. The possible uses of aprotic lithium salts as electrolytes in glymes as solvents in energy storage devices, as well as monoglyme and tetraglyme, require more investigation.

As possible electrolytes, a number of new halogen-free ionic liquids (ILs) were created and evaluated. To examine the impact of Li salts on the physical characteristics of the IL-Li mixes, the appropriate lithium salts were made and explained by (Shi *et al.*, 2013). The findings shown that, while maintaining a competitive electrochemical window (EW), when compared to ILs with more spherical geometries, those with both planar anions and cations exhibit better conductivities and lower viscosities. A qualitative understanding of the ILs' appropriateness as electrolytes can be gained from their Walden plot behavior. Because of their greater delocalized charge distribution and weaker cation-anion interaction, anions have higher conductivity than ILs with more

spherical ions. The broadest EWs are seen in phosphorus-based ILs, indicating that AHA-based ILs could be useful in electrochemical domains.

The possibility of glyme-Li salt complexes as innovative liquid electrolytes for LiBs is examined by (Tamura *et al.*, 2010). At normal temperature, tetraglyme (G4) and triclyme (G3) combine to form 1:1 complex with LiCTFSI, resulting in solid and liquid forms. These complexes have more thermal stability than pure G4, and at temperatures lower than 100 °C, the vapor pressure is insignificant. At 30°C, these complexes have a comparatively high ionic conductivity, which is marginally less than that of a typical organic electrolyte solution. It was shown that lithium exhibits reversible deposition-stripping behavior using cyclic voltammetry. The [LiCoO<sub>2</sub>|[Li(G<sub>4</sub>)][CTFSI]|Li metal] cell exhibits consistent charge-discharge cycle behavior for more than 50 cycles, indicating that the [Li(G<sub>4</sub>)][CTFSI] complex is appropriate for a 4 V class LiB. Comprising an anion and a complex cation [Li(glyme)]<sup>+</sup>, as the electrolyte, Glyme-Li salt equimolar complexes appear to be a new type of RTILs that may increase the safety of LIBs.

Although grid-connected renewable energy sources can help meet the increasing demand, their intermittent nature can limit their effectiveness and lead to issues with power quality and instability. Li-ion batteries are being employed in stationary energy storage applications to address this, while it is yet unclear if they are cost-effective as explained by (Kebede *et al.*, 2021). Li-ion and lead-acid batteries integrated with Photovoltaic Grid-Connected Systems (PVGCS) were the subject of a techno-economic analysis and a state-of-the-art simulation model that took into account resource data and actual commercial load profiles. The analysis was conducted using the Hybrid Optimization Model for Electric Renewables (HOMER). The findings demonstrated that, given the specifications and application profile taken into consideration, Li-ion batteries are more economically feasible than lead-acid batteries. Compared to lead-acid batteries, the PVGCS system using Li-ion batteries uses 40% fewer batteries, offering a more dependable and affordable power source. Additionally, systems with a higher renewable proportion need more batteries, and Li-ion batteries offer lower NPC and COE. Li-ion batteries are suggested as a feasible alternative for

stationary applications based on renewable energy since they show promise in both technical and financial aspects.

The properties and deposition process of a surface coating on lithium metal are investigated in the work by (Xiong *et al.*, 2012) using LiNO<sub>3</sub> as a lithium salt in an electrolyte solution. The production of the film is investigated using X-ray photoelectron spectroscopy (XPS), electrochemical impedance spectroscopy (EIS), scanning electron microscopy (SEM), and scanning probe microscopy (SPM). Both inorganic and organic species make up the surface coating, and LiNO<sub>3</sub> is crucial to its production. For a uniform surface coating to form, the rate at which lithium metal and electrolyte solution react with LiNO<sub>3</sub> is essential. The compact and homogeneous surface coating extends the cycle life of lithium-sulfur batteries and the stability of the lithium anode. The study found that a compact and consistent surface coating on the lithium anode is necessary for the use of SEI layer additives in electrolyte solutions for lithium-sulfur batteries.

Electrolytes' conventional function in batteries is subordinated to that of electrode materials. Cell performance, encompassing cycle efficiency, rate capability, capacity retention, and abuse tolerance, is greatly impacted by the chemical makeup of electrolytes as reviewed by (Xu, 2004). Today's lithium-ion cell electrolyte systems are tailored to the chemistry of the cell thanks to ad-hoc surface chemistries on graphitic anodes and metal oxide cathodes. Rate performance, temperature range, safety, and electrolyte "solidification" will all continue to be innovative. However, the development of new cell chemistries necessitates electrolyte reformulation, such as the usage of olivine iron phosphate family and mixed metal oxides of the 5.0 V class.

Between 2003 and 2014, energy storage research grew dramatically, particularly in the fields of electrolytes and interphases by (Xu, 2014). These elements are crucial to electrochemical devices due to their high reactivities and instability in high-voltage batteries. Graphitic structures' mature Li<sup>+</sup>-intercalation chemistry has improved our understanding of these elements. As cathode materials with larger capacity and operating voltage are produced, electrolytes and interphases encounter more challenges. The development of "beyond Li-ion" battery chemistries demonstrates that

robust electrolyte and interphase systems are necessary to ensure respectable reversibility.

Given that the most popular technology in portable electronics like laptops, tablets, and cell phones are lithium-ion batteries, they significantly improve the quality of life in contemporary society as reviewed by (Zubi *et al.*, 2018). Lithium-ion batteries continue to be the favoured choice for the expanding electric vehicle industry despite their continued underutilization in power supply systems, especially when paired with photovoltaics and wind power. As a technological component, these batteries have great promise for global carbon emission reductions and energy sustainability. With a focus on this potential, a thorough analysis of the current state of the art and prospects for Liion batteries is investigated and effectively discussed here.

### References

Adolph, R. (2016). Compatibility of Aprotic Electrolytes with Negative Electrode Materials in Lithium-ion Batteries. 63(1), 1–23.

Anouti, M., Dougassa, Y. R., Tessier, C., El Ouatani, L., & Jacquemin, J. (2012). Low pressure carbon dioxide solubility in pure electrolyte solvents for lithium-ion batteries as a function of temperature. Measurement and prediction. *Journal of Chemical Thermodynamics*, 50, 71–79. https://doi.org/10.1016/j.jct.2012.01.027

Aravindan, V., Gnanaraj, J., Madhavi, S., & Liu, H. K. (2011). Lithium-ion conducting electrolyte salts for lithium batteries. *Chemistry - A European Journal*, *17*(51), 14326–14346. https://doi.org/10.1002/chem.201101486

Armand, M., Axmann, P., Bresser, D., Copley, M., Edström, K., Ekberg, C., Guyomard, D., Lestriez, B., Novák, P., Petranikova, M., Porcher, W., Trabesinger, S., Wohlfahrt-Mehrens, M., & Zhang, H. (2020). Lithium-ion batteries – Current state of the art and anticipated developments. *Journal of Power Sources*, 479(July). https://doi.org/10.1016/j.jpowsour.2020.228708

Arya, A., & Sharma, A. L. (2017). Polymer electrolytes for lithium ion batteries: a critical study. In *Ionics* (Vol. 23, Issue 3). Ionics. https://doi.org/10.1007/s11581-016-1908-6

Bai, Y., Muralidharan, N., Sun, Y. K., Passerini, S., Stanley Whittingham, M., & Belharouak, I. (2020). Energy and environmental aspects in recycling lithium-ion batteries: Concept of Battery Identity Global Passport. *Materials Today*, 41(xx), 304–315. https://doi.org/10.1016/j.mattod.2020.09.001

Barthel, J., Bachhuber, K., Buchner, R., Gill, J. B., & Kleebauer, M. (1990). Dielectric spectra of some common solvents in the microwave region. Dipolar aprotic solvents and amides. *Chemical Physics Letters*, *167*(1–2), 62–66.

https://doi.org/10.1016/0009-2614(90)85071-J

Beaudin, M., Zareipour, H., Schellenberglabe, A., & Rosehart, W. (2010). Energy storage for mitigating the variability of renewable electricity sources: An updated

review. *Energy for Sustainable Development*, 14(4), 302–314. https://doi.org/10.1016/j.esd.2010.09.007

Boisset, A., Menne, S., Jacquemin, J., Balducci, A., & Anouti, M. (2013). Deep eutectic solvents based on N-methylacetamide and a lithium salt as suitable electrolytes for lithium-ion batteries. *Physical Chemistry Chemical Physics*, *15*(46), 20054–20063. https://doi.org/10.1039/c3cp53406e

Chawla, N., & Safa, M. (2019). Sodium batteries: A review on sodium-sulfur and sodium-air batteries. *Electronics (Switzerland)*, 8(10).

https://doi.org/10.3390/electronics8101201

Chen, P., Wang, C., & Wang, T. (2022). Review and prospects for room-temperature sodium-sulfur batteries. *Materials Research Letters*, *10*(11), 691–719. https://doi.org/10.1080/21663831.2022.2092428

Chen, X., & Zhang, Q. (2020). Atomic insights into the fundamental interactions in lithium battery electrolytes. *Accounts of Chemical Research*, *53*(9), 1992–2002. https://doi.org/10.1021/acs.accounts.0c00412

Chrétien, F., Jones, J., Damas, C., Lemordant, D., Willmann, P., & Anouti, M. (2014). Impact of Solid Electrolyte Interphase lithium salts on cycling ability of Li-ion battery: Beneficial effect of glymes additives. *Journal of Power Sources*, *248*, 969–977. https://doi.org/10.1016/j.jpowsour.2013.09.092

Coadou, E., Timperman, L., Jacquemin, J., Galiano, H., Hardacre, C., & Anouti, M. (2013). Comparative study on performances of trimethyl-sulfonium and trimethyl-ammonium based ionic liquids in molecular solvents as electrolyte for electrochemical double layer capacitors. *Journal of Physical Chemistry C*, 117(20), 10315–10325. https://doi.org/10.1021/jp402485z

Cox, B. G., Hedwig, G. R., Parker, A. J., & Watts, D. W. (1974). Solvation of ions. XIX. Thermodynamic properties for transfer of single ions between protic and dipolar aprotic solvents. *Australian Journal of Chemistry*, *27*(3), 477–501. https://doi.org/10.1071/CH9740477

Daniel, C. (2008). Materials and processing for lithium-ion batteries. *Jom*, 60(9), 43–48. https://doi.org/10.1007/s11837-008-0116-x

Davidson, W. R., & Kebarle, P. (1976). Ionic Solvation by Aprotic Solvents. Gas Phase Solvation of the Alkali Ions by Acetonitrile. *Journal of the American Chemical Society*, 98(20), 6125–6133. https://doi.org/10.1021/ja00436a010

Deng, D. (2015). Li-ion batteries: Basics, progress, and challenges. *Energy Science and Engineering*, *3*(5), 385–418. https://doi.org/10.1002/ese3.95

Díaz-González, F., Sumper, A., Gomis-Bellmunt, O., & Villafáfila-Robles, R. (2012). A review of energy storage technologies for wind power applications. *Renewable and Sustainable Energy Reviews*, *16*(4), 2154–2171. https://doi.org/10.1016/j.rser.2012.01.029

Ding, S., Yu, X., Ma, Z. F., & Yuan, X. (2021). A review of rechargeable aprotic lithium-oxygen batteries based on theoretical and computational investigations. *Journal of Materials Chemistry A*, 9(13), 8160–8194. https://doi.org/10.1039/d1ta00646k

Diouf, B., & Pode, R. (2015). Potential of lithium-ion batteries in renewable energy. *Renewable Energy*, 76, 375–380. https://doi.org/10.1016/j.renene.2014.11.058

Farret, F. A., & Simões, M. G. (2006). Integration of Alternative Sources of Energy. In *Integration of Alternative Sources of Energy*. https://doi.org/10.1002/0471755621

Feng, S., Huang, M., Lamb, J. R., Zhang, W., Tatara, R., Zhang, Y., Guang Zhu, Y., Perkinson, C. F., Johnson, J. A., & Shao-Horn, Y. (2019). Molecular Design of Stable Sulfamide- and Sulfonamide-Based Electrolytes for Aprotic Li-O2 Batteries. *Chem*, 5(10), 2630–2641. https://doi.org/10.1016/j.chempr.2019.07.003

Fletcher, S., Kirkpatrick, I., Thring, R., Dring, R., Tate, J. L., Geary, H. R. M., & Black, V. J. (2018). Ternary Mixtures of Sulfolanes and Ionic Liquids for Use in High-Temperature Supercapacitors. *ACS Sustainable Chemistry and Engineering*, *6*(2), 2612–2620. https://doi.org/10.1021/acssuschemeng.7b04117

Ghalami-Choobar, B., & Fallahkar, T. N. (2019). Thermophysical properties of 1-ethyl-3-methylimidazolium bromide ionic liquid in water + ethylene carbonate mixtures at T = (298.2, 308.2 and 318.2)K. *Fluid Phase Equilibria*, 496, 42–60. https://doi.org/10.1016/j.fluid.2019.05.015

Guo, X., Sun, B., Su, D., Liu, X., Liu, H., Wang, Y., & Wang, G. (2017). Recent developments of aprotic lithium-oxygen batteries: functional materials determine the electrochemical performance. *Science Bulletin*, 62(6), 442–452. https://doi.org/10.1016/j.scib.2017.01.037

Hall, P. J., & Bain, E. J. (2008). Energy-storage technologies and electricity generation. *Energy Policy*, *36*(12), 4352–4355. https://doi.org/10.1016/j.enpol.2008.09.037

Han, H. B., Zhou, S. S., Zhang, D. J., Feng, S. W., Li, L. F., Liu, K., Feng, W. F., Nie, J., Li, H., Huang, X. J., Armand, M., & Zhou, Z. Bin. (2011). Lithium bis(fluorosulfonyl)imide (LiFSI) as conducting salt for nonaqueous liquid electrolytes for lithium-ion batteries: Physicochemical and electrochemical properties. *Journal of Power Sources*, 196(7), 3623–3632. https://doi.org/10.1016/j.jpowsour.2010.12.040

Henderson, W. A. (2014). *Nonaqueous Electrolytes: Advances in Lithium Salts*. https://doi.org/10.1007/978-1-4939-0302-3\_1

Horwitz, G., Calvo, E. J., Méndez De Leo, L. P., & De La Llave, E. (2020). Electrochemical stability of glyme-based electrolytes for Li-O2batteries studied by: In situ infrared spectroscopy. *Physical Chemistry Chemical Physics*, 22(29), 16615–16623. https://doi.org/10.1039/d0cp02568b

Horwitz, G., Factorovich, M., Rodriguez, J., Laria, D., & Corti, H. R. (2018). Ionic Transport and Speciation of Lithium Salts in Glymes: Experimental and Theoretical Results for Electrolytes of Interest for Lithium-Air Batteries. *ACS Omega*, *3*(9), 11205–11215. https://doi.org/10.1021/acsomega.8b01443

Hu, A., Zhou, M., Lei, T., Hu, Y., Du, X., Gong, C., Shu, C., Long, J., Zhu, J., Chen, W., Wang, X., & Xiong, J. (2020). Optimizing Redox Reactions in Aprotic Lithium—

Sulfur Batteries. *Advanced Energy Materials*, 10(42), 1–26. https://doi.org/10.1002/aenm.202002180

Kalhoff, J., Eshetu, G. G., Bresser, D., & Passerini, S. (2015). Safer electrolytes for lithium-ion batteries: State of the art and perspectives. *ChemSusChem*, 8(13), 2154–2175. https://doi.org/10.1002/cssc.201500284

Kawakami, N., Iijima, Y., Sakanaka, Y., Fukuhara, M., Ogawa, K., Bando, M., & Matsuda, T. (2010). Development and field experiences of stabilization system using 34MW NAS batteries for a 51MW Wind farm. *IEEE International Symposium on Industrial Electronics*, 2371–2376. https://doi.org/10.1109/ISIE.2010.5637487

Kebede, A. A., Coosemans, T., Messagie, M., Jemal, T., Behabtu, H. A., Van Mierlo, J., & Berecibar, M. (2021). Techno-economic analysis of lithium-ion and lead-acid batteries in stationary energy storage application. *Journal of Energy Storage*, 40(June), 102748. https://doi.org/10.1016/j.est.2021.102748

Khan, I. A., Gnezdilov, O. I., Filippov, A., & Shah, F. U. (2021). Ion Transport and Electrochemical Properties of Fluorine-Free Lithium-Ion Battery Electrolytes Derived from Biomass. *ACS Sustainable Chemistry and Engineering*, *9*(23), 7769–7780. https://doi.org/10.1021/acssuschemeng.1c00939

Kim, J. I. (1978). Preferential solvation of single ions. A critical study of the Ph4AsPh4B assumption for single ion thermodynamics in amphiprotic and dipolar-aprotic solvents. *Journal of Physical Chemistry*, 82(2), 191–199. https://doi.org/10.1021/j100491a013

Kim, T., Song, W., Son, D. Y., Ono, L. K., & Qi, Y. (2019). Lithium-ion batteries: outlook on present, future, and hybridized technologies. *Journal of Materials Chemistry A*, 7(7), 2942–2964. https://doi.org/10.1039/C8TA10513H

Kousksou, T., Bruel, P., Jamil, A., El Rhafiki, T., & Zeraouli, Y. (2014). Energy storage: Applications and challenges. *Solar Energy Materials and Solar Cells*, *120*(PART A), 59–80. https://doi.org/10.1016/j.solmat.2013.08.015

Laino, T., & Curioni, A. (2013). Chemical reactivity of aprotic electrolytes on a solid Li2O 2 surface: Screening solvents for Li-air batteries. *New Journal of Physics*, *15*. https://doi.org/10.1088/1367-2630/15/9/095009

Li, T., Xu, J., Wang, C., Wu, W., Su, D., & Wang, G. (2019). The latest advances in the critical factors (positive electrode, electrolytes, separators) for sodium-sulfur battery. *Journal of Alloys and Compounds*, 792, 797–817.

https://doi.org/10.1016/j.jallcom.2019.03.343

Lombardo, L., Brutti, S., Navarra, M. A., Panero, S., & Reale, P. (2013). Mixtures of ionic liquid-Alkylcarbonates as electrolytes for safe lithium-ion batteries. *Journal of Power Sources*, 227, 8–14. https://doi.org/10.1016/j.jpowsour.2012.11.017

Manthiram, A. (2017). An Outlook on Lithium Ion Battery Technology. *ACS Central Science*, *3*(10), 1063–1069. https://doi.org/10.1021/acscentsci.7b00288

May, G. J., Davidson, A., & Monahov, B. (2018). Lead batteries for utility energy storage: A review. *Journal of Energy Storage*, *15*, 145–157. https://doi.org/10.1016/j.est.2017.11.008

McDowall, J. (2006). Integrating energy storage with wind power in weak electricity grids. *Journal of Power Sources*, *162*(2 SPEC. ISS.), 959–964. https://doi.org/10.1016/j.jpowsour.2005.06.034

Morioka, Y., Narukawa, S., & Itou, T. (2001). State-of-the-art of alkaline rechargeable batteries. *Journal of Power Sources*, 100(1–2), 107–116.

https://doi.org/10.1016/S0378-7753(01)00888-6

Mozhzhukhina, N., Longinotti, M. P., Corti, H. R., & Calvo, E. J. (2015). A conductivity study of preferential solvation of lithium ion in acetonitrile-dimethyl sulfoxide mixtures. *Electrochimica Acta*, *154*, 456–461.

https://doi.org/10.1016/j.electacta.2014.12.022

Nasrabadi, A. T., & Ganesan, V. (2019). Structure and Transport Properties of Lithium-Doped Aprotic and Protic Ionic Liquid Electrolytes: Insights from Molecular Dynamics Simulations [Research-article]. *Journal of Physical Chemistry B*, 123(26), 5588–5600.

https://doi.org/10.1021/acs.jpcb.9b04477

Nasybulin, E., Xu, W., Engelhard, M. H., Nie, Z., Burton, S. D., Cosimbescu, L., Gross, M. E., & Zhang, J. G. (2013). Effects of electrolyte salts on the performance of Li-O2 batteries. *Journal of Physical Chemistry C*, *117*(6), 2635–2645. https://doi.org/10.1021/jp311114u

Omar, N., Van den Bossche, P., Coosemans, T., & Van Mierlo, J. (2013). Peukert revisited-critical appraisal and need for modification for lithium-ion batteries. *Energies*, 6(11), 5625–5641. https://doi.org/10.3390/en6115625

Parker, A. J., & Alexander, R. (1968). Solvation of Ions. XIII. Solvent Activity Coefficients of Ions in Protic and Dipolar Aprotic Solvents. A Comparison of Extrathermodynamic Assumptions. *Journal of the American Chemical Society*, 90(13), 3313–3319. https://doi.org/10.1021/ja01015a003

Pigłowska, M., Kurc, B., Galiński, M., Fuć, P., Kamińska, M., Szymlet, N., & Daszkiewicz, P. (2021). Challenges for safe electrolytes applied in lithium-ion cells—a review. *Materials*, *14*(22), 1–52. https://doi.org/10.3390/ma14226783

Ray, P., Vogl, T., Balducci, A., & Kirchner, B. (2017). Structural Investigations on Lithium-Doped Protic and Aprotic Ionic Liquids. *Journal of Physical Chemistry B*, 121(20), 5279–5292. https://doi.org/10.1021/acs.jpcb.7b02636

Rivki, M., Bachtiar, A. M., Informatika, T., Teknik, F., & Indonesia, U. K. (n.d.). *Glyme-based electrolytes: suitable solutions for next-generation lithium batteries Daniele.* 112.

Scheers, J., Fantini, S., & Johansson, P. (2014). A review of electrolytes for lithium-sulphur batteries. *Journal of Power Sources*, 255, 204–218.

https://doi.org/10.1016/j.jpowsour.2014.01.023

Sharma, C., & Thakur, R. C. (2022). Potential solvents and electrolytes for energy storage applications: A Review. *Journal of Physics: Conference Series*, 2267(1). https://doi.org/10.1088/1742-6596/2267/1/012051

Shi, C., Quiroz-Guzman, M., DeSilva, A., & Brennecke, J. F. (2013). Physicochemical

and Electrochemical Properties of Ionic Liquids Containing Aprotic Heterocyclic Anions Doped With Lithium Salts. *Journal of The Electrochemical Society*, *160*(9), A1604–A1610. https://doi.org/10.1149/2.116309jes

Syali, M. S., Kumar, D., Mishra, K., & Kanchan, D. K. (2020). Recent advances in electrolytes for room-temperature sodium-sulfur batteries: A review. *Energy Storage Materials*, *31*, 352–372. https://doi.org/10.1016/j.ensm.2020.06.023

Tamura, T., Hachida, T., Yoshida, K., Tachikawa, N., Dokko, K., & Watanabe, M. (2010). New glyme-cyclic imide lithium salt complexes as thermally stable electrolytes for lithium batteries. *Journal of Power Sources*, *195*(18), 6095–6100. https://doi.org/10.1016/j.jpowsour.2009.11.061

Väyrynen, A., & Salminen, J. (2012). Lithium ion battery production. *Journal of Chemical Thermodynamics*, 46, 80–85. https://doi.org/10.1016/j.jct.2011.09.005

Vraneš, M., Cvjetićanin, N., Papović, S., Šarac, B., Prislan, I., Megušar, P., Gadžurić, S., & Bešter-Rogač, M. (2017). Electrical, electrochemical and thermal properties of the ionic liquid + lactone binary mixtures as the potential electrolytes for lithium-ion batteries. *Journal of Molecular Liquids*, 243, 52–60.

https://doi.org/10.1016/j.molliq.2017.07.129

Wang, Y., Zhang, Y., Cheng, H., Ni, Z., Wang, Y., Xia, G., Li, X., & Zeng, X. (2021). Research progress toward room temperature sodium sulfur batteries: A review. *Molecules*, 26(6). https://doi.org/10.3390/molecules26061535

Wei, S., Inoue, S., Di Lecce, D., Li, Z., Tominaga, Y., & Hassoun, J. (2020). Towards a High-Performance Lithium-Metal Battery with Glyme Solution and an Olivine Cathode. *ChemElectroChem*, 7(11), 2344. https://doi.org/10.1002/celc.202000554

Xiong, S., Xie, K., Diao, Y., & Hong, X. (2012). Properties of surface film on lithium anode with LiNO 3 as lithium salt in electrolyte solution for lithium-sulfur batteries. *Electrochimica Acta*, 83, 78–86. https://doi.org/10.1016/j.electacta.2012.07.118

Xu, K. (2004). Nonaqueous Liquid Electrolytes for Lithium-Based Rechargeable Batteries Kang. *Chemical Reviews*, *104*(10), 4303–4417.

https://doi.org/10.1021/cr030203g

Xu, K. (2014). Electrolytes and interphases in Li-ion batteries and beyond. *Chemical Reviews*, 114(23), 11503–11618. https://doi.org/10.1021/cr500003w

Younesi, R., Veith, G. M., Johansson, P., Edström, K., & Vegge, T. (2015). Lithium salts for advanced lithium batteries: Li-metal, Li-O2, and Li-S. *Energy and Environmental Science*, 8(7), 1905–1922. https://doi.org/10.1039/c5ee01215e

Zhang, M., Liu, Y., Li, D., Cui, X., Wang, L., Li, L., & Wang, K. (2023). Electrochemical Impedance Spectroscopy: A New Chapter in the Fast and Accurate Estimation of the State of Health for Lithium-Ion Batteries. *Energies*, *16*(4), 1–16. https://doi.org/10.3390/en16041599

Zhao, Z., Liu, B., Shen, Y., Wu, T., Zang, X., Zhao, Y., Zhong, C., Ma, F., & Hu, W. (2021). Comparative study of intrinsically safe zinc-nickel batteries and lead-acid batteries for energy storage. *Journal of Power Sources*, 510(June), 230393. https://doi.org/10.1016/j.jpowsour.2021.230393

Zubi, G., Dufo-López, R., Carvalho, M., & Pasaoglu, G. (2018). The lithium-ion battery: State of the art and future perspectives. *Renewable and Sustainable Energy Reviews*, 89(April 2017), 292–308. https://doi.org/10.1016/j.rser.2018.03.002

## Chapter 3 Experimental

### 3. EXPERIMENTAL

### 3.1. MATERIALS

The complete details of experimental work that includes chemicals used. Also, various techniques used to carry out the experiments also stated in this chapter.

 Table 3.1: Details of chemical utilized during research work.

| S.No. | Chemicals                                   | als Molecular Formula   |               | CAS<br>number | Mass fraction purity <sup>a</sup> |
|-------|---|---|---------------|---------------|-----------------------------------|
| 1     | Lithium bis(trifluoromethanesulphonyl)imide | CF <sub>3</sub> SO <sub>2</sub> NLiSO <sub>2</sub> CF <sub>3</sub>                | Sigma Aldrich | 90076-65-6    | 99%                               |
| 2     | Lithium trifluoromethanesulfonate           | CF <sub>3</sub> SO <sub>3</sub> Li  | Sigma Aldrich | 33454-82-9    | 99.9%                             |
| 3     | Lithium bis(fluorosulphonyl)imide           | CF <sub>3</sub> SO <sub>2</sub> NLiSO <sub>2</sub> CF <sub>3</sub>                | Sigma Aldrich | 90076-65-6    | 99.5%                             |
| 4     | Lithium hexafluorophosphate                 | LiPF <sub>6</sub>   | Sigma Aldrich | 21324-40-3    | 98%                               |
| 5     | Lithium tetrafluoroborate                   | LiBF <sub>4</sub>   | Sigma Aldrich | 14283-07-9    | 98.5%                             |
| 6     | 1,2-dimethoxyethane                         | CH <sub>3</sub> OCH <sub>2</sub> CH <sub>2</sub> OCH <sub>3</sub>                 | Sigma Aldrich | 110-71-4      | 99%                               |
| 7     | Tetraethylene glycol dimethyl ether         | CH <sub>3</sub> O(CH <sub>2</sub> CH <sub>2</sub> O) <sub>4</sub> CH <sub>3</sub> | Sigma Aldrich | 143-24-8      | 98.0%                             |

<sup>&</sup>lt;sup>a</sup> as stated by the supplier.

### 3.2. BRIEF OVERVIEW OF LITHIUM SALTS USED IN STUDY

### 3.2.1. Lithium bis(trifluoromethanesulphonyl)imide:

The chemical structure of LiTFSI consists of a lithium cation (Li<sup>+</sup>) coordinated with two trifluoromethanesulfonyl imide anions (N(CF<sub>3</sub>SO<sub>2</sub>)<sup>2-</sup>). LiTFSI is highly soluble in many organic solvents, including common ones like diethyl carbonate (DEC), dimethyl carbonate (DMC) and ethylene carbonate (EC). This solubility makes it a suitable choice for formulating non-aqueous electrolytes in lithium-ion (Li-ion) batteries. It has a high electrochemical stability window i.e., it can withstand diverse voltages without undergoing decomposition, making it useful in high-voltage battery systems(Shah et al.. 2017). The molecular structure of Lithium bis(trifluoromethanesulphonyl)imide is represented in Figure 3.1.

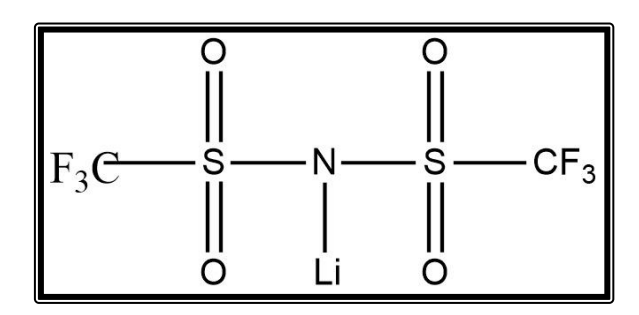


Figure 3.1: General structure of Lithium bis(trifluoromethanesulphonyl)imide.

### 3.2.2. Lithium trifluoromethanesulfonate

Lithium triflate is known for its high ionic conductivity, which makes it a popular choice in lithium-ion batteries and other electrochemical devices. It is mainly utilized as an electrolyte salt in Li-ion batteries, helping the Li-ions move between the cathode and anode throughout charge-discharge cycles(de Araujo Lima e Souza *et al.*, 2024). The molecular structure of **Lithium trifluoromethanesulfonate** is represented in **Figure 3.2.** 

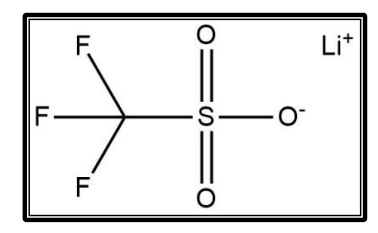


Figure 3.2: General structure of Lithium trifluoromethanesulfonate.

### 3.2.3. Lithium bis(fluorosulphonyl)imide (LiFSI)

LiFSI is known for its high ionic conductivity and stability, which makes it a valuable component in advanced battery technologies. LiFSI dissolves quite well in several polar solvents, such as acetone, acetonitrile, and dimethyl carbonate. It exhibits excellent thermal and electrochemical stability. Also, it has a high ionic conductivity, making it a desirable component in lithium-ion battery electrolytes(Scrosati *et al.*, 2011). The molecular structure of **Lithium bis(fluorosulphonyl)imide** is represented in **Figure 3.3**.

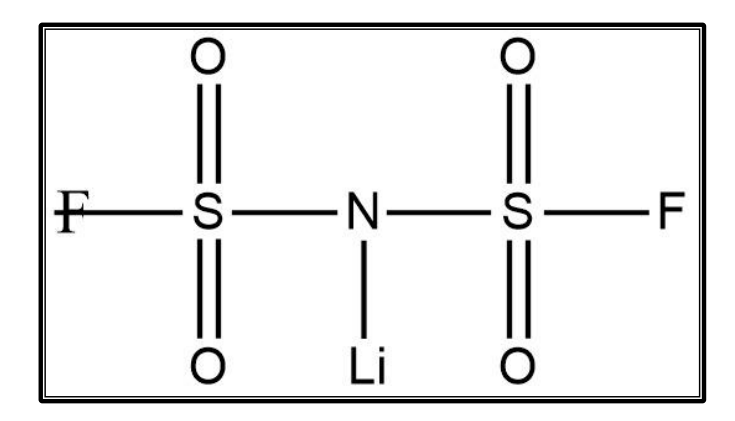


Figure 3.3: General structure of Lithium bis(fluorosulphonyl)imide.

### 3.2.4. Lithium hexafluorophosphate (LiPF<sub>6</sub>)

A key component of the electrolyte specifically in Li-ion batteries, which comprises the substance that allows ions move between the two electrodes, making it easier for the battery to charge and discharge (Nikiforidis *et al.*, 2021). It helps enhance the battery's performance and stability. LiPF<sub>6</sub> increases the ionic conductivity of the electrolyte, allowing lithium ions to move more freely between the battery's anode and

cathode, thereby improving the battery's overall efficiency. The molecular structure of **Lithium hexafluorophosphate** is represented in **Figure 3.4.** 

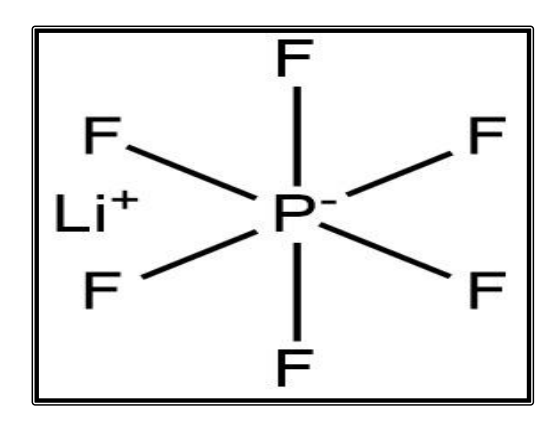
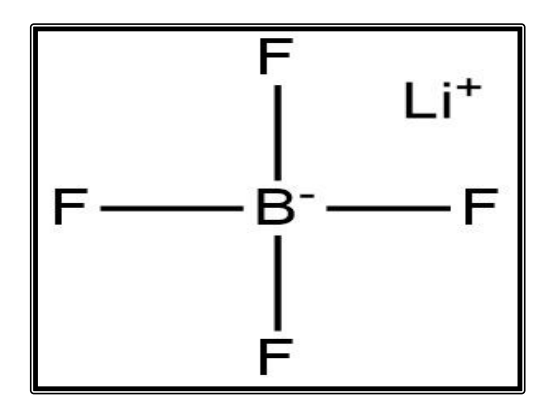


Figure 3.4: General structure of Lithium hexafluorophosphate.

### 3.2.5. Lithium tetrafluoroborate (LiBF4)

LiBF<sub>4</sub> is a white crystalline powder or solid, soluble in many polar solvents, including water, acetone, and some organic solvents (Rana *et al.*, 2023). LiBF<sub>4</sub> is utilized for various electrochemical applications, including supercapacitors, lithium-ion capacitors, and in the synthesis of organofluoride compounds. The molecular structure of **Lithium tetrafluoroborate** is represented in **Figure 3.5.** 



**Figure 3.5:** General structure of Lithium tetrafluoroborate.

### 3.3 EXPERIMENTAL TECHNIQUES

To interpret the interactions, present among the Lithium salts and glycols multiple techniques were employed to get the ultimate results. The various techniques used to collect the experimental data are discussed below:

- Density and speed of sound measurements
- Conductivity measurements
- FT-IR Spectroscopic Studies
- Cyclic Voltammetry

A Sartorius CPA 225D scale with an accuracy of  $\pm$  0.00001 g was used to weigh the chemicals. Degassed and triple-distilled water with a specific conductance  $<10^{-6}$  S.cm<sup>-1</sup> was used to make the solution.

### 3.3.1. Density and Speed of sound measurements

Anton Paar DSA 5000M, which stands for "density and speed of sound analyzer," was used to determine the data for density and speed of sound. It can simultaneously determine two physically independent parameters in one setup with high accuracy. It works on Pulsed Excitation Method that conveys the most stable results considering oscillation characteristics. To calibrate the device, the speed & density of sound were measured through dry air and fresh triple-distilled and deionized water at 293.15 K. This was done prior to each set of measures in the experimental temperature range. As the speed and intensity of sound change with temperature, inbuilt Peltier method was used to keep it at  $1 \times 10^{-3}$  K. The transmission time method was used to determine the speed of sound. The sample studied was kept between two piezoelectric ultrasound sensors. A transducer sent out 3 MHz sound waves through a sample hole that was filled with air and then received by another transducer. The accuracy of the density measurements was found to be 1×10<sup>-3</sup> kg.m<sup>-3</sup> & speed of sound measurements was found to be 1×10<sup>-2</sup> ms<sup>-1</sup>. As an average, there was 0.15 kg m<sup>-3</sup> of error in the mass and 1.0 ms<sup>-1</sup> in the speed of sound. There are about  $2 \times 10^{-5}$  mol.kg<sup>-1</sup> of errors in the molality of the solution. This instrument has a density cell and a pulseecho speed of sound cell, as shown in Figure 3.6. These cells are composed of stainless steel and are temperature controlled by build-in thermostat. The extraordinary longterm stability is offered by a reference oscillator along with the U-tube oscillator that allows adjustments at the desired temperatures. Two integrated Pt 100 thermometers offer the maximum accurateness in temperature control and are traceable to national standards. The DSA 5000 simultaneously fixes any errors in the density values that are

caused by viscosity by measuring how much the filled-in sample slows down the oscillation of the U-tube as shown in **Figure 3.7.** Another thing that makes the speed of the filled-in sample accurate is an extra measurement cell made of stainless steel & high-resolution electronics.



Figure 3.6: Anton Paar DSA 5000M (Anton Paar, 2011a)

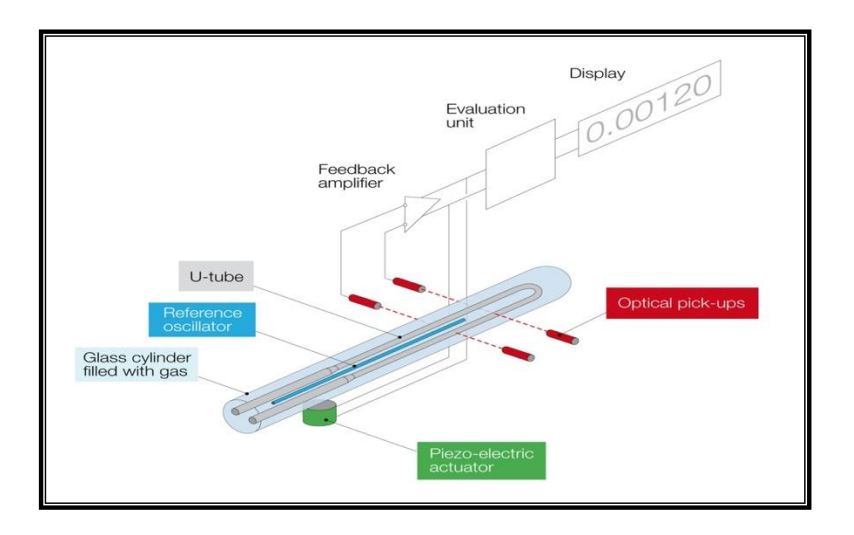
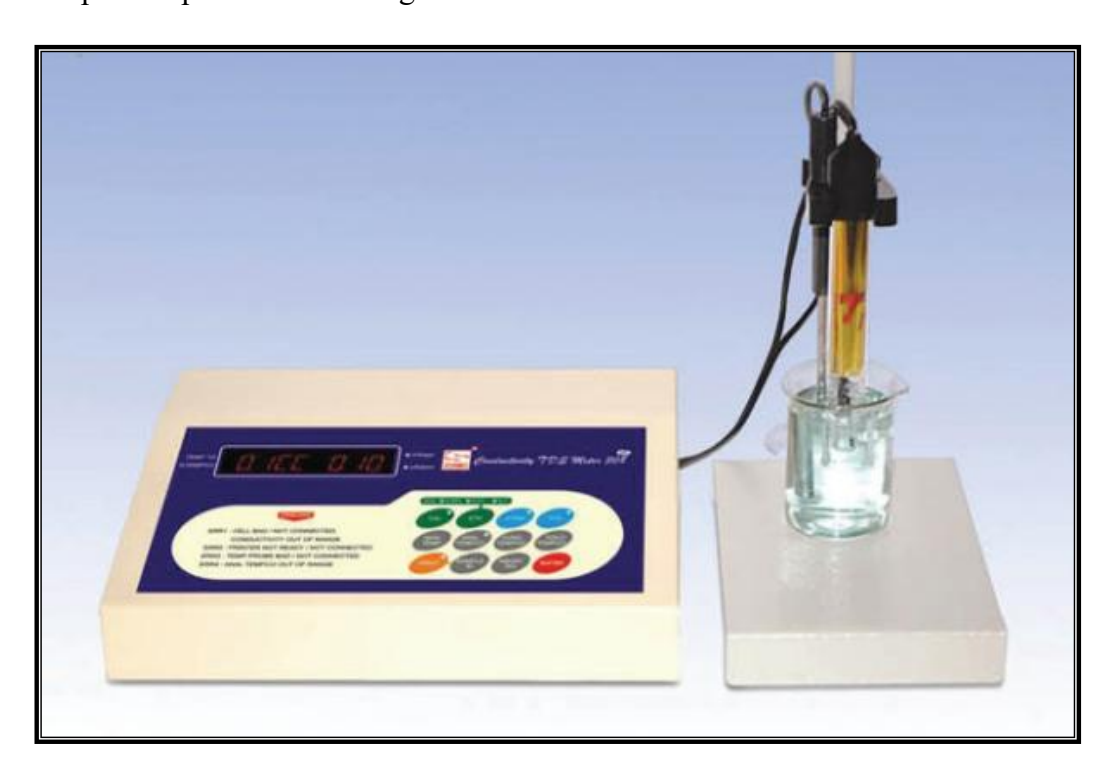


Figure 3.7: Density and sound velocity cell of DSA 5000M (Anton Paar, 2011b)

In order to carry out a measurement, the sample under investigation is filled in the measuring cells using a syringe. Once the measurement is complete, an acoustic signal informed. The built-in conversion tables and functions take the data and turn them into units of concentration, specific gravity, or other density or speed of sound-related units.

### 3.3.2. Conductivity measurements

Systronics 308-Digital conductivity meter (**shown in Figure 3.8**) was used for conductivity measurements. It includes a dip type conductivity cell that has a cell constant of 1 cm<sup>-1</sup>. The Systronics 308 digital conductivity meter measures the ability of a solution to conduct electric current between two electrodes of a dip-type conductivity cell. When an alternating voltage is applied, ions in the solution move and carry current; the instrument detects this current and converts it into conductivity using the cell constant (1 cm<sup>-1</sup>). Calibration with standard KCl solutions ensures accuracy, and the measured conductivity reflects the ionic strength of the test solution at controlled temperature. Before measuring the conductivities of the experiments, KCl solution with a concentration of 0.01 to 1.0 mol kg<sup>-1</sup> is used to calibrate the conductivity meter. After it is set up correctly, the solution whose conductivity needs to be tested is put into a jar with two jackets. With the help of a refrigerated circulated water thermometer (Macro Scientific Works Pvt. Ltd. Delhi) that was accurate to within 0.1 K, the right temperature was kept. The conductivity values have been recorded three times per sample and the average value have been considered.



**Figure 3.8:** Systronics Conductivity meter 308 (Limited, 2008)

### 3.3.3. FT-IR Spectroscopic Studies

FTIR spectra was recorded using Shimadzu spectrometer 8400S (**shown in Figure 3.9**). It achieves best signal-to-noise ratio 20,000:1. FTIR-8400S can be operated using a laptop PC or an ordinary desktop. This instrument provides consistently reproducible spectra without any laborious mechanical adjustments. FTIR-spectroscopy is one of the important tools that offers information regarding the interactions prevailing in the system at molecular level. This technique is an absorption spectroscopy and measurements based on the amount of light absorbed by a sample at each wavelength. The spectra of the solvent as well as investigated system were recorded in 4500 cm<sup>-1</sup> to 500 cm<sup>-1</sup> wave region.

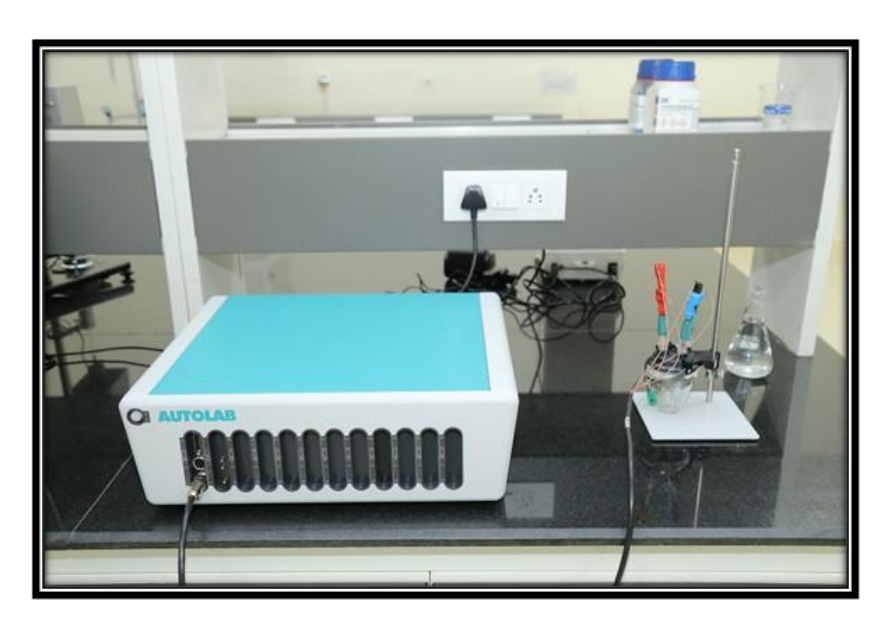


Figure 3.9: Shimadzu FTIR-8400S Spectrophotometer

### 3.3.4. Cyclic Voltammetry

Cyclic voltammetry helps us in the determination of the electrochemical properties of the electrode being used. To determine the electrochemical properties with the help of CV graphs, Metrohm Autolab PGSTAT204 multi-channel Potentiostat/Galvanostat electrochemical workstation (shown in **Figure 3.10**) was used. It has a three-electrode cell that is tightly closed and is in a neutral environment with argon flow. There is an overlap between the reduction and oxidation potential peaks in the cyclic voltammograms of the ternary mixtures as a function of concentration at room

temperature in the potential range from -1.0 V to +2.0 V shown in the graph or cyclic voltogramms. As a standard, 10 mM AgCl mixed with Ag wire was used in all the systems as reference electrode. Counter electrode was made of Pt wire, and working electrode is platinum with a width of 3 mm. These voltammograms began with a potential of 0 V and no current moving. For final results, 3 cycles were repeated.



**Figure 3.10:** Metrohm Autolab PGSTAT204 multi-channel Potentiostat/galvanostat electrochemical workstation

### References

Anton Paar, A. (2011a). Instruction Manual DSA 5000 M. Anton Paar.

Anton Paar, A. (2011b). Instruction Manual DSA 5000 M. Anton Paar.

de Araujo Lima e Souza, G., Di Pietro, M. E., Castiglione, F., Fazzio Martins

Martinez, P., Middendorf, M., Schönhoff, M., Fraenza, C. C., Stallworth, P.,

Greenbaum, S., Triolo, A., Appetecchi, G. B., & Mele, A. (2024). Unveiling the transport properties of protic ionic liquids: Lithium ion dynamics modulated by the anion fluorine reservoir. *Electrochimica Acta*, 475(November 2023).

https://doi.org/10.1016/j.electacta.2023.143598

Limited, systronics I. (2008). Manufacturers of electronic instruments and scientific equipments.

Nikiforidis, G., Raghibi, M., Sayegh, A., & Anouti, M. (2021). Low-Concentrated Lithium Hexafluorophosphate Ternary-based Electrolyte for a Reliable and Safe NMC/Graphite Lithium-Ion Battery. *Journal of Physical Chemistry Letters*, *12*(7), 1911–1917. https://doi.org/10.1021/acs.jpclett.0c03736

Rana, S., Thakur, R. C., Kaur, H., Sharma, A., Sharma, R., Thakur, V., Singh, H., & Fatma, I. (2023). Investigating the Solvation Behavior of Some Lithium Salts in Binary Aqueous Mixtures of 1-Ethyl-3-methylimidazolium Tetrafluoroborate ([EMIM][BF4]) at Equidistant Temperatures (T = 298.15, 303.15, 308.15, 313.15, 318.15) K. *Journal of Chemical & Engineering Data*, 68(6), 1291–1304. https://doi.org/10.1021/acs.jced.3c00037

Scrosati, B., Hassoun, J., & Sun, Y. K. (2011). Lithium-ion batteries. A look into the future. *Energy and Environmental Science*, *4*, 3287–3295.

https://doi.org/10.1039/c1ee01388b

Shah, F. U., Gnezdilov, O. I., Gusain, R., & Filippov, A. (2017). Transport and Association of Ions in Lithium Battery Electrolytes Based on Glycol Ether Mixed with Halogen-Free Orthoborate Ionic Liquid. *Scientific Reports*, 7, 16340. https://doi.org/10.1038/s41598-017-16597-7

# Chapter 4 Results and Discussion

## SECTION-I

Thermodynamic, Acoustic and Conductance Measurements of LiOTf (Lithium trifluoromethanesulfonate) in aqueous TEGDME (Tetraethylene glycol dimethyl ether) and DME (1,2-dimethoxyethane) Solutions at different temperatures.

### 4.1 Section -I

### 4.1.1 Density and Acoustic measurements

The densities ( $\rho$ ) of LiOTf in an aqueous solution of DME as well as TEGDME with concentrations of glyme  $m=(0.01,\ 0.03\ \text{and}\ 0.05)\ \text{mol\cdot kg}^{-1}$  and LiOTf concentrations ranging from (0.05 to 0.30) mol·kg<sup>-1</sup> at T= (293.15, 298.15, 303.15, 308.15 and 313.15) K were ascertained in this study. **Tables 4.1** and **4.6** present the measured density and acoustic values.

### 4.1.2 Thermophysical parameters derived from Density measurements

**Table 4.1** shows the uprise of the density values of LiOTf as the concentration of Li salt in the aqueous solution of DME and aqueous TEGDME increases, but drops down when the temperature rises. Furthermore, with the increase in the concentration of DME, the density decreases whereas in the case of LiOTf in TEGDME, the density values increase with the concentration of the glyme.

### 4.1.3 Apparent molar volume

The apparent molar volume ( $V_{\phi}$ ) has been determined by utilizing the equation (1.13). In this equation M and m<sub>A</sub> denote the molar mass (kg·mol<sup>-1</sup>) and molality of LiOTf correspondingly, and  $\rho_{\theta}$  and  $\rho$  denote the densities (kg·m<sup>-3</sup>) of solvent and solution. The resulting apparent molar volume values are presented in **Table 4.1**(Pradhan & Singh, 2024). In both cases, the  $V_{\phi}$  values increase with rising temperature, which can be attributed primarily to thermal expansion effects rather than changes in solute-solvent affinity. It is evident from data analysis that  $V_{\phi}$  values are larger at higher temperatures because there is a greater thermal movement of molecules at higher temperatures, which results in an increase in volume. Moreover, the values of  $V_{\phi}$  increase as the concentration of Li salt in the ternary solution (LiOTf + Water+ DME/ TEGDME) increases. It was found that the density values for LiOTf decrease as the concentration of DME increases, while the density values increase for increasing concentrations of TEGDME. **Figure 4.1** includes the diagrammatic representation of  $V_{\phi}$  of LiOTf in 0.01 mol.kg<sup>-1</sup> and 0.05 mol.kg<sup>-1</sup> in (a) aqueous DME solution and (b) aqueous TEGDME solution at T = (293.15, 298.15, 303.15, 308.15, and 313.15) K.

**Table 4.1:** The molality, densities ( $\rho$ ), apparent molar volumes ( $V_{\phi}$ ) of LiOTf in aqueous DME and aqueous TEGDME solutions at various temperatures, P = 0.1 MPa.

| <sup>a</sup> m <sub>A</sub> / | $ ho \times 10^{-3} / (\text{kg} \cdot \text{m}^{-3})$ |          |          |            |                         |          | $V_{\phi} \times 10^6 / (\mathrm{m}^3 \cdot \mathrm{mol}^{-1})$ |          |          |          |  |  |
|-------------------------------|--|----------|----------|------------|-------------------------|----------|---|----------|----------|----------|--|--|
| (mol·kg-1)                    | T=293.15   | T=298.15 | T=303.15 | T=308.15   | T=313.15                | T=293.15 | T=298.15  | T=303.15 | T=308.15 | T=313.15 |  |  |
|                               | K  | K        | K        | K          | K                       | K        | K   | K        | K        | K        |  |  |
|                               |  |          |          | LiOTf+ 0.0 | 01 mol·kg <sup>-1</sup> | DME      |   |          |          |          |  |  |
| 0.00000                       | 0.998273   | 0.996680 | 0.995411 | 0.993617   | 0.992051                |          |   |          |          |          |  |  |
| 0.04999                       | 1.002167   | 1.000548 | 0.999246 | 0.997421   | 0.995825                | 78.13    | 78.41   | 78.85    | 79.21    | 79.59    |  |  |
| 0.09983                       | 1.006050   | 1.004406 | 1.003070 | 1.001214   | 0.999588                | 78.43    | 78.70   | 79.15    | 79.50    | 79.88    |  |  |
| 0.14999                       | 1.009957   | 1.008288 | 1.006918 | 1.005031   | 1.003375                | 78.73    | 79.00   | 79.45    | 79.79    | 80.16    |  |  |
| 0.19951                       | 1.013815   | 1.012120 | 1.010717 | 1.008800   | 1.007114                | 79.03    | 79.29   | 79.74    | 80.08    | 80.44    |  |  |
| 0.24983                       | 1.017735   | 1.016015 | 1.014578 | 1.012629   | 1.010913                | 79.33    | 79.58   | 80.03    | 80.37    | 80.73    |  |  |
| 0.29986                       | 1.021632   | 1.019886 | 1.018416 | 1.016436   | 1.014690                | 79.62    | 79.87   | 80.32    | 80.65    | 81.01    |  |  |

|         |          |          |          | LiOTf+ 0.  | 03 mol·kg <sup>-1</sup> I | OME   |       |       |       |       |
|---------|----------|----------|----------|------------|---------------------------|-------|-------|-------|-------|-------|
| 0.00000 | 0.997518 | 0.996162 | 0.994835 | 0.992985   | 0.991648                  |       |       |       |       |       |
| 0.04993 | 1.001410 | 1.000032 | 0.998679 | 0.996799   | 0.995437                  | 77.97 | 78.19 | 78.50 | 78.81 | 79.11 |
| 0.09855 | 1.005200 | 1.003801 | 1.002424 | 1.000515   | 0.999128                  | 78.26 | 78.49 | 78.79 | 79.10 | 79.39 |
| 0.14993 | 1.009205 | 1.007783 | 1.006380 | 1.004440   | 1.003028                  | 78.57 | 78.79 | 79.09 | 79.40 | 79.69 |
| 0.19831 | 1.012976 | 1.011533 | 1.010105 | 1.008136   | 1.006700                  | 78.86 | 79.08 | 79.37 | 79.68 | 79.97 |
| 0.24855 | 1.016893 | 1.015427 | 1.013974 | 1.011974   | 1.010513                  | 79.15 | 79.37 | 79.67 | 79.97 | 80.26 |
| 0.29962 | 1.020873 | 1.019386 | 1.017906 | 1.015876   | 1.014389                  | 79.45 | 79.67 | 79.96 | 80.26 | 80.55 |
|         |          |          |          | LiOTf+ 0.0 | 05 mol·kg <sup>-1</sup> l | OME   |       |       |       |       |
| 0.00000 | 0.996974 | 0.995741 | 0.994188 | 0.992591   | 0.990711                  |       |       |       |       |       |
| 0.04979 | 1.000908 | 0.999650 | 0.998071 | 0.996450   | 0.994542                  | 76.83 | 77.12 | 77.40 | 77.64 | 77.90 |
| 0.09983 | 1.004861 | 1.003578 | 1.001974 | 1.000328   | 0.998393                  | 77.14 | 77.44 | 77.71 | 77.95 | 78.20 |
| 0.14981 | 1.008809 | 1.007501 | 1.005872 | 1.004201   | 1.002239                  | 77.45 | 77.74 | 78.01 | 78.25 | 78.50 |
| 0.20215 | 1.012944 | 1.011610 | 1.009953 | 1.008257   | 1.006266                  | 77.77 | 78.06 | 78.33 | 78.56 | 78.81 |
| 0.24599 | 1.016407 | 1.015051 | 1.013373 | 1.011655   | 1.009640                  | 78.04 | 78.33 | 78.59 | 78.82 | 79.07 |
| 0.29951 | 1.020635 | 1.019253 | 1.017547 | 1.015803   | 1.013758                  | 78.36 | 78.65 | 78.91 | 79.14 | 79.38 |

## LiOTf+ 0.01 mol·kg<sup>-1</sup> TEGDME

| 0.00000 | 0.998601 | 0.997162 | 0.995575 | 0.993951   | 0.992427                |       |       |       |       |       |
|---------|----------|----------|----------|------------|-------------------------|-------|-------|-------|-------|-------|
| 0.04995 | 1.002542 | 1.001083 | 0.999476 | 0.997832   | 0.996287                | 77.19 | 77.36 | 77.51 | 77.66 | 77.83 |
| 0.09981 | 1.006476 | 1.004997 | 1.003370 | 1.001707   | 1.000142                | 77.50 | 77.67 | 77.82 | 77.96 | 78.13 |
| 0.14972 | 1.010414 | 1.008915 | 1.007268 | 1.005584   | 1.003999                | 77.80 | 77.97 | 78.12 | 78.26 | 78.43 |
| 0.19867 | 1.014276 | 1.012757 | 1.011091 | 1.009387   | 1.007782                | 78.10 | 78.27 | 78.41 | 78.55 | 78.72 |
| 0.24314 | 1.017784 | 1.016248 | 1.014564 | 1.012843   | 1.011219                | 78.37 | 78.54 | 78.68 | 78.82 | 78.98 |
| 0.29987 | 1.022261 | 1.020702 | 1.018995 | 1.017251   | 1.015604                | 78.71 | 78.87 | 79.02 | 79.15 | 79.32 |
|         |          |          | L        | iOTf+ 0.03 | mol·kg <sup>-1</sup> TE | GDME  |       |       |       |       |
| 0.00000 | 0.999412 | 0.997889 | 0.996373 | 0.994742   | 0.993179                |       |       |       |       |       |
| 0.04992 | 1.003345 | 1.001797 | 1.000257 | 0.998598   | 0.997010                | 77.42 | 77.68 | 77.94 | 78.23 | 78.50 |
| 0.10109 | 1.007378 | 1.005805 | 1.004238 | 1.002551   | 1.000937                | 77.73 | 77.99 | 78.25 | 78.54 | 78.81 |
| 0.14978 | 1.011215 | 1.009617 | 1.008026 | 1.006313   | 1.004673                | 78.03 | 78.28 | 78.54 | 78.83 | 79.09 |
| 0.19995 | 1.015168 | 1.013545 | 1.011929 | 1.010188   | 1.008523                | 78.33 | 78.58 | 78.84 | 79.12 | 79.39 |
| 0.24328 | 1.018583 | 1.016938 | 1.015300 | 1.013536   | 1.011848                | 78.59 | 78.84 | 79.09 | 79.38 | 79.64 |
| 0.29950 | 1.023013 | 1.021340 | 1.019674 | 1.017878   | 1.016163                | 78.93 | 79.17 | 79.42 | 79.71 | 79.96 |

LiOTf+ 0.05 mol·kg<sup>-1</sup> TEGDME

| 0.00000 | 1.000032 | 0.998702 | 0.997111 | 0.995511 | 0.993876 |       |       |       |       |       |
|---------|----------|----------|----------|----------|----------|-------|-------|-------|-------|-------|
| 0.04997 | 1.003930 | 1.002574 | 1.000955 | 0.999328 | 0.997666 | 78.31 | 78.60 | 78.90 | 79.20 | 79.50 |
| 0.09987 | 1.007822 | 1.006442 | 1.004795 | 1.003141 | 1.001451 | 78.61 | 78.90 | 79.20 | 79.50 | 79.79 |
| 0.14993 | 1.011727 | 1.010322 | 1.008647 | 1.006966 | 1.005248 | 78.91 | 79.19 | 79.49 | 79.79 | 80.08 |
| 0.19738 | 1.015428 | 1.013999 | 1.012299 | 1.010591 | 1.008848 | 79.19 | 79.47 | 79.76 | 80.06 | 80.35 |
| 0.24978 | 1.019515 | 1.018060 | 1.016331 | 1.014595 | 1.012822 | 79.50 | 79.78 | 80.07 | 80.36 | 80.65 |
| 0.29955 | 1.023397 | 1.021917 | 1.020160 | 1.018397 | 1.016597 | 79.79 | 80.06 | 80.35 | 80.64 | 80.93 |

 $<sup>^</sup>a\overline{m}_A$  denotes the molality of LiOTf in aqueous DME and aqueous TEGDME solution. Standard uncertainties in the molality of LiOTf  $u_r$  ( $m_A$ ) is 1%. Standard uncertainties in the molality of DME and TEGDME  $u_r$  is 1.5%. Standard uncertainty in density,  $u(\rho) = \pm 5 \times 10^{-3}$  kg·m<sup>-3</sup>, temperature, u(T) = 0.001 K, and pressure, u(p) = 0.01 MPa.

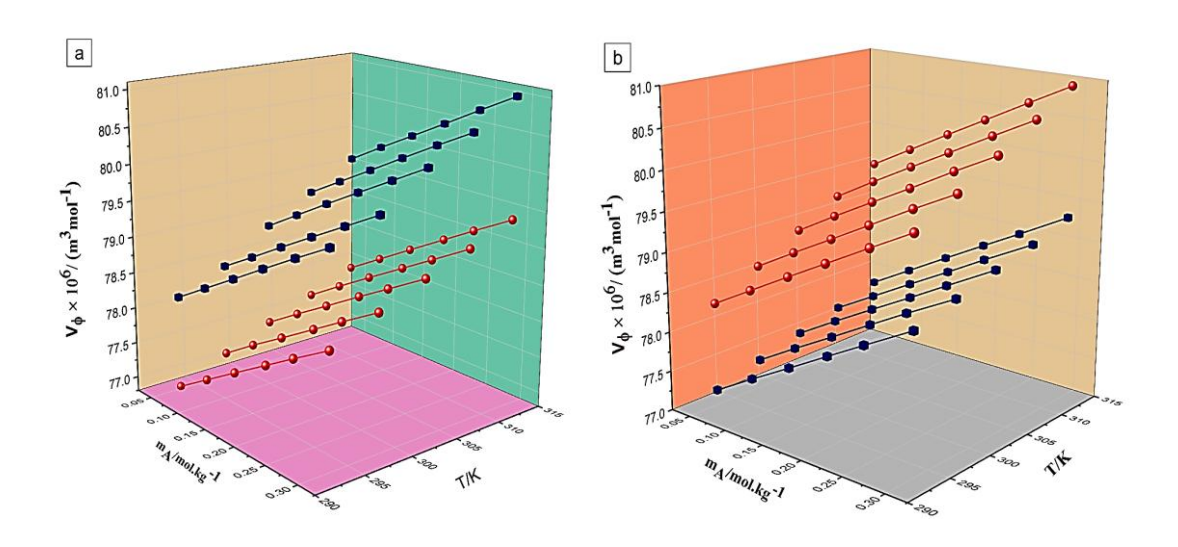


**Figure 4.1:** Plots of variation of apparent molar volume  $(V_{\phi})$  of LiOTf in 0.01 mol.kg<sup>-1</sup> (labelled as Blue) and 0.05 mol.kg<sup>-1</sup> (labelled as red) in (a) aqueous DME solution (b) aqueous TEGDME solution at T = (293.15 K, 298.15 K, 303.15 K, 308.15 K and 313.15 K...

### 4.1.4 Partial molar volume

The apparent molar volume at infinite dilution, also known as partial molar volume  $(V_{\phi}^{0})$ , was calculated utilizing Masson's least square fitting approach in equation 1.15. In this equation,  $V_{\phi}^{0}$  denotes partial molar volume.  $V_{\phi}^{0}$ , depicts the solute-solvent interactions, assuming that the solute molecules are apart at infinite dilution and hence no solute-solute interactions exist. The positive  $V_{\phi}^{0}$  (Table 4.2) proves the occurrence of solute-solvent interactions in ternary systems. The electrostriction, which decreases as the temperature increases, could be responsible for the increase of  $V_{\phi}^{0}$  values with temperature (Ravinder Sharma, Harsh Kumar, Meenu Singla, Vaneet Kumar, Abdullah A. Al-Kahtani, 2022). Some solvation molecules emerge solute's loose solvation layers and penetrate the bulk solution sequentially. The water molecules that enclose LiOTf are compressed by the electric field induced by their head groups. As a result, increased partial molar volume values in the ternary (LiOTf + H<sub>2</sub>O + DME/TEGDME) solutions indicate the prevalence of solute-solvent interactions(Rana et al., 2023a). Furthermore, in the case of Li salt in DME, the  $V_\phi^0$  values decrease with the increase in the concentration of the aqueous solvent. In contrast to this, the  $V_{\phi}^{0}$  values of LiOTf in TEGDME increase with the concentration of TEGDME.

**Table 4.2:** Partial molar volumes,  $(V_{\phi}^{0})$  of LiOTf in aqueous DME and aqueous TEGDME solutions at various temperatures.

| $V_{\phi}^0 \times 10^6/(\mathrm{m}^3 \cdot \mathrm{mol}^{-1})$ |  |  |  |  |  |  |  |  |
|---|--|--|--|--|--|--|--|--|
| T=293.15 K  | T=298.15 K   | T=303.15 K   | T=308.15 K   | T=313.15 K   |  |  |  |  |
| LiOTf in Aqueous DME  |  |  |  |  |  |  |  |  |
| 80.44   | 79.85  | 79.34  | 78.59  | 77.89  |  |  |  |  |
| $(\pm 0.003)$   | $(\pm 0.006)$  | $(\pm 0.003)$  | $(\pm 0.003)$  | $(\pm 0.013)$  |  |  |  |  |
| 77.84   | 78.12  | 78.56  | 78.93  | 79.31  |  |  |  |  |
| $(\pm 0.003)$   | $(\pm 0.003)$  | $(\pm 0.006)$  | $(\pm 0.003)$  | $(\pm 0.003)$  |  |  |  |  |
| 77.67   | 77.90  | 78.21  | 78.53  | 78.83  |  |  |  |  |
| (±0.003)  | $(\pm 0.003)$  | $(\pm 0.003)$  | $(\pm 0.003)$  | $(\pm 0.003)$  |  |  |  |  |
| 76.53   | 76.82  | 77.11  | 77.35  | 77.61  |  |  |  |  |
| $(\pm 0.003)$   | $(\pm 0.006)$  | $(\pm 0.003)$  | $(\pm 0.003)$  | $(\pm 0.003)$  |  |  |  |  |
| L   | iOTf in Aqueo  | us TEGDME  |  |  |  |  |  |  |
| 76.89   | 77.06  | 77.22  | 77.36  | 77.54  |  |  |  |  |
| $(\pm 0.003)$   | $(\pm 0.003)$  | $(\pm 0.003)$  | $(\pm 0.003)$  | $(\pm 0.003)$  |  |  |  |  |
| 77.12   | 77.38  | 77.64  | 77.94  | 78.21  |  |  |  |  |
| $(\pm 0.003)$   | $(\pm 0.003)$  | $(\pm 0.003)$  | $(\pm 0.003)$  | $(\pm 0.003)$  |  |  |  |  |
| 78.01   | 78.31  | 78.61  | 78.92  | 79.22  |  |  |  |  |
| $(\pm 0.003)$   | $(\pm 0.003)$  | $(\pm 0.003)$  | $(\pm 0.003)$  | $(\pm 0.003)$  |  |  |  |  |
|   | 80.44<br>(±0.003)<br>77.84<br>(±0.003)<br>77.67<br>(±0.003)<br>76.53<br>(±0.003)<br>II<br>76.89<br>(±0.003)<br>77.12<br>(±0.003) | T=293.15 K LiOTf in Aqu 80.44 79.85  (±0.003) (±0.006)  77.84 78.12  (±0.003) (±0.003)  77.67 77.90 (±0.003) (±0.003)  76.53 76.82  (±0.003) (±0.006)  LiOTf in Aqueo  76.89 77.06  (±0.003) (±0.003)  77.12 77.38  (±0.003) (±0.003)  78.01 78.31 | T=293.15 K         T=298.15 K         T=303.15 K           80.44         79.85         79.34           (±0.003)         (±0.006)         (±0.003)           77.84         78.12         78.56           (±0.003)         (±0.003)         (±0.006)           77.67         77.90         78.21           (±0.003)         (±0.003)         (±0.003)           76.53         76.82         77.11           (±0.003)         (±0.006)         (±0.003)           LiOTf in Aqueous TEGDME           76.89         77.06         77.22           (±0.003)         (±0.003)         (±0.003)           77.12         77.38         77.64           (±0.003)         (±0.003)         (±0.003)           78.01         78.31         78.61 | T=293.15 K         T=298.15 K         T=303.15 K         T=308.15 K           LiOTf in Aqueous DME $80.44$ $79.85$ $79.34$ $78.59$ ( $\pm 0.003$ )         ( $\pm 0.006$ )         ( $\pm 0.003$ )         ( $\pm 0.003$ )         ( $\pm 0.003$ ) $77.84$ $78.12$ $78.56$ $78.93$ ( $\pm 0.003$ )         ( $\pm 0.006$ )         ( $\pm 0.003$ )         ( $\pm 0.003$ ) $77.67$ $77.90$ $78.21$ $78.53$ ( $\pm 0.003$ )         ( $\pm 0.003$ )         ( $\pm 0.003$ )         ( $\pm 0.003$ ) $76.53$ $76.82$ $77.11$ $77.35$ ( $\pm 0.003$ )         ( $\pm 0.003$ )         ( $\pm 0.003$ )         ( $\pm 0.003$ )           LiOTf in Aqueous TEGDME $76.89$ $77.06$ $77.22$ $77.36$ ( $\pm 0.003$ )         ( $\pm 0.003$ )         ( $\pm 0.003$ )         ( $\pm 0.003$ )         ( $\pm 0.003$ ) $77.12$ $77.38$ $77.64$ $77.94$ ( $\pm 0.003$ )         ( $\pm 0.003$ )         ( $\pm 0.003$ )         ( $\pm 0.003$ ) $78.01$ $78.31$ $78.61$ $78.92$ |  |  |  |  |

 $<sup>^{</sup>a}m_{\textrm{B}}$  is the molality of aqueous DME and aqueous TEGDME solution.

The partial molar volume of transfer,  $\Delta V_{\phi}^{0}$  of LiOTf from water to aqueous solvent (DME/TEGDME), at infinite dilution, have been evaluated by employing the equation 1.18.

 $\Delta V_{\phi}^{0}$  values given in Table 4.3 signifies solute-solvent interactions particularly, thus the contribution from solute-solute interactions is considered to be negligible. Co-sphere overlap model is useful in predicting the possibility of shrinkage or expansion in the volume as a consequence of solute-solvent interactions(Gaba *et al.*, 2019). The negative values of the transfer volumes at lower temperatures suggest that hydrophobic-hydrophobic interactions are predominant attributable to the increase in the electrostriction. Whereas at elevated temperatures, ion-ion interactions are significant as here higher  $\Delta V_{\phi}^{0}$  values are observed because the H<sub>2</sub>O molecules earlier existing near hydrophilic centres are now discharged to the bulk that is highly compressible in comparison to the electrostricted region.

**Table 4.3.** Partial molar volume of transfer,  $\Delta V_{\phi}^{0} \times 10^{6} / (\text{m}^{3} \, \text{mol}^{-1})$  of LiOTf in aqueous DME and aqueous TEGDME solutions at various temperatures.

| <sup>a</sup> m <sub>B</sub> | $\Delta V_{m{\phi}}^0$ |              |             |            |            |  |  |  |  |
|-----------------------------|------------------------|--------------|-------------|------------|------------|--|--|--|--|
| (mol·kg <sup>-1</sup> )     | T=293.15 K             | T=298.15 K   | T=303.15 K  | T=308.15 K | T=313.15 K |  |  |  |  |
| LiOTf in Aqueous DME        |                        |              |             |            |            |  |  |  |  |
| 0.01                        | -2.60                  | -1.73        | -0.78       | 0.34       | 1.42       |  |  |  |  |
| 0.03                        | -2.77                  | -1.95        | -1.14       | -0.06      | 0.93       |  |  |  |  |
| 0.05                        | -3.91                  | -3.04        | -2.24       | -1.24      | -0.28      |  |  |  |  |
|                             |                        | LiOTf in Aqu | eous TEGDMI | E          |            |  |  |  |  |
| 0.01                        | -3.55                  | -2.79        | -2.13       | -1.23      | -0.35      |  |  |  |  |
| 0.03                        | -3.32                  | -2.48        | -1.70       | -0.65      | 0.32       |  |  |  |  |
| 0.05                        | -2.43                  | -1.55        | -0.73       | 0.33       | 1.33       |  |  |  |  |

<sup>&</sup>lt;sup>a</sup>m<sub>B</sub> is molality of aqueous DME and aqueous TEGDME solution.

### 4.1.5 Temperature dependence of partial molar volume

Temperature has a significant impact on the interactions in a system. The influence of temperature on apparent molar volume ( $V_{\phi}^{0}$ ) (at infinite dilution) has been evaluated utilizing the polynomial equation 1.19. In this reaction,  $T_{\rm ref}$  is reference temperature (298.15 K), whereas the empirical constants are a, b and c. **Table 4.4** enlists the values of these empirical constants. Apart from c at  $m_{\rm DME} = 0.05$  mol·kg<sup>-1</sup> and  $m_{\rm TEGDME} = 0.01$  mol·kg<sup>-1</sup> for LiOTf wherein empirical constant c has minor negative values, and all empirical constants are positive (Kumar, 2016).

**Table 4.4:** Values of empirical parameters determined from Eq. (1.13) for LiOTf in aqueous DME and aqueous TEGDME.

| amB / (mol·kg-1)     | a×10 <sup>6</sup> / (mol·kg <sup>-1</sup> ) | b ×10 <sup>6</sup> / (m <sup>3</sup> ·mol <sup>-1</sup> ·K) | c×10 <sup>6</sup> /(m <sup>3</sup> ·mol <sup>-1</sup> ·K <sup>-2</sup> ) | R <sup>2</sup> | ARD(σ) |  |  |  |  |  |
|----------------------|---|---|--|----------------|--------|--|--|--|--|--|
| LiOTf in Aqueous DME |   |   |  |                |        |  |  |  |  |  |
| 0.01                 | 78.17                                       | 0.071   | 0.0003   | 0.9999         | 0.0013 |  |  |  |  |  |
| 0.03                 | 77.92                                       | 0.054   | 0.0004   | 0.9999         | 0.0007 |  |  |  |  |  |
| 0.05                 | 76.82                                       | 0.056   | -0.0003  | 0.9999         | 0.0003 |  |  |  |  |  |
|                      |   | LiOTf in Aqueo  | ous TEGDME   |                |        |  |  |  |  |  |
| 0.01                 | 77.05                                       | 0.032   | -0.00001   | 0.9999         | 0.0003 |  |  |  |  |  |
| 0.03                 | 77.38                                       | 0.053   | 0.0002   | 0.9999         | 0.0003 |  |  |  |  |  |
| 0.05                 | 78.31                                       | 0.06  | 0.0001   | 0.9999         | 0.0001 |  |  |  |  |  |

<sup>&</sup>lt;sup>a</sup>m<sub>B</sub> is the molality of aqueous DME and aqueous TEGDME solution.

The experimental values of  $V_{\phi}^{0}$  deviate from the theoretical values. The ARD  $(\sigma)$  deviations could be determined by using the equation 1.20 where,  $(Y = V_{\phi}^{0})$ . **Table 4.4** summarizes the ARD data, demonstrating a strong fit to the experimental data for the ternary compositions studied. Furthermore, partial molar expansibilities,  $\phi_{E}^{0}$ , were used to confirm the presence of solute-solvent interactions in the mixtures under study by utilizing the equation (1.21). For all quantities of DME and experimental

temperatures, the positive partial molar expansibilities (given in **Table 4.5**) are consistent with the expected thermal expansion behaviour of the solution as temperature increases and should not be directly interpreted as evidence of unusual solute-solvent interactions.

Additionally, the packing effect phenomena verifies the occurrence of substantial interactions between LiOTf and DME as well as LiOTf in TEGDME with the reported positive values of,  $\phi_E^0$ . In a mixed solvent solution, the Hepler constant contributes to evaluating the solute's potential to function as a structure breaker/maker. Hepler's thermodynamic equation is found in equation 1.22(Hepler, 1969). Positive & negative values of  $(\partial \phi_E^0/\partial T)_P$  has been reported for the ternary systems investigated for (LiOTf + H<sub>2</sub>O + DME) (given in **Table 4.5**). The sign of  $(\partial \phi_E^0/\partial T)$  could be used to evaluate the function of a solute as a structure maker/breaker(Kumar *et al.*, 2019)(Raheem *et al.*, 2023). Structure makers have positive values of  $(\partial \phi_E^0/\partial T)$  and minor negative values of  $(\partial \phi_E^0/\partial T)$ , while structure breaker solutes have negative values. In aqueous solution,  $m_{DME/TEGDME} = (0.01, 0.03, \text{ and } 0.05) \text{ molkg}^{-1}$ , LiOTf behaves as structure makers.

**Table 4.5:** Limiting apparent molar expansibilities  $(\phi_E^0)$  of LiOTf in aqueous solution of DME and aqueous TEGDME solutions at various temperatures.

| <sup>a</sup> m <sub>B</sub> / |            | $\phi_E^0 	imes 10$                       | 0 <sup>6</sup> /(m <sup>3</sup> ·mol <sup>-1</sup> ·m | ıol <sup>-1</sup> •K <sup>-1</sup> ) |        | $(\partial \phi_E^0 / \partial \mathbf{T})$ |  |  |  |  |  |
|-------------------------------|------------|---|---|--------------------------------------|--------|---|--|--|--|--|--|
| (mol·kg <sup>-1</sup> )       | T=293.15 K | 293.15 K T=298.15 K T=303.15 K T=308.15 K |   | T=313.15 K                           | _      |   |  |  |  |  |  |
| LiOTf in Aqueous DME          |            |   |   |                                      |        |   |  |  |  |  |  |
| 0.01                          | 0.0680     | 0.0714                                    | 0.0748  | 0.0782                               | 0.0816 | 0.00068                                     |  |  |  |  |  |
| 0.03                          | 0.0501     | 0.0544                                    | 0.0587  | 0.0629                               | 0.0672 | 0.00086                                     |  |  |  |  |  |
| 0.05                          | 0.0594     | 0.0566                                    | 0.0538  | 0.0510                               | 0.0482 | -0.00056                                    |  |  |  |  |  |
|                               |            | LiOTf i                                   | n Aqueous TEO   | GDME                                 |        |   |  |  |  |  |  |
| 0.01                          | 0.0320     | 0.0319                                    | 0.0318  | 0.0317                               | 0.0316 | -0.00002                                    |  |  |  |  |  |
| 0.03                          | 0.0519     | 0.0535                                    | 0.0550  | 0.0566                               | 0.0581 | 0.00031                                     |  |  |  |  |  |
| 0.05                          | 0.0596     | 0.0601                                    | 0.0606  | 0.0610                               | 0.0615 | 0.00010                                     |  |  |  |  |  |

<sup>a</sup>m<sub>B</sub> is the molality of aqueous DME and aqueous TEGDME solution.

# 4.1.6 Acoustic parameters derived from the speed of sound (acoustic) measurements

Acoustic measurements give valuable information about the solution's physical properties and interactions. **Table 4.6** shows the sound speed of LiOTf in  $m_{DME/TEGDME} = (0.01, 0.03 \text{ and } 0.05) \text{ mol·kg}^{-1}$  of aqueous solutions at above specified temperatures.

#### 4.1.7 Apparent molar isentropic compressibility:

The apparent molar isentropic compressibility  $(K_{\phi,s})$  can be determined by utilizing the equation 1.23 where  $\kappa_S$  denotes solution isentropic compressibility and  $\kappa_{S,0}$ denotes pure solvent isentropic compressibility. The molality of the solute is m<sub>A</sub>, the molar mass of LiOTf (solute) is M, and the density values of the solute and solvent are  $\rho$  and  $\rho_0$  correspondingly.  $\kappa_S$  can be calculated using Laplace Newton's equation (equation 1.24) where u and  $\rho$  refers to the density and acoustic values of the given solution. The values of  $K_{\phi,s}$  determined employing (equation 1.23) have been indexed in **Table 4.6**. $K_{\phi,s}$  is negative at all the aqueous DME and aqueous TEGDME concentrations and temperatures. As the molality of the LiOTf as well as DME and TEGDME increases and the temperature increases, the  $K_{\phi,s}$  values of LiOTf ascent. Furthermore, as the concentration of solvent increased,  $K_{\phi,s}$  decreases. The occurrence of solute-solvent interactions is confirmed by the negative  $K_{\phi,s}$  values. Negative values of  $K_{\phi,s}$  indicate that H<sub>2</sub>O molecules in the bulk solution are much more deformable than those near the solute. Because of the charge on ions, the electrostricted H<sub>2</sub>O molecules are mainly compacted. The electrostriction reduces as the temperature rises, and some H<sub>2</sub>O molecules are discharged from the hydration sphere and into the bulk solution, resulting in less conformational distortion of the water and showing a reduced regulating influence by the solute on the solvent. As  $V_{\phi}^{0}$  is defined at infinite dilution, it reflects solute-solvent interactions in the absence of significant solute-solute interactions. Therefore, the observed  $V_{\phi}^{0}$  values confirm the typical behavior expected in such dilute systems(Gerald R. Van Hecke, Oliver W. M. Baldwin, 2022a).

**Table 4.6:** Values of ultrasonic speed, (u) and apparent molar isentropic compressibility,  $(K_{\phi,s})$  of LiOTf in aqueous DME and aqueous TEGDME solution at various temperatures, P = 0.1 MPa.

| <sup>a</sup> m <sub>A</sub> / |          |          | u / (m·s <sup>-1</sup> )  |            |            |          |          |          |          |          |
|-------------------------------|----------|----------|---------------------------|------------|------------|----------|----------|----------|----------|----------|
| (mol·kg-1)                    | T=293.15 | T=298.15 | F298.15 T=303.15 T=308.15 |            | T=313.15   | T=293.15 | T=298.15 | T=303.15 | T=308.15 | T=313.15 |
|                               | K        | K        | K                         | K          | K          | K        | K        | K        | K        | K        |
|                               |          |          | Ι                         | iOTf+ 0.01 | mol·kg-1 D | ME       |          |          |          |          |
| 0.00000                       | 1483.54  | 1497.11  | 1509.66                   | 1520.66    | 1529.20    |          |          |          |          |          |
| 0.04999                       | 1484.81  | 1498.23  | 1510.64                   | 1521.49    | 1529.90    | -15.87   | -13.26   | -10.81   | -8.52    | -6.43    |
| 0.09983                       | 1486.09  | 1499.34  | 1511.61                   | 1522.32    | 1530.59    | -15.96   | -13.37   | -10.91   | -8.62    | -6.55    |
| 0.14999                       | 1487.37  | 1500.47  | 1512.59                   | 1523.15    | 1531.29    | -16.07   | -13.48   | -11.03   | -8.74    | -6.68    |
| 0.19951                       | 1488.63  | 1501.57  | 1513.56                   | 1523.98    | 1531.99    | -16.17   | -13.59   | -11.14   | -8.86    | -6.81    |
| 0.24983                       | 1489.91  | 1502.70  | 1514.54                   | 1524.82    | 1532.69    | -16.28   | -13.70   | -11.26   | -8.98    | -6.93    |
| 0.29986                       | 1491.19  | 1503.82  | 1515.52                   | 1525.65    | 1533.39    | -16.38   | -13.81   | -11.37   | -9.10    | -7.05    |

|         | LiOTf+ 0.03 mol·kg <sup>-1</sup> DME |         |         |            |            |        |       |       |       |       |  |  |
|---------|--------------------------------------|---------|---------|------------|------------|--------|-------|-------|-------|-------|--|--|
| 0.00000 | 1484.68                              | 1498.35 | 1510.19 | 1520.69    | 1529.69    |        |       |       |       |       |  |  |
| 0.04993 | 1485.43                              | 1499.02 | 1510.78 | 1521.20    | 1530.12    | -9.38  | -8.03 | -6.47 | -5.11 | -3.73 |  |  |
| 0.09855 | 1486.15                              | 1499.68 | 1511.35 | 1521.70    | 1530.53    | -9.53  | -8.16 | -6.60 | -5.24 | -3.86 |  |  |
| 0.14993 | 1486.92                              | 1500.37 | 1511.95 | 1522.22    | 1530.97    | -9.66  | -8.28 | -6.73 | -5.37 | -3.99 |  |  |
| 0.19831 | 1487.64                              | 1501.02 | 1512.51 | 1522.72    | 1531.39    | -9.79  | -8.40 | -6.85 | -5.49 | -4.11 |  |  |
| 0.24855 | 1488.39                              | 1501.70 | 1513.10 | 1523.23    | 1531.82    | -9.91  | -8.53 | -6.98 | -5.62 | -4.24 |  |  |
| 0.29962 | 1489.15                              | 1502.39 | 1513.70 | 1523.76    | 1532.25    | -10.04 | -8.65 | -7.10 | -5.74 | -4.37 |  |  |
|         |                                      |         | L       | iOTf+ 0.05 | mol·kg-1 D | ME     |       |       |       |       |  |  |
| 0.00000 | 1485.96                              | 1499.43 | 1512.31 | 1521.74    | 1530.81    |        |       |       |       |       |  |  |
| 0.04979 | 1486.51                              | 1499.92 | 1512.74 | 1522.09    | 1531.09    | -7.98  | -6.80 | -5.57 | -4.25 | -3.00 |  |  |
| 0.09983 | 1487.06                              | 1500.42 | 1513.17 | 1522.44    | 1531.37    | -8.11  | -6.92 | -5.69 | -4.37 | -3.14 |  |  |
| 0.14981 | 1487.60                              | 1500.91 | 1513.60 | 1522.79    | 1531.64    | -8.23  | -7.05 | -5.81 | -4.50 | -3.26 |  |  |
| 0.20215 | 1488.18                              | 1501.43 | 1514.05 | 1523.16    | 1531.94    | -8.36  | -7.18 | -5.94 | -4.63 | -3.40 |  |  |
| 0.24599 | 1488.66                              | 1501.86 | 1514.43 | 1523.47    | 1532.18    | -8.47  | -7.28 | -6.05 | -4.73 | -3.50 |  |  |
| 0.29951 | 1489.25                              | 1502.39 | 1514.89 | 1523.84    | 1532.48    | -8.59  | -7.41 | -6.17 | -4.86 | -3.63 |  |  |

## LiOTf+ 0.01 mol·kg<sup>-1</sup> TEGDME

| 0.00000 | 1484.54                                 | 1497.38 | 1509.6  | 1521.1  | 1530.70 |        |        |        |       |       |  |
|---------|---|---------|---------|---------|---------|--------|--------|--------|-------|-------|--|
| 0.04995 | 1485.76                                 | 1498.42 | 1510.37 | 1521.60 | 1531.10 | -16.13 | -13.26 | -9.84  | -6.61 | -3.36 |  |
| 0.09981 | 1486.98                                 | 1499.46 | 1511.15 | 1522.10 | 1531.50 | -16.19 | -13.38 | -9.97  | -6.73 | -3.51 |  |
| 0.14972 | 1488.20                                 | 1500.51 | 1511.92 | 1522.60 | 1531.89 | -16.29 | -13.50 | -10.09 | -6.85 | -3.64 |  |
| 0.19867 | 1489.40                                 | 1501.53 | 1512.68 | 1523.09 | 1532.28 | -16.38 | -13.61 | -10.20 | -6.97 | -3.77 |  |
| 0.24314 | 1490.49                                 | 1502.46 | 1513.37 | 1523.53 | 1532.64 | -16.47 | -13.71 | -10.30 | -7.08 | -3.88 |  |
| 0.29987 | 1491.88                                 | 1503.64 | 1514.25 | 1524.10 | 1533.09 | -16.58 | -13.83 | -10.43 | -7.21 | -4.02 |  |
|         | LiOTf+ 0.03 mol·kg <sup>-1</sup> TEGDME |         |         |         |         |        |        |        |       |       |  |
| 0.00000 | 1487.46                                 | 1499.90 | 1511.73 | 1522.89 | 1532.40 |        |        |        |       |       |  |
| 0.04992 | 1488.63                                 | 1501.20 | 1512.54 | 1523.46 | 1532.72 | -16.06 | -12.93 | -9.78  | -6.32 | -2.98 |  |
| 0.10109 | 1489.84                                 | 1502.53 | 1513.38 | 1524.05 | 1533.04 | -16.12 | -13.08 | -9.87  | -6.49 | -3.15 |  |
| 0.14978 | 1490.98                                 | 1503.80 | 1514.18 | 1524.61 | 1533.35 | -16.22 | -13.20 | -9.98  | -6.62 | -3.29 |  |
| 0.19995 | 1492.16                                 | 1505.10 | 1514.99 | 1525.18 | 1533.66 | -16.32 | -13.31 | -10.09 | -6.75 | -3.42 |  |
| 0.24328 | 1493.18                                 | 1506.23 | 1515.70 | 1525.68 | 1533.94 | -16.40 | -13.40 | -10.19 | -6.86 | -3.53 |  |
| 0.29950 | 1494.50                                 | 1507.69 | 1516.62 | 1526.32 | 1534.29 | -16.51 | -13.52 | -10.32 | -6.99 | -3.67 |  |
|         |   |         |         |         |         |        |        |        |       |       |  |

### LiOTf+ 0.05 mol·kg<sup>-1</sup> TEGDME

| 0   | 0.00000 | 1490.09 | 1502.85 | 1513.73 | 1524.89 | 1534.71 |        |        |       |       |       |
|-----|---------|---------|---------|---------|---------|---------|--------|--------|-------|-------|-------|
| 0   | .04997  | 1491.31 | 1503.87 | 1514.56 | 1525.51 | 1534.99 | -14.86 | -11.87 | -8.94 | -6.05 | -2.91 |
| 0   | .09987  | 1492.53 | 1504.88 | 1515.38 | 1526.13 | 1535.28 | -14.99 | -11.95 | -9.10 | -6.21 | -3.08 |
| 0   | .14993  | 1493.75 | 1505.90 | 1516.21 | 1526.75 | 1535.56 | -15.11 | -12.05 | -9.24 | -6.35 | -3.23 |
| 0   | .19738  | 1494.91 | 1506.86 | 1517.00 | 1527.34 | 1535.83 | -15.21 | -12.15 | -9.36 | -6.47 | -3.36 |
| 0   | .24978  | 1496.19 | 1507.93 | 1517.87 | 1527.99 | 1536.13 | -15.33 | -12.27 | -9.49 | -6.61 | -3.49 |
| 0.2 | 29955   | 1497.41 | 1508.94 | 1518.69 | 1528.61 | 1536.41 | -15.43 | -12.38 | -9.61 | -6.73 | -3.62 |

 $<sup>^{</sup>a}$ m<sub>A</sub> denotes the molality of LiOTf in an aqueous DME medium and aqueous TEGDME solution. Standard uncertainties in the molality of LiOTf u<sub>r</sub> (m<sub>A</sub>) is 1%. Standard uncertainties in the molality of DME and TEGDME u<sub>r</sub> is 1.5%. Standard uncertainty in acoustic, u(u)= 0.5m·s<sup>-1</sup>, u(T) = 0.001 K, and pressure, u(p) = 0.01 MPa.

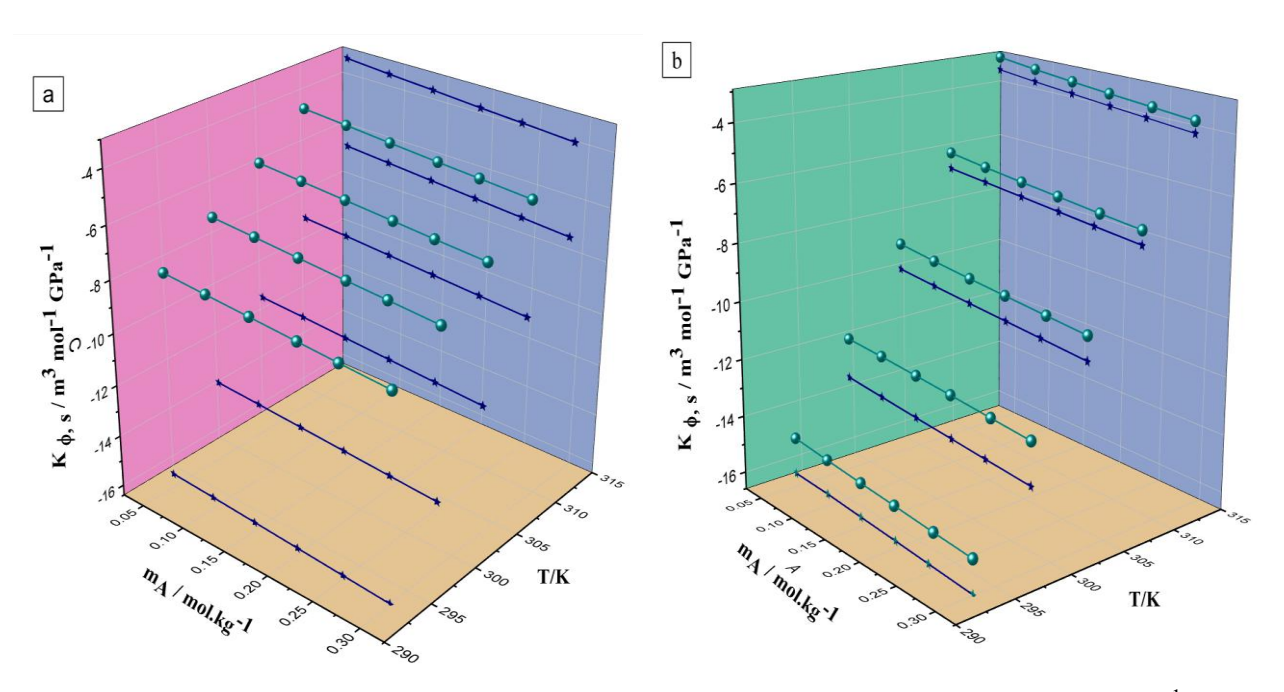


**Figure 4.2:** Plots of variation of apparent molar isentropic compressibility ( $K_{\phi,S}$ ) of LiOTf in 0.01 mol.kg<sup>-1</sup> (labelled as Blue) and 0.05 mol.kg<sup>-1</sup> (labelled as cyan) in (a) aqueous DME solution (b) aqueous TEGDME solution at T = (293.15 K, 298.15 K, 303.15 K, 308.15 K and 313.15 K)

#### 4.1.8 Partial molar isentropic compressibility:

 $^{a}m_{B}$  /

 $K_{\phi,s}^0$  (Partial molar isentropic compressibility) referred to as limiting molar isentropic compressibility, indicates the existence of (solute-solvent) interactions. The equation 1.25 used to calculate the variation of  $K_{\phi,s}^0$  with molality of solute. The molality of LiOTf utilized in an aqueous DME solution is denoted by  $m_A$ . **Table 4.7** shows the calculated values of  $K_{\phi,s}^0$  of the ternary systems. While raising the temperature,  $K_{\phi,s}^0$  lowers because water molecules are firmly bound to solute molecules at low temperatures, but as the temperature rises, the electrostriction between them reduces, and some  $H_2O$  molecules are discharged into the bulk solution. As a result, partial molar isentropic compressibility inference suggests that in this investigation, solute-solvent interactions are predominant (Sharma *et al.*, 2022).  $K_{\phi,s}^0$  deduces that the solvent molecules are bound to the solute molecules, which enhances the interactions between the ions.

**Table 4.7:** Partial molar isentropic compressibility,  $(K_{\phi,s}^0)$  of LiOTf in an aqueous solution of DME and aqueous TEGDME at various temperatures.

 $K_{\phi c}^{0} \times 10^{6}/(\text{m}^{3} \cdot \text{mol}^{-1} \cdot \text{GPa}^{-1})$ 

|                         |               | $\varphi$ ,s  | , (           | ·· )          |               |
|-------------------------|---------------|---------------|---------------|---------------|---------------|
| (mol·kg <sup>-1</sup> ) |               |               |               |               |               |
|                         | T=293.15 K    | T=298.15 K    | T=303.15 K    | T=308.15 K    | T=313.15 K    |
|                         |               | LiOTf in Ac   | queous DME    |               |               |
| 0.01                    | -15.77        | -13.15        | -10.69        | -8.39         | -6.3          |
|                         | $(\pm 0.005)$ | $(\pm 0.003)$ | $(\pm 0.005)$ | $(\pm 0.004)$ | $(\pm 0.002)$ |
| 0.03                    | -9.26         | -7.91         | -6.35         | -4.99         | -3.61         |
|                         | $(\pm 0.01)$  | $(\pm 0.003)$ | $(\pm 0.004)$ | $(\pm 0.002)$ | $(\pm 0.002)$ |
| 0.05                    | -7.86         | -6.68         | -5.45         | -4.13         | -2.88         |
|                         | $(\pm 0.004)$ | $(\pm 0.002)$ | $(\pm 0.002)$ | $(\pm 0.002)$ | $(\pm 0.002)$ |

#### **LiOTf in Aqueous TEGDME**

| 0.01 | -16.02        | -13.16        | -9.73         | -6.49         | -3.24        |
|------|---------------|---------------|---------------|---------------|--------------|
|      | $(\pm 0.01)$  | $(\pm 0.004)$ | $(\pm 0.003)$ | $(\pm 0.003)$ | $(\pm 0.01)$ |
| 0.03 | -15.95        | -12.83        | -9.66         | -6.21         | -2.87        |
|      | $(\pm 0.01)$  | $(\pm 0.01)$  | $(\pm 0.007)$ | $(\pm 0.01)$  | $(\pm 0.01)$ |
| 0.05 | -14.76        | -11.75        | -8.83         | -5.93         | -2.79        |
|      | $(\pm 0.007)$ | $(\pm 0.01)$  | $(\pm 0.01)$  | $(\pm 0.01)$  | $(\pm 0.01)$ |

<sup>&</sup>lt;sup>a</sup>m<sub>B</sub> is the molality of aqueous DME and aqueous TEGDME solution.

#### 4.1.9 Pair and triplet interaction coefficient

Pair interaction coefficients ( $V_{AB}$ ,  $K_{AB}$ ) & triplet interaction coefficients ( $V_{ABB}$ ,  $K_{ABB}$ ) assist in the interpretation of the interactions existing in the solvation sphere. These parameters represent the divergence in the properties because of the interactions between two or more solute molecules. In order to determine the interaction coefficients McMillan and Mayer put forward a theory that was revised further by Friedman and Krishanan (Millero *et al.*, 1978). The interaction coefficients are calculated using the equations 1.27 and 1.28. In the mentioned equations, A stands for LiOTf and B represents DME/TEGDME,  $m_B$  is the concentration of aqueous solvent. Here,  $V_{AB}$  and  $V_{ABB}$  are volumes &  $V_{ABB}$  and  $V_{ABB}$  are isentropic compressions signifying pair & triplet interaction coefficients. The values of the interaction coefficients are recorded in **Table 4.8**. From the results obtained, it is clear that at low temperatures  $V_{ABB} > V_{ABB}$  and  $V_{ABB} > V_{ABB}$ 

**Table 4.8:** Pair interaction coefficients,  $(V_{AB}, K_{AB})$  and triplet interaction coefficients,  $(V_{ABB}, K_{ABB})$  of LiOTf in an aqueous solution of DME and aqueous TEGDME at various temperatures.

| T / (K) | $V_{AB} \times 10^6$ / | $V_{ABB} \times 10^6$ / | $K_{AB} \times 10^6$ /                                   | $K_{ABB} \times 10^6$ /     |
|---------|------------------------|-------------------------|--|-----------------------------|
|         | $(m^3  mol^{-2}  kg)$  | $(m^3mol^{-3}kg^2)$     | (m <sup>3</sup> mol <sup>-2</sup> kg GPa <sup>-1</sup> ) | $(m^3mol^{-3}kg^2GPa^{-1})$ |
|         |                        | LiOTf in A              | queous DME   |                             |
| 293.15  | -88.54                 | 686.86                  | -54.60   | 1339.28                     |
| 298.15  | -57.34                 | 378.41                  | 8.98   | 563.70                      |
| 303.15  | -23.53                 | 23.87                   | 73.06  | -211.86                     |
| 308.15  | 18.78                  | -418.07                 | 129.73   | -868.63                     |
| 313.15  | 58.43                  | -829.71                 | 178.66   | -1444.61                    |
|         |                        | LiOTf in Aqu            | eous TEGDME  |                             |
| 293.15  | -139.67                | 1571.06                 | -158.01  | 1753.57                     |
| 298.15  | -110.08                | 1287.03                 | -73.17   | 942.69                      |
| 303.15  | -83.57                 | 1037.52                 | -4.37  | 914.87                      |
| 308.15  | -47.18                 | 686.23                  | 199.97   | -1869.02                    |
| 313.15  | 8.88                   | 131.67                  | 323.47   | -3192.49                    |

#### 4.1.10 Cyclic voltammetry Studies

CV is a powerful and widely used electrochemical technique for studying the electrochemical properties of materials, particularly for determining the electrochemical window (EW) of solvents and electrolytes. In this study, CV analysis was conducted using a Metrohm Autolab PGSTAT204 multi-channel Potentiostat/galvanostat, which is a sophisticated and versatile electrochemical workstation(Satheesh & Kandasamy, 2024; Wu & Si, 2023; Zahra *et al.*, 2024). This apparatus offers accurate control and monitoring of electrochemical processes, making

it perfect for extensive investigations on electrochemical behavior. In the CV analysis, a silver chloride (Ag/AgCl) reference electrode was used, which consists of a silver wire coated with solid silver chloride, immersed in a 3 M KCl solution. This standard configuration ensures stable and reproducible potential measurements during the electrochemical testing.

In the analysis, solutions of DME and TEGDME were prepared, along with these solvents containing various concentrations of LiOTf. The CV measurements were performed at a scan rate of 100 mV/s, which is a typical rate that balances sensitivity and resolution in detecting electrochemical processes. By cycling the potential between predetermined lower and upper limits and recording the corresponding current, the CV plots (cyclic voltammograms) were obtained. These plots display the working electrode potential against the current, revealing the electrochemical activity within the tested potential range (Khan *et al.*, 2022; Singh Thakur *et al.*, 2024). The electrochemical window was identified by locating the potential values at the beginning and end of the flat current region in the CV plots. These values represent the limits where only capacitive currents flow, and no significant Faradaic reactions occur. The electrochemical window was calculated by taking the difference between upper and lower potential limit.

In this analysis, CV studies have been performed in order to determine the electrochemical window of the pure systems & systems with different concentrations of LiOTf (Macchieraldo *et al.*, 2018). CV analysis was carried out at room temperature in a glove box in an inert environment of argon flow. CV was performed on the salt solutions at various concentrations and scan rates. Optimal electrochemical window (EW) values were observed at a scan rate of 100 mV/s for the solvent system containing pure DME, TEGDME and these systems with different concentrations of LiOTf. CV graphs (**Figure. 4.3**) were employed to determine the electrochemical window. These graphs plot the working electrode potential against the corresponding current (Le Donne *et al.*, 2018; J. Singh *et al.*, 2021). From the two studied systems, TEGDME was found to have a higher EW of 1.36 V in 0.01 TEGDME and 1.40 V in 0.05 TEGDME compared to that of 1.25 V in 0.01 DME and 1.38 V in 0.05 DME. Similar

patterns were seen in the other samples and clearly, EW also increases with an increase in the concentration of TEGDME & DME. The EW was also found to be increasing with the increasing concentration of LiOTf, as EW of 0.01 TEGDME system with 0.05 LiOTf is 2.23 V and with 0.30 LiOTf is 2.30 V. The remaining samples showed similar patterns (as shown in the **Table 4.9**) with the approximate EW ranges from 2.2 V to 2.32 V with different LiOTf concentrations. This result implies optimistic outcomes of these investigated systems, producing favourable and comparable working electrochemical windows (Zhang *et al.*, 2018).

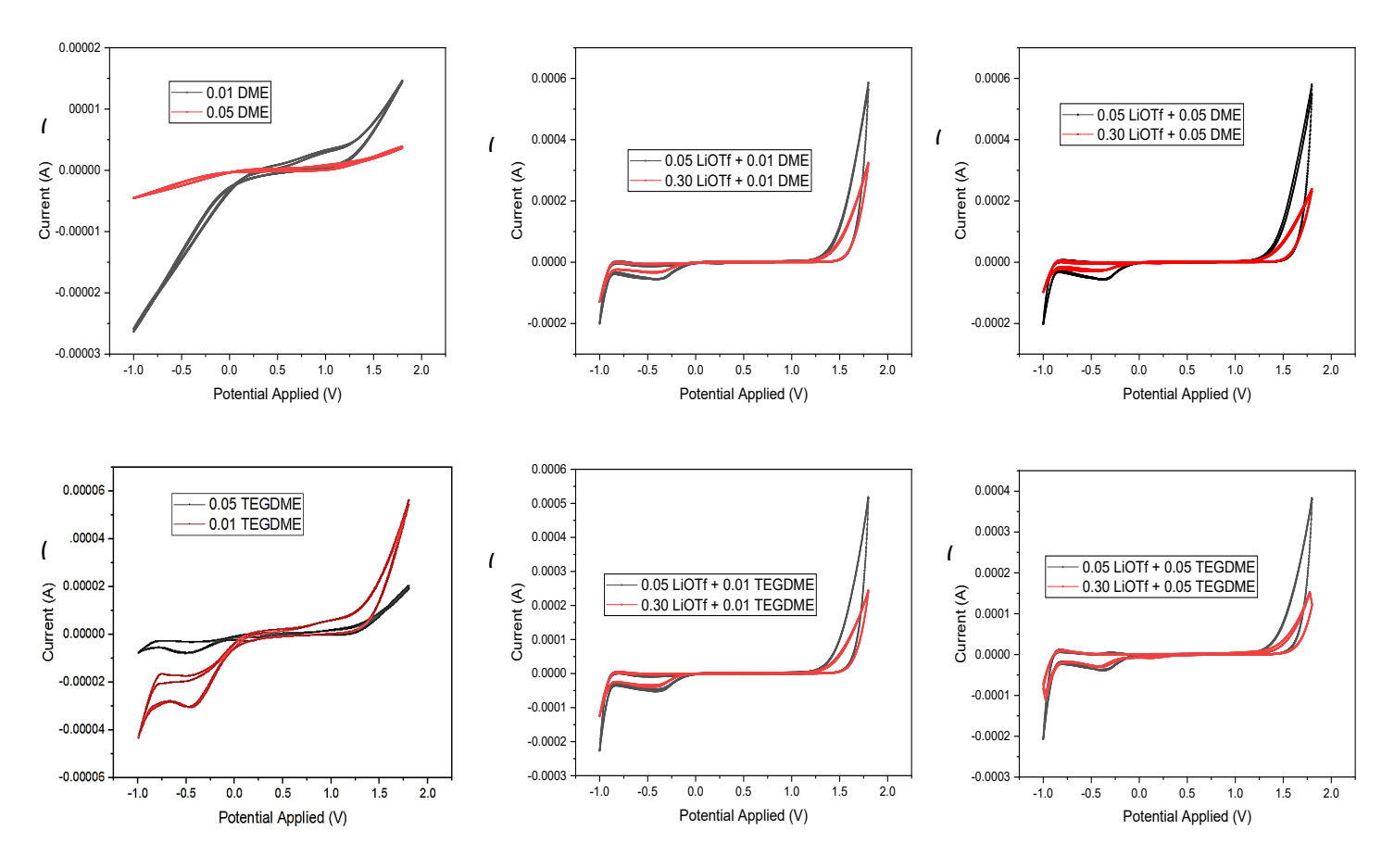


**Fig. 4.3:** Depiction of the CV plots (V vs. A) for (a) 0.01 DME and 0.05 DME, (b) 0.05 LiOTf + 0.01 DME and 0.30 LiOTf + 0.01 DME, (c) 0.05 LiOTf + 0.05 DME and 0.30 LiOTf + 0.05 DME, (d) 0.05 TEGDME and 0.01 TEGDME, (e) 0.05 LiOTf + 0.01 TEGDME and 0.30 LiOTf + 0.01 TEGDME, (f) 0.05 LiOTf + 0.05 TEGDME and 0.30 LiOTf + 0.05 TEGDME at ambient temperature.

**Table 4.9:** Several EW values attained from the CV analysis of LiOTf in an aqueous solution of DME and aqueous TEGDME at ambient temperature.

|            | Electrochemical Window (V) |          |  |  |  |  |  |  |  |
|------------|----------------------------|----------|--|--|--|--|--|--|--|
|            | 0.01 TEGDME                | 0.01 DME |  |  |  |  |  |  |  |
|            | 1.36                       | 1.25     |  |  |  |  |  |  |  |
| 0.05 LiOTf | 2.23                       | 2.20     |  |  |  |  |  |  |  |
| 0.30 LiOTf | 2.30                       | 2.28     |  |  |  |  |  |  |  |
|            | 0.05 TEGDME                | 0.05 DME |  |  |  |  |  |  |  |
|            | 1.40                       | 1.38     |  |  |  |  |  |  |  |
| 0.05 LiOTf | 2.22                       | 2.21     |  |  |  |  |  |  |  |
| 0.30 LiOTf | 2.32                       | 2.27     |  |  |  |  |  |  |  |

#### 4.1.11 Conductance Studies

The specific conductivity (K) for LiOTf in aqueous DME and TEGDME solutions at different temperatures have been given in Table 4.10. Both the solute's concentration & temperature increase cause the values of κ to rise. From κ values molar conductivity  $(\Lambda_m)$  have been calculated and presented in tabular form in **Table 4.10**. The resultant molar conductivity data has been analysed to obtain limiting molar conductivity  $(\Lambda_m^0)$  values at infinite dilution using Onsager relation given in equation 1.32. The intercept of graph plot between  $\Lambda_m$  versus  $\sqrt{C}$  represents  $\Lambda_m^0$ . The values of  $\Lambda_m^0$  have been listed in **Table 4.11** (Kant *et al.*, 2009a). It has been demonstrated that the values of limiting molar conductivity elevated with temperature due to high ionic mobility at higher temperatures. Increase in temperature results in higher frequency and bond breaking as a consequence of the increase in translational & vibrational degrees of freedom and therefore the mobility of ions accelerates. There are no other ions within a limited radius of the solute ions at infinite dilution because they are encircled by solvent molecules. Further, positive activation energy of conductance values are obtained for LiOTf in aqueous DME and TEGDME solutions (given in Table 4.12) which infers that ionic movement is thermally activated, and as the concentration increase, the values of activation energy of conductance increases due to the greater ion-ion interactions.

**Table 4.10:** Specific conductance ( $\kappa$ ) and molar conductance ( $\Lambda_m$ ) of LiOTf in aqueous DME and TEGDME solutions at different temperatures.

|                               |          | <b>κ</b> /(μS | cm <sup>-1</sup> ) |             |                         |        | $\Lambda_m$ | (S cm <sup>2</sup> m | ol <sup>-1</sup> ) |        |
|-------------------------------|----------|---------------|--------------------|-------------|-------------------------|--------|-------------|----------------------|--------------------|--------|
| <sup>a</sup> m <sub>A</sub> / | 293.15K  | 298.15K       | 303.15K            | 308.15K     | 313.15K                 | 293.15 | 298.15      | 303.15               | 308.15             | 313.15 |
| (mol.kg-1)                    |          |               |                    |             |                         | K      | K           | K                    | K                  | K      |
|                               |          |               | LiC                | OTf+ 0.01 m | ol·kg <sup>-1</sup> DME | 2      |             |                      |                    |        |
| 0.04999                       | 4536.00  | 4746.03       | 4997.93            | 5305.98     | 6350.39                 | 91.25  | 95.63       | 100.83               | 107.25             | 128.56 |
| 0.09983                       | 6652.72  | 7024.71       | 7424.60            | 7855.52     | 9313.81                 | 67.27  | 71.15       | 75.30                | 79.82              | 94.79  |
| 0.14999                       | 8783.04  | 9318.01       | 9866.85            | 10421.44    | 12296.25                | 59.34  | 63.06       | 66.86                | 70.75              | 83.62  |
| 0.19951                       | 10886.17 | 11582.06      | 12277.94           | 12954.61    | 15240.64                | 55.50  | 59.14       | 62.78                | 66.37              | 78.21  |
| 0.24983                       | 13023.28 | 13882.68      | 14727.98           | 15528.71    | 18232.59                | 53.22  | 56.82       | 60.37                | 63.77              | 75.01  |
| 0.29986                       | 15148.07 | 16170.04      | 17163.90           | 18087.98    | 21207.30                | 51.76  | 55.35       | 58.83                | 62.12              | 72.96  |
|                               |          |               | LiC                | OTf+ 0.03 m | ol·kg <sup>-1</sup> DME | 2      |             |                      |                    |        |
| 0.04993                       | 5068.01  | 5277.99       | 5558.01            | 5809.95     | 7095.22                 | 91.43  | 95.79       | 101.01               | 107.44             | 128.76 |
| 0.09855                       | 7442.43  | 7810.53       | 8223.35            | 8617.82     | 10419.40                | 68.19  | 72.10       | 76.31                | 80.89              | 96.05  |
| 0.14993                       | 9951.63  | 10486.83      | 11039.99           | 11585.09    | 13932.28                | 59.40  | 63.11       | 66.92                | 70.82              | 83.68  |
| 0.19831                       | 12314.33 | 13006.87      | 13692.17           | 14379.10    | 17240.06                | 55.87  | 59.52       | 63.19                | 66.80              | 78.70  |
| 0.24855                       | 14767.86 | 15623.79      | 16446.32           | 17280.53    | 20675.00                | 53.52  | 57.14       | 60.71                | 64.13              | 75.41  |
| 0.29962                       | 17261.92 | 18283.95      | 19245.97           | 20229.89    | 24166.69                | 51.84  | 55.42       | 58.91                | 62.20              | 73.04  |

| LiOTf+ 0.05 mol·kg <sup>-1</sup> DME |                    |                    |                                |                                |                                |                         |                |                |                |                 |  |
|--------------------------------------|--------------------|--------------------|--------------------------------|--------------------------------|--------------------------------|-------------------------|----------------|----------------|----------------|-----------------|--|
| 0.04979                              | 5515.99            | 5760.96            | 5950.02                        | 6188.05                        | 7722.39                        | 91.73                   | 96.10          | 101.36         | 107.78         | 129.24          |  |
| 0.09983                              | 8302.89            | 8689.51            | 9031.43                        | 9412.59                        | 11624.05                       | 67.35                   | 71.21          | 75.38          | 79.89          | 94.90           |  |
| 0.14981                              | 11086.45           | 11614.55           | 12109.15                       | 12633.26                       | 15521.03                       | 59.47                   | 63.18          | 67.01          | 70.89          | 83.81           |  |
| 0.20215                              | 14001.44           | 14677.71           | 15332.19                       | 16006.00                       | 19602.02                       | 54.84                   | 58.42          | 62.03          | 65.56          | 77.29           |  |
| 0.24599                              | 16443.04           | 17243.41           | 18031.82                       | 18831.02                       | 23020.26                       | 54.09                   | 57.73          | 61.35          | 64.79          | 76.23           |  |
| 0.29951                              | 19423.75           | 20375.62           | 21327.53                       | 22279.80                       | 27193.25                       | 51.87                   | 55.44          | 58.95          | 62.23          | 73.11           |  |
| LiOTf+ 0.01 mol·kg-1 TEGDME          |                    |                    |                                |                                |                                |                         |                |                |                |                 |  |
|                                      |                    |                    | LIGI                           | - 0001 11101                   | ng ILODA                       |                         |                |                |                |                 |  |
| 0.04979                              | 2920.33            | 3513.95            | 4115.97                        | 4689.99                        | 5259.81                        | 58.77                   | 70.82          | 83.09          | 94.83          | 106.52          |  |
| 0.04979<br>0.09983                   | 2920.33<br>6064.16 | 3513.95<br>6634.89 |                                |                                | J                              |                         | 70.82<br>67.17 | 83.09<br>73.14 | 94.83<br>78.90 | 106.52<br>84.63 |  |
|                                      |                    |                    | 4115.97                        | 4689.99                        | 5259.81                        | 58.77                   |                |                |                |                 |  |
| 0.09983                              | 6064.16            | 6634.89            | 4115.97<br>7212.34             | 4689.99<br>7767.37             | 5259.81<br>8319.04             | 58.77<br>61.31          | 67.17          | 73.14          | 78.90          | 84.63           |  |
| 0.09983<br>0.14981                   | 6064.16<br>9211.15 | 6634.89<br>9758.95 | 4115.97<br>7212.34<br>10311.81 | 4689.99<br>7767.37<br>10847.84 | 5259.81<br>8319.04<br>11381.34 | 58.77<br>61.31<br>62.31 | 67.17<br>66.11 | 73.14<br>69.97 | 78.90<br>73.73 | 84.63<br>77.48  |  |

| LiOTf+ 0.03 mol·kg <sup>-1</sup> TEGDME |          |          |          |              |                        |       |       |        |        |        |  |
|---|----------|----------|----------|--------------|------------------------|-------|-------|--------|--------|--------|--|
| 0.04992                                 | 3620.39  | 4241.99  | 4816.01  | 5403.98      | 5922.00                | 72.99 | 85.35 | 97.05  | 109.07 | 119.91 |  |
| 0.10109                                 | 7028.93  | 7608.90  | 8165.73  | 8730.70      | 9234.40                | 70.26 | 75.90 | 81.58  | 87.36  | 92.70  |  |
| 0.14978                                 | 10272.27 | 10812.63 | 11353.11 | 11896.20     | 12386.26               | 69.54 | 73.06 | 76.83  | 80.63  | 84.24  |  |
| 0.19995                                 | 13614.19 | 14113.75 | 14637.37 | 15157.91     | 15633.92               | 69.31 | 71.70 | 74.48  | 77.25  | 79.95  |  |
| 0.24328                                 | 16500.49 | 16964.80 | 17473.86 | 17974.93     | 18438.81               | 69.23 | 71.06 | 73.31  | 75.53  | 77.75  |  |
| 0.2995                                  | 20245.41 | 20664.00 | 21154.17 | 21629.97     | 22078.11               | 69.31 | 70.59 | 72.39  | 74.14  | 75.93  |  |
|   |          |          | LiOT     | f+ 0.05 mol· | kg <sup>-1</sup> TEGDN | Æ     |       |        |        |        |  |
| 0.04997                                 | 4320.40  | 4927.95  | 5516.04  | 6090.06      | 6650.01                | 86.79 | 99.13 | 111.14 | 122.91 | 134.43 |  |
| 0.09987                                 | 7817.59  | 8386.51  | 8936.53  | 9484.56      | 10016.49               | 78.88 | 84.74 | 90.44  | 96.15  | 101.71 |  |
| 0.14993                                 | 11325.99 | 11856.16 | 12367.98 | 12889.94     | 13393.77               | 76.41 | 80.10 | 83.70  | 87.38  | 90.95  |  |
| 0.19738                                 | 14651.48 | 15144.91 | 15620.53 | 16117.77     | 16594.96               | 75.35 | 78.00 | 80.59  | 83.29  | 85.91  |  |
| 0.24978                                 | 18323.88 | 18776.74 | 19212.38 | 19682.33     | 20130.11               | 74.76 | 76.72 | 78.63  | 80.69  | 82.67  |  |
| 0.29955                                 | 21811.96 | 22226.29 | 22623.95 | 23067.99     | 23487.82               | 74.48 | 76.00 | 77.49  | 79.15  | 80.73  |  |

 $<sup>^{</sup>a}m_{A}$  is the molality of LiOTf in aqueous DME and TEGDME solutions.

**Table 4.11:** Limiting molar conductance  $(\Lambda_m^0)$  of LiOTf in aqueous DME and TEGDME solutions at different temperatures.

|         | Limiting molar conductance $(\Lambda_m^0)$ , |                                  |                                  |  |  |  |  |  |  |  |  |
|---------|--|----------------------------------|----------------------------------|--|--|--|--|--|--|--|--|
| T (K)   | LiOTf+ 0.01 mol·kg <sup>-1</sup>             | LiOTf+ 0.03 mol·kg <sup>-1</sup> | LiOTf+ 0.05 mol·kg <sup>-1</sup> |  |  |  |  |  |  |  |  |
|         | DME  | DME                              | DME                              |  |  |  |  |  |  |  |  |
| 293.15K | 109.89                                       | 110.37                           | 110.39                           |  |  |  |  |  |  |  |  |
| 298.15K | 114.63                                       | 115.11                           | 115.10                           |  |  |  |  |  |  |  |  |
| 303.15K | 120.65                                       | 121.16                           | 121.17                           |  |  |  |  |  |  |  |  |
| 308.15K | 128.54                                       | 129.09                           | 129.08                           |  |  |  |  |  |  |  |  |
| 313.15K | 154.82                                       | 155.44                           | 155.53                           |  |  |  |  |  |  |  |  |
| T (K)   | LiOTf+ 0.01 mol·kg <sup>-1</sup>             | LiOTf+ 0.03 mol·kg <sup>-1</sup> | LiOTf+ 0.05 mol·kg <sup>-1</sup> |  |  |  |  |  |  |  |  |
|         | TEGDME                                       | TEGDME                           | TEGDME                           |  |  |  |  |  |  |  |  |
| 293.15K | 92.71  | 107.75                           | 126.07                           |  |  |  |  |  |  |  |  |
| 298.15K | 98.40  | 114.64                           | 131.46                           |  |  |  |  |  |  |  |  |
| 303.15K | 105.38                                       | 122.43                           | 138.04                           |  |  |  |  |  |  |  |  |
| 308.15K | 117.22                                       | 135.17                           | 152.00                           |  |  |  |  |  |  |  |  |
| 313.15K | 130.59                                       | 151.78                           | 177.59                           |  |  |  |  |  |  |  |  |

**Table 4.12:** Activation energy of conductance  $(E_{\lambda})$  of LiOTf in aqueous DME and TEGDME solutions.

|                               | Eλ(ŀ                        | kJ mol <sup>-1</sup> ) |                      |
|-------------------------------|-----------------------------|------------------------|----------------------|
| <sup>a</sup> m <sub>A</sub> / | LiOTf+ 0.01                 | LiOTf+ 0.03            | LiOTf+ 0.05          |
| (mol.kg- <sup>1</sup> )       | mol·kg <sup>-1</sup> DME    | mol·kg-1 DME           | mol·kg-1 DME         |
| 0.05                          | 0.01172                     | 0.01277                | 0.01543              |
| 0.1                           | 0.01154                     | 0.01266                | 0.01468              |
| 0.15                          | 0.01152                     | 0.01269                | 0.01447              |
| 0.2                           | 0.01155                     | 0.01276                | 0.01441              |
| 0.25                          | 0.01160                     | 0.01284                | 0.01442              |
| 0.3                           | 0.01166                     | 0.01292                | 0.01444              |
| <sup>a</sup> m <sub>A</sub> / | LiOTf+ 0.01                 | LiOTf+ 0.03            | LiOTf+ 0.05          |
| (mol.kg-1)                    | mol·kg <sup>-1</sup> TEGDME | mol·kg <sup>-1</sup>   | mol·kg <sup>-1</sup> |
|                               |                             | TEGDME                 | TEGDME               |
| 0.05                          | 0.00624                     | 0.00688                | 0.00747              |
| 0.1                           | 0.00918                     | 0.01019                | 0.01100              |
| 0.15                          | 0.01246                     | 0.01372                | 0.01510              |
| 0.2                           | 0.01603                     | 0.01777                | 0.01960              |
| 0.25                          | 0.01959                     | 0.02164                | 0.02537              |
| 0.3                           | 0.02461                     | 0.02722                | 0.03179              |

## **SECTION-2**

Thermophysical and Acoustic measurements of Lithium tetrafluoroborate and Lithium hexafluorophosphate in binary aqueous mixtures of tetra ethylene glycol dimethyl ether at various temperatures

#### 4.2 Results (Section -II)

The densities ( $\rho$ ) of LiBF<sub>4</sub> and LiPF<sub>6</sub> in aqueous media of TEGDME where  $m_{TEGDME}$ = (0.01, 0.03 and 0.05) mol·kg<sup>-1</sup> and LiBF<sub>4</sub> and LiPF<sub>6</sub> concentrations ranging between (0.05 - 0.30) mol/kg at T= (293.15K, 298.15K, 303.15K, 308.15K and 313.15K) have been ascertained in this study.

#### 4.2.1 Thermophysical parameters derived from density measurements

**Table 4.13** shows that density values are enhanced with a rise in the concentration of Li salt in the binary aqueous solution of TEGDME but decline when the temperature rises. Utilizing the density data apparent molar volume  $(V_{\phi})$  has been determined employing the equation (1.13). In this equation, M and  $m_A$  denote the molar mass (kg·mol<sup>-1</sup>) and molality of LiBF<sub>4</sub> and LiPF<sub>6</sub> correspondingly, and  $\rho$  and  $\rho_0$  denote the density (kg·m<sup>-3</sup>) of solution and solvent respectively. **Table 4.13** presents the resulting  $V_{\phi}$  values.  $V_{\phi}$  values are more at elevated temperatures since a rise in temperature leads to the thermal movement of molecules, which results in increasing the volume (Widegren & Magee, 2007).

**Table 4.13:** Temperature-dependent densities and  $V_{\phi}$  of LiBF<sub>4</sub> and LiPF<sub>6</sub> in aqs. TEGDME medium, P = 0.1 MPa.

| <sup>a</sup> m <sub>A</sub> / |          | $ ho \times$ | 10 <sup>-3</sup> / (kg·m | -3)             |            | $V_{\phi} \times 10^6 / (\text{m}^3 \cdot \text{mol}^{-1})$ |          |          |          |          |
|-------------------------------|----------|--------------|--------------------------|-----------------|------------|---|----------|----------|----------|----------|
| (mol·kg-1)                    | T=293.15 | T=298.15     | T=303.15                 | T=308.15        | T=313.15   | T=293.15  | T=298.15 | T=303.15 | T=308.15 | T=313.15 |
|                               | K        | K            | K                        | K               | K          | K   | K        | K        | K        | K        |
|                               |          |              | I                        | $JiBF_4 + 0.01$ | mol·kg-1 T | EGDME   |          |          |          |          |
| 0.00000                       | 0.998601 | 0.997162     | 0.995575                 | 0.993951        | 0.992427   |   |          |          |          |          |
| 0.04907                       | 1.001054 | 0.999600     | 0.997996                 | 0.996355        | 0.994812   | 43.73   | 43.90    | 44.10    | 44.27    | 44.42    |
| 0.10027                       | 1.003615 | 1.002143     | 1.000521                 | 0.998864        | 0.997300   | 43.86   | 44.03    | 44.22    | 44.39    | 44.54    |
| 0.15345                       | 1.006274 | 1.004786     | 1.003145                 | 1.001470        | 0.999885   | 43.99   | 44.16    | 44.35    | 44.52    | 44.67    |
| 0.20034                       | 1.008618 | 1.007115     | 1.005458                 | 1.003768        | 1.002164   | 44.10   | 44.28    | 44.47    | 44.63    | 44.78    |
| 0.24941                       | 1.011072 | 1.009553     | 1.007878                 | 1.006172        | 1.004548   | 44.22   | 44.40    | 44.58    | 44.75    | 44.90    |
| 0.30075                       | 1.013639 | 1.012103     | 1.010411                 | 1.008688        | 1.007044   | 44.35   | 44.52    | 44.71    | 44.87    | 45.02    |

| $LiBF_4 + 0.03 mol \cdot kg^{-1} TEGDME$             |          |          |          |          |          |       |       |       |       |       |  |
|--|----------|----------|----------|----------|----------|-------|-------|-------|-------|-------|--|
| 0.00000  | 0.999412 | 0.997889 | 0.996373 | 0.994742 | 0.993179 |       |       |       |       |       |  |
| 0.04904  | 1.001835 | 1.000295 | 0.998763 | 0.997113 | 0.995533 | 44.41 | 44.60 | 44.78 | 45.00 | 45.20 |  |
| 0.09315  | 1.004014 | 1.002459 | 1.000912 | 0.999246 | 0.997650 | 44.51 | 44.70 | 44.88 | 45.10 | 45.30 |  |
| 0.14928  | 1.006786 | 1.005213 | 1.003647 | 1.001960 | 1.000344 | 44.65 | 44.84 | 45.02 | 45.24 | 45.43 |  |
| 0.20117  | 1.009350 | 1.007758 | 1.006176 | 1.004468 | 1.002835 | 44.77 | 44.96 | 45.14 | 45.36 | 45.55 |  |
| 0.25660  | 1.012088 | 1.010478 | 1.008877 | 1.007149 | 1.005496 | 44.91 | 45.09 | 45.27 | 45.49 | 45.68 |  |
| 0.30063  | 1.014263 | 1.012638 | 1.011023 | 1.009278 | 1.007609 | 45.01 | 45.20 | 45.37 | 45.59 | 45.78 |  |
| LiBF <sub>4</sub> + 0.05 mol·kg <sup>-1</sup> TEGDME |          |          |          |          |          |       |       |       |       |       |  |
| 0.00000  | 1.000321 | 0.998702 | 0.997110 | 0.995511 | 0.993876 |       |       |       |       |       |  |
| 0.04906  | 1.002700 | 1.001057 | 0.999440 | 0.997817 | 0.996162 | 45.39 | 45.73 | 46.10 | 46.38 | 46.68 |  |
| 0.09862  | 1.005104 | 1.003436 | 1.001795 | 1.000146 | 0.998472 | 45.51 | 45.85 | 46.20 | 46.49 | 46.79 |  |
| 0.14919  | 1.007557 | 1.005863 | 1.004197 | 1.002523 | 1.000828 | 45.63 | 45.96 | 46.31 | 46.60 | 46.90 |  |
| 0.19120  | 1.009594 | 1.007879 | 1.006192 | 1.004497 | 1.002786 | 45.72 | 46.06 | 46.41 | 46.70 | 46.99 |  |
| 0.25227  | 1.012556 | 1.010811 | 1.009093 | 1.007368 | 1.005632 | 45.86 | 46.20 | 46.54 | 46.83 | 47.12 |  |
| 0.30069  | 1.014905 | 1.013135 | 1.011393 | 1.009644 | 1.007888 | 45.97 | 46.31 | 46.65 | 46.94 | 47.23 |  |

 $LiPF_6 + 0.01 \ mol \cdot kg^{\text{--}1} \ TEGDME$ 

| 0.00000  | 0.998601 | 0.997162 | 0.995575 | 0.993951 | 0.992427 |       |       |       |       |       |
|--|----------|----------|----------|----------|----------|-------|-------|-------|-------|-------|
| 0.05002  | 1.002963 | 1.001485 | 0.999862 | 0.998243 | 0.996639 | 64.84 | 65.35 | 65.81 | 66.28 | 66.77 |
| 0.10005  | 1.007325 | 1.005809 | 1.004149 | 1.002535 | 1.000851 | 65.21 | 65.72 | 66.17 | 66.64 | 67.13 |
| 0.14980  | 1.011663 | 1.010109 | 1.008413 | 1.006804 | 1.005040 | 65.58 | 66.09 | 66.54 | 67.00 | 67.48 |
| 0.20657  | 1.016613 | 1.015015 | 1.013278 | 1.011674 | 1.009820 | 66.00 | 66.51 | 66.95 | 67.41 | 67.88 |
| 0.24967  | 1.020372 | 1.018741 | 1.016971 | 1.015372 | 1.013449 | 66.32 | 66.82 | 67.26 | 67.71 | 68.18 |
| 0.29954  | 1.024721 | 1.023051 | 1.021245 | 1.019651 | 1.017648 | 66.68 | 67.18 | 67.61 | 68.07 | 68.53 |
| LiPF <sub>6</sub> + 0.03 mol·kg <sup>-1</sup> TEGDME |          |          |          |          |          |       |       |       |       |       |
| 0  | 0.999412 | 0.997889 | 0.996373 | 0.994742 | 0.993179 |       |       |       |       |       |
| 0.04977  | 1.003732 | 1.002170 | 1.000614 | 0.998943 | 0.997340 | 65.37 | 65.90 | 66.44 | 66.96 | 67.50 |
| 0.10268  | 1.008325 | 1.006719 | 1.005121 | 1.003408 | 1.001763 | 65.77 | 66.29 | 66.83 | 67.34 | 67.87 |
| 0.14998  | 1.012430 | 1.010787 | 1.009151 | 1.007400 | 1.005717 | 66.12 | 66.64 | 67.17 | 67.68 | 68.20 |
| 0.19734  | 1.016541 | 1.014860 | 1.013186 | 1.011398 | 1.009677 | 66.46 | 66.98 | 67.50 | 68.01 | 68.53 |
| 0.24865  | 1.020995 | 1.019273 | 1.017558 | 1.015728 | 1.013966 | 66.83 | 67.35 | 67.87 | 68.37 | 68.89 |
| 0.29972  | 1.025428 | 1.023665 | 1.021909 | 1.020038 | 1.018235 | 67.20 | 67.71 | 68.22 | 68.72 | 69.23 |
|  |          |          |          |          |          |       |       |       |       |       |

LiPF<sub>6</sub> + 0.05 mol·kg<sup>-1</sup> TEGDME

| 0       | 1.000321 | 0.998702 | 0.997110 | 0.995511 | 0.993876 |       |       |       |       |       |
|---------|----------|----------|----------|----------|----------|-------|-------|-------|-------|-------|
| 0.04997 | 1.004659 | 1.003000 | 1.001371 | 0.999729 | 0.998049 | 65.53 | 66.05 | 66.53 | 67.10 | 67.72 |
| 0.10879 | 1.009764 | 1.008058 | 1.006384 | 1.004693 | 1.002960 | 65.97 | 66.48 | 66.96 | 67.52 | 68.13 |
| 0.15004 | 1.013344 | 1.011605 | 1.009900 | 1.008174 | 1.006404 | 66.27 | 66.78 | 67.25 | 67.81 | 68.42 |
| 0.20129 | 1.017793 | 1.016013 | 1.014269 | 1.012500 | 1.010683 | 66.64 | 67.15 | 67.62 | 68.17 | 68.77 |
| 0.24602 | 1.021675 | 1.019860 | 1.018082 | 1.016275 | 1.014418 | 66.97 | 67.47 | 67.93 | 68.48 | 69.08 |
| 0.29954 | 1.026321 | 1.024462 | 1.022644 | 1.020792 | 1.018887 | 67.35 | 67.84 | 68.31 | 68.85 | 69.44 |

 $<sup>^{</sup>a}m_{A}$  denotes the molality of LiBF<sub>4</sub> and LiPF<sub>6</sub> in an aqueous TEGDME solution. Standard uncertainties in LiBF<sub>4</sub> and LiPF<sub>6</sub> ur (mA) molality are 1%. Standard uncertainties in the molality of TEGDME  $u_{r}$  is 1.5%. Standard uncertainty in density,  $u(\rho) = \pm 5 \times 10^{-3} \text{ kg} \cdot \text{m}^{-3}$ , temperature, u(T) = 0.001 K, and pressure, u(p) = 0.01 MPa.

Partial molar volume  $(V_{\phi}^{0})$ , have been calculated utilizing Masson's least square fitting approach in equation (1.15). In this equation, partial molar volume is denoted by  $V_{\phi}^{0}$ . The slope of the graph represented as  $S_{V}^{*}$ .  $V_{\phi}^{0}$ , depicts the solute-solvent linkages, predicting that the solute molecules are apart at infinite dilution and therefore, no solute-solute linkages persist. **Table 4.14** shows the  $V_{\phi}^{0}$  and  $S_{V}^{*}$  values. The positive  $V_{\phi}^{0}$  proves the emergence of solute-solvent interactions in current systems (Srinivasa Reddy *et al.*, 2016). The electrostriction, which decreases as the temperature increases, might be accountable for the enhancement of  $V_{\phi}^{0}$  values in accordance with the temperature. The minimal values of the  $S_{V}^{*}$  clearly illustrate negligible solute-solute interactions.

**Table 4.14:** Temperature-dependent  $V_{\phi}^{0}$  and  $S_{v}^{*}$  of LiBF<sub>4</sub> and LiPF<sub>6</sub> in aqs. media of TEGDME.

| <sup>a</sup> m <sub>B</sub> |          | $V_{\phi}^{0}$ × | 10 <sup>6</sup> /(m <sup>3</sup> ·1 | mol <sup>-1</sup> ) |                   |          | $S_v^* \times 10$ | <sup>06</sup> /(m <sup>3</sup> ⋅ kg·r | nol <sup>-2</sup> ) |          |
|-----------------------------|----------|------------------|-------------------------------------|---------------------|-------------------|----------|-------------------|---------------------------------------|---------------------|----------|
| (mol·kg-                    | T=293.15 | T=298.15         | T=303.15                            | T=308.15            | T=313.1           | T=293.15 | T=298.15          | T=303.15                              | T=308.1             | T=313.15 |
| 1)                          | K        | K                | K                                   | K                   | 5 K               | K        | K                 | K                                     | 5 K                 | K        |
|                             |          |                  |                                     |                     | LiBF4             |          |                   |                                       |                     |          |
| 0.00                        | 43.57    | 43.75            | 43.91                               | 44.06               | 44.26             |          |                   |                                       |                     |          |
| 0.01                        | 43.61    | 43.79            | 43.98                               | 44.15               | 44.30             | 2.47     | 2.45              | 2.42                                  | 2.40                | 2.39     |
| 0.03                        | 44.29    | 44.48            | 44.66                               | 44.89               | 45.09             | 2.40     | 2.38              | 2.36                                  | 2.34                | 2.31     |
| 0.05                        | 45.28    | 45.62            | 45.99                               | 46.27               | 46.57             | 2.31     | 2.27              | 2.18                                  | 2.21                | 2.18     |
|                             |          |                  |                                     |                     | LiPF <sub>6</sub> |          |                   |                                       |                     |          |
| 0.00                        | 62.60    | 63.39            | 64.06                               | 64.88               | 65.54             |          |                   |                                       |                     |          |
| 0.01                        | 64.47    | 64.99            | 65.45                               | 65.93               | 66.42             | 7.41     | 7.31              | 7.22                                  | 7.16                | 7.04     |
| 0.03                        | 65.01    | 65.55            | 66.09                               | 66.62               | 67.16             | 7.32     | 7.22              | 7.12                                  | 7.03                | 6.93     |
| 0.05                        | 65.17    | 65.69            | 66.18                               | 66.75               | 67.38             | 7.30     | 7.21              | 7.12                                  | 7.01                | 6.90     |

Moreover, the values of  $\Delta V_{\phi}^{0}$  of Li salts from water to aqueous (TEGDME), during infinite dilution, have been evaluated by employing the following relation 1.18. The computed values of  $\Delta V_{\phi}^{0}$  are given in **Table 4.15**. The positive transfer volumes are attributed to an enhancement in the volume of that specific Li salt on being transferred from pure water to aqueous TEGDME.  $\Delta V_{\phi}^{0}$  signifies solute-solvent interactions. Following the co-sphere model, ion-ion linkages culminated in positive  $\Delta V_{\phi}^{0}$  values because the H<sub>2</sub>O molecules earlier existing near hydrophilic centres are now discharged to the bulk that is highly compressible in comparison to the electro strictive region (Zheng *et al.*, 2019)

**Table 4.15:** Temperature-dependent  $\Delta V_{\phi}^{0}$  of LiBF<sub>4</sub> and LiPF<sub>6</sub> in aqs. media of TEGDME media.

| m <sub>B</sub>          |                   | $\Delta V_{\phi}^{0}$ | $\times$ 10 <sup>6</sup> /(m <sup>3</sup> mol |      |            |  |  |  |  |
|-------------------------|-------------------|-----------------------|---|------|------------|--|--|--|--|
| (mol kg <sup>-1</sup> ) | T=293.15 K        | T=298.15 K            | T=298.15 K T=303.15 K                         |      | T=313.15 K |  |  |  |  |
|                         | LiBF <sub>4</sub> |                       |   |      |            |  |  |  |  |
| 0.01                    | 0.04              | 0.03                  | 0.07  | 0.09 | 0.04       |  |  |  |  |
| 0.03                    | 0.72              | 0.73                  | 0.75  | 0.83 | 0.83       |  |  |  |  |
| 0.05                    | 1.71              | 1.87                  | 2.08  | 2.22 | 2.31       |  |  |  |  |
|                         |                   | LiP                   | <b>F</b> 6                                    |      |            |  |  |  |  |
| 0.01                    | 1.87              | 1.60                  | 1.40  | 1.05 | 0.89       |  |  |  |  |
| 0.03                    | 2.41              | 2.16                  | 2.04  | 1.74 | 1.62       |  |  |  |  |
| 0.05                    | 2.57              | 2.30                  | 2.12  | 1.87 | 1.84       |  |  |  |  |

Further, the effect of temperature on  $V_{\phi}^{0}$  has been evaluated utilizing the polynomial equation (1.19). In this equation,  $T_{\rm ref} = 298.15$  K, while a, b, and c are the empirical constants as enlisted in **Table 4.16**. The empirical findings of  $V_{\phi}^{0}$  differ from the attained theoretical findings. The ARD ( $\sigma$ ) deviation could be determined by using the equation (1.20). Table 4.16 summarizes the ARD data, demonstrating that the polynomial equation fits significantly during the ternary compositions undergoing examination.

**Table 4.16:** Empirical variables computed using Eqn. (1.18) for LiBF<sub>4</sub> and LiPF<sub>6</sub> in aqueous media of TEGDME.

| $a_{\rm m_B}$ /         | a×10 <sup>6</sup> /     | b ×10 <sup>6</sup> /                   | c×10 <sup>6</sup> /                                   | $\mathbb{R}^2$ | 4 DD(-) |
|-------------------------|-------------------------|--|---|----------------|---------|
| (mol·kg <sup>-1</sup> ) | (mol·kg <sup>-1</sup> ) | (m <sup>3</sup> ·mol <sup>-1</sup> ·K) | (m <sup>3</sup> ·mol <sup>-1</sup> ·K <sup>-2</sup> ) | K-             | ARD(σ)  |
|                         |                         | LiBF <sub>4</sub>                      | ı   |                |         |
| 0.01                    | 43.80                   | 0.037                                  | -0.0002   | 0.9999         | 0.0005  |
| 0.03                    | 44.48                   | 0.038                                  | 0.0002  | 0.9999         | 0.0005  |
| 0.05                    | 45.64                   | 0.070                                  | -0.0005   | 0.9999         | 0.0011  |
|                         | ${ m LiPF_6}$           |  | j   |                |         |
| 0.01                    | 0.01 64.97 0.           |  | -0.0001   | 0.9999         | 0.0009  |
| 0.03                    | 65.55                   | 0.108                                  | -0.0001   | 0.9999         | 0.0005  |
| 0.05                    | 0.05 65.66 0.101        |  | 0.0009  | 0.9999         | 0.0010  |

Furthermore, partial molar expansibilities,  $\phi_E^0$ , have been calculated using the equation (1.21). For all quantities of TEGDME and experimental temperatures, positive partial molar expansibilities have been obtained, demonstrating a remarkable solute—solvent linkages in the ternary systems studied as provided in **Table 4.17**. Also, Hepler's constant was used to calculate the equation given 1.22 (Hepler, 1969). Positive values of  $(\partial \phi_E^0/\partial T)_p$  has been reported for the ternary systems investigated for (LiBF<sub>4</sub> and LiPF<sub>6</sub>+ H<sub>2</sub>O + TEGDME (given in **Table 4.14**). The sign of  $(\partial \phi_E^0/\partial T)$  signifies that in aqueous media of the tetraglyme, LiBF<sub>4</sub> and LiPF<sub>6</sub> operate as structure makers (Kumar & Behal, 2016a).

**Table 4.17:** Temperature-dependent  $\phi_E^0$  of LiBF<sub>4</sub> and LiPF<sub>6</sub> in aqueous media of TEGDME.

| <sup>a</sup> m <sub>B</sub> / |            | $\phi_E^0 \times 10^6/(\mathrm{m}^3 \cdot \mathrm{mol}^{-1} \cdot \mathrm{Mol}^{-1} \cdot \mathrm{K}^{-1})$ |            |            |            |         |  |  |  |
|-------------------------------|------------|---|------------|------------|------------|---------|--|--|--|
| (mol·kg <sup>-1</sup> )       | T=293.15 K | T=298.15 K  | T=303.15 K | T=308.15 K | T=313.15 K | -       |  |  |  |
|                               |            |   | LiBF4      |            |            |         |  |  |  |
| 0.01                          | 0.039      | 0.037   | 0.035      | 0.033      | 0.031      | -0.0004 |  |  |  |
| 0.03                          | 0.036      | 0.038   | 0.040      | 0.042      | 0.043      | 0.0004  |  |  |  |
| 0.05                          | 0.075      | 0.070   | 0.065      | 0.060      | 0.055      | -0.0010 |  |  |  |
|                               |            |   | LiPF6      |            |            |         |  |  |  |
| 0.01                          | 0.099      | 0.098   | 0.097      | 0.096      | 0.095      | -0.0002 |  |  |  |
| 0.03                          | 0.109      | 0.108   | 0.107      | 0.106      | 0.105      | -0.0002 |  |  |  |
| 0.05                          | 0.092      | 0.101   | 0.110      | 0.118      | 0.127      | 0.0017  |  |  |  |

#### 4.2.2 Acoustic parameters derived using the speed of sound measurements

The apparent molar isentropic compression ( $K_{\phi,s}$ ) (indexed in **Table 4.18**) can be determined by utilizing the equation (1.23). In this equation,  $\kappa_S$  denotes solution isentropic compressibility and  $\kappa_{S,0}$  denotes pure solvent isentropic compressibility,  $m_A$ =molality whereas, M=molar mass of the LiBF<sub>4</sub> or LiPF<sub>6</sub>.  $\kappa_S$  can be calculated using Laplace Newton's equation (1.24).

 $K_{\phi,s}$  is negative in all the aqueous TEGDME quantities and temperatures. Negative values obtained for  $K_{\phi,s}$  indicate the excessive deformability of the H<sub>2</sub>O molecules in the core media as compared to those nearby the solute. Higher temperatures cause less electrostriction & the release of fewer water molecules into the core media, causing less conformational distortion of the water and demonstrating a decreased regulatory influence by the solute on the solvent.  $V_{\phi}^{0}$  values have also determined that (solute–solvent) interactions predominate (Kumar *et al.*, 2021a)

**Table 4.18:** Values of ultrasonic speed and  $K_{\phi,S}$  of LiBF<sub>4</sub> and LiPF<sub>6</sub> in aqueous media of TEGDME at various temp., P = 0.1 MPa.

| <sup>a</sup> m <sub>A</sub> / |          |          | u / (1   | n·s <sup>-1</sup> ) |            | $K_{\phi}$ ,s × 10 <sup>6</sup> (m <sup>3</sup> ·mol <sup>-1</sup> ·GPa <sup>-1</sup> ) |          |          |          |          |  |  |
|-------------------------------|----------|----------|----------|---------------------|------------|---|----------|----------|----------|----------|--|--|
| (mol·kg-                      | T=293.15 | T=298.15 | T=303.15 | T=308.15            | T=313.15   | T=293.15  | T=298.15 | T=303.15 | T=308.15 | T=313.15 |  |  |
| 1)                            | K        | K        | K        | K                   | K          | K   | K        | K        | K        | K        |  |  |
|                               |          |          | LiB      | F4+ aqueo           | us 0.01 mo | l·kg <sup>-1</sup> TEG  | DME      |          |          |          |  |  |
| 0.00000                       | 1484.54  | 1497.38  | 1509.59  | 1521.13             | 1530.70    |   |          |          |          |          |  |  |
| 0.04907                       | 1485.01  | 1497.84  | 1510.04  | 1521.58             | 1531.14    | -8.77   | -8.24    | -7.76    | -7.41    | -7.02    |  |  |
| 0.10027                       | 1485.49  | 1498.31  | 1510.50  | 1522.04             | 1531.60    | -8.81   | -8.29    | -7.80    | -7.45    | -7.06    |  |  |
| 0.15345                       | 1486.00  | 1498.81  | 1510.99  | 1522.53             | 1532.09    | -8.85   | -8.33    | -7.84    | -7.49    | -7.10    |  |  |
| 0.20034                       | 1486.44  | 1499.24  | 1511.42  | 1522.96             | 1532.52    | -8.88   | -8.36    | -7.87    | -7.52    | -7.14    |  |  |
| 0.24941                       | 1486.91  | 1499.70  | 1511.87  | 1523.41             | 1532.97    | -8.91   | -8.40    | -7.91    | -7.56    | -7.18    |  |  |
| 0.30075                       | 1487.40  | 1500.18  | 1512.33  | 1523.87             | 1533.43    | -8.95   | -8.44    | -7.95    | -7.60    | -7.21    |  |  |

|  |         |                    | LiB                | F4+ aqueo | us 0.03 mol | kg <sup>-1</sup> TEGI | OME            |                |                |                |
|--|---------|--------------------|--------------------|-----------|-------------|-----------------------|----------------|----------------|----------------|----------------|
| 0.00000  | 1487.46 | 1499.90            | 1511.73            | 1522.89   | 1532.40     |                       |                |                |                |                |
| 0.04904  | 1487.94 | 1500.38            | 1512.20            | 1523.34   | 1532.84     | -8.26                 | -7.86          | -7.37          | -6.83          | -6.37          |
| 0.09315  | 1488.36 | 1500.80            | 1512.61            | 1523.75   | 1533.24     | -8.29                 | -7.89          | -7.41          | -6.87          | -6.41          |
| 0.14928  | 1488.91 | 1501.35            | 1513.15            | 1524.27   | 1533.74     | -8.33                 | -7.94          | -7.45          | -6.91          | -6.45          |
| 0.20117  | 1489.41 | 1501.85            | 1513.64            | 1524.75   | 1534.21     | -8.37                 | -7.97          | -7.49          | -6.96          | -6.49          |
| 0.25660  | 1489.95 | 1502.39            | 1514.17            | 1525.26   | 1534.71     | -8.41                 | -8.02          | -7.53          | -7.00          | -6.54          |
| 0.30063  | 1490.38 | 1502.82            | 1514.59            | 1525.67   | 1535.11     | -8.44                 | -8.05          | -7.57          | -7.03          | -6.57          |
| LiBF4 + aqueous 0.05 mol·kg <sup>-1</sup> TEGDME |         |                    |                    |           |             |                       |                |                |                |                |
| 0.00000  | 1490.09 | 1502.85            | 1513.73            | 1524.89   | 1534.71     |                       |                |                |                |                |
| 0.04906  | 1490.63 | 1503.36            | 1514.21            | 1525.31   | 1535.09     | -8.13                 | -7.25          | -6.35          | -5.22          | -4.39          |
| 0.09862  | 1491.17 | 1503.88            | 1514.69            | 1525.74   | 1535.47     | -8.17                 | -7.29          | -6.40          | -5.27          | -4.44          |
| 0.14919  | 1491.73 | 1504.40            | 1515.18            | 1526.17   | 1535.87     | -8.21                 | -7.33          | -6.44          | -5.31          | -4.48          |
| 0.10120  | 1402 10 | 150404             | 4 - 4 0            | 1506 50   | 1526 10     | 0.25                  | 7.26           | C 40           | 5.25           | 4.50           |
| 0.19120  | 1492.19 | 1504.84            | 1515.59            | 1526.53   | 1536.19     | -8.25                 | -7.36          | -6.48          | -5.35          | -4.52          |
| 0.19120  | 1492.19 | 1504.84<br>1505.48 | 1515.59<br>1516.19 | 1526.53   | 1536.19     | -8.25<br>-8.30        | -7.36<br>-7.41 | -6.48<br>-6.53 | -5.35<br>-5.40 | -4.52<br>-4.57 |

LiPF<sub>6</sub> + aqueous 0.01 mol·kg<sup>-1</sup> TEGDME

| 0.00000 | 1484.54 | 1497.38 | 1509.59 | 1521.13                | 1531.51     |            |        |        |        |        |
|---------|---------|---------|---------|------------------------|-------------|------------|--------|--------|--------|--------|
| 0.05002 | 1485.02 | 1497.85 | 1510.06 | 1521.51                | 1531.93     | -16.30     | -15.32 | -14.51 | -13.49 | -12.53 |
| 0.10005 | 1485.50 | 1498.32 | 1510.52 | 1521.88                | 1532.35     | -16.38     | -15.40 | -14.59 | -13.57 | -12.61 |
| 0.14980 | 1485.98 | 1498.79 | 1510.98 | 1522.26                | 1532.77     | -16.44     | -15.47 | -14.66 | -13.64 | -12.69 |
| 0.20657 | 1486.52 | 1499.32 | 1511.51 | 1522.69                | 1533.24     | -16.52     | -15.55 | -14.74 | -13.72 | -12.78 |
| 0.24967 | 1486.94 | 1499.73 | 1511.91 | 1523.01                | 1533.60     | -16.58     | -15.61 | -14.80 | -13.78 | -12.84 |
| 0.29954 | 1487.42 | 1500.20 | 1512.38 | 1523.39                | 1534.02     | -16.64     | -15.68 | -14.87 | -13.85 | -12.92 |
|         |         |         | LiP     | F <sub>6</sub> + aqueo | us 0.03 mol | ·kg-1 TEGI | OME    |        |        |        |
| 0       | 1487.46 | 1499.90 | 1511.73 | 1522.89                | 1532.97     |            |        |        |        |        |
| 0.04977 | 1487.95 | 1500.38 | 1512.20 | 1523.33                | 1533.39     | -15.98     | -14.95 | -13.99 | -12.92 | -11.91 |
| 0.10268 | 1488.48 | 1500.89 | 1512.70 | 1523.80                | 1533.83     | -16.05     | -15.03 | -14.07 | -13.01 | -12.00 |
| 0.14998 | 1488.95 | 1501.35 | 1513.14 | 1524.22                | 1534.23     | -16.12     | -15.10 | -14.15 | -13.09 | -12.08 |
| 0.19734 | 1489.42 | 1501.80 | 1513.59 | 1524.65                | 1534.63     | -16.18     | -15.17 | -14.22 | -13.16 | -12.15 |
| 0.24865 | 1489.93 | 1502.30 | 1514.07 | 1525.10                | 1535.06     | -16.25     | -15.24 | -14.29 | -13.24 | -12.23 |
| 0.29972 | 1490.43 | 1502.79 | 1514.55 | 1525.56                | 1535.49     | -16.32     | -15.31 | -14.36 | -13.32 | -12.31 |

LiPF<sub>6</sub>+ aqueous 0.05 mol·kg<sup>-1</sup> TEGDME

| 0       | 1490.09 | 1502.85 | 1531.73 | 1524.89 | 1534.71 |        |        |        |        |        |
|---------|---------|---------|---------|---------|---------|--------|--------|--------|--------|--------|
| 0.04997 | 1490.55 | 1503.30 | 1532.20 | 1525.31 | 1535.12 | -15.36 | -14.42 | -13.35 | -12.55 | -11.66 |
| 0.10879 | 1491.09 | 1503.83 | 1532.75 | 1525.81 | 1535.61 | -15.44 | -14.51 | -13.51 | -12.64 | -11.77 |
| 0.15004 | 1491.47 | 1504.20 | 1533.13 | 1526.16 | 1535.96 | -15.50 | -14.57 | -13.59 | -12.71 | -11.84 |
| 0.20129 | 1491.94 | 1504.66 | 1533.61 | 1526.59 | 1536.38 | -15.58 | -14.64 | -13.68 | -12.79 | -11.92 |
| 0.24602 | 1492.35 | 1505.06 | 1534.03 | 1526.97 | 1536.75 | -15.64 | -14.71 | -13.75 | -12.86 | -11.99 |
| 0.29954 | 1492.84 | 1505.55 | 1534.53 | 1527.42 | 1537.20 | -15.71 | -14.78 | -13.83 | -12.94 | -12.07 |

 $<sup>^{</sup>a}m_{A}$  denotes the molality of LiBF<sub>4</sub> and LiPF<sub>6</sub> in aqueous. media of TEGDME solution. Standard uncertainties in molality of LiBF<sub>4</sub> and LiPF<sub>6</sub> u<sub>r</sub> (m<sub>A</sub>) is 1%. Standard uncertainties in the molality of TEGDME u<sub>r</sub> is 1.5%. Standard uncertainty in acoustic, u(u) = 0.5 m·s<sup>-1</sup>, u(T) = 0.001 K, and pressure, u(p) = 0.01 MPa.

#### 4.2.3 Partial molar isentropic compression

 $K_{\phi,s}^0$  (Partial molar isentropic compression) referred to as limiting molar isentropic compression, have been determined utilizing the equation 1.25. **Table 4.19** shows the computed values of  $K_{\phi,s}^0$  and,  $S_K^*$  of the ternary systems. In ternary systems (LiBF<sub>4</sub>/LiPF<sub>6</sub> + H<sub>2</sub>O + TEGDME), less negative value of the slope  $S_K^*$  indicate that interactions between solute molecules are insignificant, while solute—solvent interactions are prominent. While raising the temperature,  $K_{\phi,s}^0$  lowers because water molecules are firmly bound to solute molecules at low temperatures, but as the temperature rises, the electrostriction between them decreases, and fewer H<sub>2</sub>O molecules are discharged into the core media. As a result, partial molar isentropic compression inference suggests that in this investigation, solute—solvent interactions exceed solute—solute interactions(Kaur *et al.*, 2021).

**Table 4.19:**  $K_{\phi,s}^0$  and  $S_K^*$  of LiBF<sub>4</sub> and LiPF<sub>6</sub> in aqs. media of TEGDME at various temp.

| $m_{\rm B} / ({\rm mol \cdot kg^{-1}})  K_{\phi,s}^0 \times 10^6 / ({\rm m^3 \cdot mol^{-1} \cdot GPa^{-1}})$ |            |               |               |               |               |               | $S_K^* \times 10^6 / (\text{kg} \cdot \text{m}^3 \cdot \text{mol}^{-2} \cdot \text{GPa}^{-1})$ |               |               |               |  |  |
|---|------------|---------------|---------------|---------------|---------------|---------------|--|---------------|---------------|---------------|--|--|
|   | T=293.15 K | T=298.15<br>K | T=303.15<br>K | T=308.15<br>K | T=313.15<br>K | T=293.15<br>K | T=298.15<br>K  | T=303.15<br>K | T=308.15<br>K | T=313.15<br>K |  |  |
| LiBF <sub>4</sub>   |            |               |               |               |               |               |  |               |               |               |  |  |
| 0.01  | -8.73      | -8.21         | -7.73         | -7.37         | -6.99         | -0.73         | -0.76  | -0.74         | -0.74         | -0.75         |  |  |
| 0.03  | -8.22      | -7.82         | -7.34         | -6.79         | -6.34         | -0.74         | -0.76  | -0.76         | -0.81         | -0.78         |  |  |
| 0.05  | -8.09      | -7.21         | -6.31         | -5.18         | -4.35         | -0.80         | -0.80  | -0.88         | -0.87         | -0.89         |  |  |
| LiPF <sub>6</sub>   |            |               |               |               |               |               |  |               |               |               |  |  |
| 0.01  | -16.24     | -15.25        | -14.44        | -13.42        | -12.84        | -1.35         | -1.43  | -1.44         | -1.44         | -1.67         |  |  |
| 0.03  | -15.91     | -14.88        | -13.92        | -12.85        | -11.83        | -1.36         | -1.44  | -1.49         | -1.58         | -1.61         |  |  |
| 0.05  | -15.29     | -14.35        | -13.29        | -12.47        | -11.59        | -1.41         | -1.44  | -1.86         | -1.58         | -1.64         |  |  |
|   |            |               |               |               |               |               |  |               |               |               |  |  |

At infinite dilution, partial molar isentropic compression of transfer ( $\Delta K_{\phi,s}^0$ ) of Li across water to aqueous TEGDME are determined using the equation (1.26). Values of  $\Delta K_{\phi,s}^0$  are listed in **Table 4.20** and are positive. Also  $\Delta K_{\phi,s}^0$  values of LiPF<sub>6</sub> are relatively high in comparison to LiBF<sub>4</sub>, which specifies (hydrophilic-hydrophilic) interactions are more significant in LiPF<sub>6</sub> and aqueous TEGDME.

**Table 4.20:**  $\Delta K_{\phi,s}^0$  of LiBF<sub>4</sub> and LiPF<sub>6</sub> in aqueous media of TEGDME medium.

| m <sub>B</sub>          | $\Delta K_{\phi,s}^0 \times 10^6/(\mathrm{m}^3\ \mathrm{mol}^{-1})$ |            |                 |            |            |  |  |  |  |  |  |  |  |  |
|-------------------------|---|------------|-----------------|------------|------------|--|--|--|--|--|--|--|--|--|
| (mol kg <sup>-1</sup> ) | T=293.15 K  | T=298.15 K | T=303.15 K      | T=308.15 K | T=313.15 K |  |  |  |  |  |  |  |  |  |
|                         | LiBF4   |            |                 |            |            |  |  |  |  |  |  |  |  |  |
| 0.01                    | 3.06  | 3.17       | 3.21            | 3.17       | 3.04       |  |  |  |  |  |  |  |  |  |
| 0.03                    | 3.57  | 3.56       | 3.60            | 3.76       | 3.70       |  |  |  |  |  |  |  |  |  |
| 0.05                    | 3.70  | 4.17       | 4.62            | 5.37       | 5.68       |  |  |  |  |  |  |  |  |  |
|                         |   | Lil        | PF <sub>6</sub> |            |            |  |  |  |  |  |  |  |  |  |
| 0.01                    | 5.18  | 5.22       | 4.69            | 4.87       | 4.26       |  |  |  |  |  |  |  |  |  |
| 0.03                    | 5.51  | 5.60       | 5.21            | 5.45       | 5.27       |  |  |  |  |  |  |  |  |  |
| 0.05                    | 6.13  | 6.13       | 5.84            | 5.82       | 5.52       |  |  |  |  |  |  |  |  |  |

The density and acoustic parameters for LiBF<sub>4</sub> and LiPF<sub>6</sub> have been evaluated in aqueous TEGDME media. When the results for  $V_{\phi}$  and  $V_{\phi}^{0}$  are compared, it could be inferred that interactions among solute & solvent molecules are of considerable importance in the ternary studies performed (Gerald R. Van Hecke, Oliver W. M. Baldwin, 2022b). Moreover, it has been confirmed through transfer volumes that solute-solvent interactions are significant in ternary mixes containing LiPF<sub>6</sub> in aqueous TEGDME. Additionally, the values of the Hepler constant indicate that LiBF<sub>4</sub> and LiPF<sub>6</sub> behave as structure makers in aqueous TEGDME.

# **Section III**

Thermophysical, Acoustic and Conductance
measurements of Lithium bis(fluorosulphonyl)imide
(LiFSI) and Lithium
bis(trifluoromethanesulphonyl)imide (LiTFSI) with
tetraglyme (TEGDME) at various temperatures.

# 4.3 Result and Discussions

# 4.3.1 Density and acoustic measurements

The densities ( $\rho$ ) of LiTFSI and LiFSI in aqueous media of TEGDME with concentrations of glyme  $m_{glyme}$ = (0.01, 0.03 and 0.05) mol·kg<sup>-1</sup> and LiTFSI and LiFSI concentrations ranging from (0.05 to 0.30) mol·kg<sup>-1</sup> at T= (293.15, 298.15, 303.15, 308.15 and 313.15) K were ascertained in this study. **Tables 4.21** and **Table 4.25** show the measured density and acoustic values.

# 4.3.2 Thermophysical parameters derived from density measurements

**Table 4.21** shows that density values enhanced with the concentration of Li salt in the aqueous media of TEGDME increases but drops down when the temperature rises. Furthermore, with the increase in the concentration of glyme, the density increases as well. The values of apparent molar volume for LiTFSI are higher as compared to LiFSI.

**Table 4.21:** The molality, densities  $(\rho)$ , apparent molar volumes  $(V_{\phi})$  of LiTFSI and LiFSI in aqueous TEGDME media at various temperatures, P = 0.1 MPa.

| am <sub>A</sub> / |   | $\rho$   | ×10 <sup>-3</sup> / (kg·m | 1-3)     |          | $V_{\phi} \times 10^6 / (\text{m}^3 \cdot \text{mol}^{-1})$ |          |          |          |          |  |  |  |  |
|-------------------|---|----------|---------------------------|----------|----------|---|----------|----------|----------|----------|--|--|--|--|
| (mol·kg-1)        | T=293.15                                  | T=298.15 | T=303.15                  | T=308.15 | T=313.15 | T=293.15  | T=298.15 | T=303.15 | T=308.15 | T=313.15 |  |  |  |  |
|                   | K   | K        | K                         | K        | K        | K   | K        | K        | K        | K        |  |  |  |  |
|                   | LiTFSI + 0.01 mol·kg <sup>-1</sup> TEGDME |          |                           |          |          |   |          |          |          |          |  |  |  |  |
| 0.00000           | 0.998601                                  | 0.997162 | 0.995575                  | 0.993951 | 0.992427 |   |          |          |          |          |  |  |  |  |
| 0.05015           | 1.005938                                  | 1.004469 | 1.002847                  | 1.001178 | 0.999649 | 139.75  | 140.34   | 140.84   | 141.40   | 142.03   |  |  |  |  |
| 0.09545           | 1.012565                                  | 1.011069 | 1.009415                  | 1.007705 | 1.006172 | 138.83  | 139.42   | 139.92   | 140.49   | 141.11   |  |  |  |  |
| 0.14966           | 1.020497                                  | 1.018968 | 1.017276                  | 1.015518 | 1.013979 | 137.75  | 138.34   | 138.84   | 139.41   | 140.02   |  |  |  |  |
| 0.19867           | 1.027666                                  | 1.026108 | 1.024382                  | 1.022579 | 1.021035 | 136.79  | 137.38   | 137.88   | 138.45   | 139.06   |  |  |  |  |
| 0.24995           | 1.035169                                  | 1.033580 | 1.031818                  | 1.029969 | 1.028420 | 135.80  | 136.39   | 136.88   | 137.45   | 138.06   |  |  |  |  |
| 0.30026           | 1.042530                                  | 1.040911 | 1.039113                  | 1.037219 | 1.035665 | 134.84  | 135.43   | 135.92   | 136.49   | 137.09   |  |  |  |  |

#### LiTFSI + 0.03 mol·kg<sup>-1</sup> TEGDME 0.00000 0.999412 0.997889 0.996373 0.994742 0.993179 0.04999 1.006861 1.005288 1.003722 1.002041 1.000438 137.05 138.04 139.03 140.02 140.82 0.09845 1.014081 1.012460 1.010845 1.009116 139.84 1.007474 136.08 137.06 138.05 139.04 1.018365 0.14960 1.021703 1.020030 1.016584 1.014902 135.06 137.03 138.02 138.81 136.04 0.20012 1.029230 1.027507 1.025791 1.023960 1.022236 134.07 135.05 136.04 137.03 137.82 0.25312 1.037127 1.035351 1.033582 1.031698 1.029932 133.05 134.03 135.01 136.00 136.79 0.29913 1.043982 1.042160 1.040345 1.038415 1.036612 132.18 133.15 134.13 135.12 135.91 LiTFSI + 0.05 mol·kg<sup>-1</sup> TEGDME 0.00000 1.000032 0.998702 0.997110 0.995511 0.993876 0.05013 1.002905 140.01 1.007607 1.006222 1.004560 1.001195 134.96 136.04 137.42 138.51 0.10014 1.015163 1.013723 1.011992 1.010282 1.008496 133.95 135.03 136.41 137.50 139.00 1.021161 0.14972 1.022655 1.019360 1.017595 1.015736 132.97 134.05 135.43 136.51 138.01 0.20031 1.026877 137.01 1.030299 1.028749 1.025057 1.023121 131.99 133.06 134.44 135.52 0.24998 1.037804 1.036199 1.034258 1.032383 1.030373 131.03 132.10 133.48 134.56 136.05 0.30014 1.045384 1.043724 1.041712 1.039782 1.037697 130.08 131.15 132.52 133.60 135.09

LiFSI + 0.01 mol·kg<sup>-1</sup> TEGDME

| 0  | 0.998601                         | 0.997162                         | 0.995575                                     | 0.993951                                     | 0.992427                                     |                         |                |                |                |                |  |
|--|----------------------------------|----------------------------------|--|--|--|-------------------------|----------------|----------------|----------------|----------------|--|
| 0.05024                                  | 1.003590                         | 1.002151                         | 1.000509                                     | 0.998860                                     | 0.997305                                     | 87.32                   | 87.88          | 88.39          | 88.88          | 89.47          |  |
| 0.09664                                  | 1.008197                         | 1.006758                         | 1.005065                                     | 1.003392                                     | 1.001810                                     | 86.92                   | 87.48          | 87.99          | 88.48          | 89.07          |  |
| 0.14954                                  | 1.013450                         | 1.012011                         | 1.010259                                     | 1.008561                                     | 1.006947                                     | 86.47                   | 87.03          | 87.54          | 88.02          | 88.61          |  |
| 0.19990                                  | 1.018451                         | 1.017012                         | 1.015205                                     | 1.013481                                     | 1.011837                                     | 86.04                   | 86.61          | 87.11          | 87.59          | 88.19          |  |
| 0.25014                                  | 1.023440                         | 1.022001                         | 1.020138                                     | 1.018389                                     | 1.016715                                     | 85.62                   | 86.18          | 86.69          | 87.17          | 87.76          |  |
| 0.30032                                  | 1.028423                         | 1.026984                         | 1.025066                                     | 1.023292                                     | 1.021588                                     | 85.21                   | 85.77          | 86.27          | 86.75          | 87.34          |  |
| LiFSI + 0.03 mol·kg <sup>-1</sup> TEGDME |                                  |                                  |  |  |  |                         |                |                |                |                |  |
|  |                                  |                                  |  | LIFSI 1 0.0                                  | Jillot Kg 1                                  | EODNIE                  |                |                |                |                |  |
| 0  | 0.999412                         | 0.997889                         | 0.996373                                     | 0.994742                                     | 0.993179                                     | EGDME                   |                |                |                |                |  |
| 0<br>0.05021                             | 0.999412<br>1.004358             | 0.997889<br>1.002808             |  |  | O  | 88.13                   | 88.64          | 89.10          | 89.59          | 90.09          |  |
|  |                                  |                                  | 0.996373                                     | 0.994742                                     | 0.993179                                     |                         | 88.64<br>88.21 | 89.10<br>88.67 | 89.59<br>89.16 | 90.09<br>89.65 |  |
| 0.05021                                  | 1.004358                         | 1.002808                         | 0.996373<br>1.001269                         | 0.994742<br>0.999612                         | 0.993179<br>0.998024                         | 88.13                   |                |                |                |                |  |
| 0.05021<br>0.10042                       | 1.004358<br>1.009304             | 1.002808<br>1.007727             | 0.996373<br>1.001269<br>1.006164             | 0.994742<br>0.999612<br>1.004483             | 0.993179<br>0.998024<br>1.002870             | 88.13<br>87.70          | 88.21          | 88.67          | 89.16          | 89.65          |  |
| 0.05021<br>0.10042<br>0.14956            | 1.004358<br>1.009304<br>1.014144 | 1.002808<br>1.007727<br>1.012542 | 0.996373<br>1.001269<br>1.006164<br>1.010956 | 0.994742<br>0.999612<br>1.004483<br>1.009250 | 0.993179<br>0.998024<br>1.002870<br>1.007612 | 88.13<br>87.70<br>87.28 | 88.21<br>87.79 | 88.67<br>88.25 | 89.16<br>88.74 | 89.65<br>89.23 |  |

LiFSI + 0.05 mol·kg<sup>-1</sup> TEGDME

| 0.00000 | 1.000032 | 0.998702 | 0.997111 | 0.995511 | 0.993876 |       |       |       |       |       |
|---------|----------|----------|----------|----------|----------|-------|-------|-------|-------|-------|
| 0.05022 | 1.004919 | 1.003563 | 1.001947 | 1.000322 | 0.998662 | 89.33 | 89.82 | 90.32 | 90.81 | 91.30 |
| 0.09617 | 1.009389 | 1.008011 | 1.006372 | 1.004724 | 1.003041 | 88.94 | 89.43 | 89.92 | 90.41 | 90.91 |
| 0.14965 | 1.014593 | 1.013189 | 1.011523 | 1.009848 | 1.008138 | 88.48 | 88.97 | 89.46 | 89.95 | 90.45 |
| 0.20191 | 1.019678 | 1.018247 | 1.016555 | 1.014854 | 1.013118 | 88.04 | 88.53 | 89.02 | 89.51 | 90.00 |
| 0.25538 | 1.024880 | 1.023423 | 1.021704 | 1.019976 | 1.018214 | 87.59 | 88.08 | 88.57 | 89.06 | 89.55 |
| 0.30218 | 1.029434 | 1.027953 | 1.026211 | 1.024460 | 1.022674 | 87.21 | 87.69 | 88.18 | 88.67 | 89.16 |

 $<sup>^</sup>am_A$  denotes molality of LiTFSI and LiFSI in aqueous TEGDME medium. Standard uncertainties in molality of LiTFSI and LiFSI  $u_r(m_A)$  and TEGDME  $u_r$  are 1% and 1.5% respectively. Standard uncertainty in density,  $u(\rho) = \pm 5 \times 10^{-3} \text{ kg} \cdot \text{m}^{-3}$ , temperature, u(T) = 0.001 K, and pressure, u(p) = 0.01 MPa.

### 4.3.3 Apparent molar volume

The apparent molar volume  $(V_{\phi})$  has been determined by utilizing the equation (1.13). In this equation, M and  $m_A$  denote the molar mass  $(kg \cdot mol^{-1})$  and molality of LiTFSI/LiFSI correspondingly, and  $\rho_0$  and  $\rho$  denote the densities  $(kg \cdot m^{-3})$  of solvent and solution. The resulting apparent molar volume values are presented in **Table 4.21**, and the trend is graphically depicted in **figure 4.4** and **4.5**.

 $V_{\phi}$  values of LiTFSI and LiFSI in (0.01 and 0.05) mol·kg<sup>-1</sup> of TEGDME at (T=293.15 K, 298.15 K, 303.15 K, 308.15 and 313.15 K) have been presented in figure 4.4 and 4.5.  $V_{\phi}$  values increases with temperature rise demonstrating that the solute has a greater affinity for the solvent at elevated temperatures that leads to more solute–solvent interactions. It is evident from the analysis of data that  $V_{\phi}$  values are larger at higher temperatures. This happens because the rising temperatures allow more thermal movements in molecules resulting in an increase in volume. Furthermore, the positive  $V_{\phi}$  values signify that LiTFSI and LiFSI in aqueous TEGDME media have strong solute–solvent interactions (Panduranga Rao *et al.*, 2024). The apparent molar volume decreases as the molality of LiTFSI and LiFSI increases.

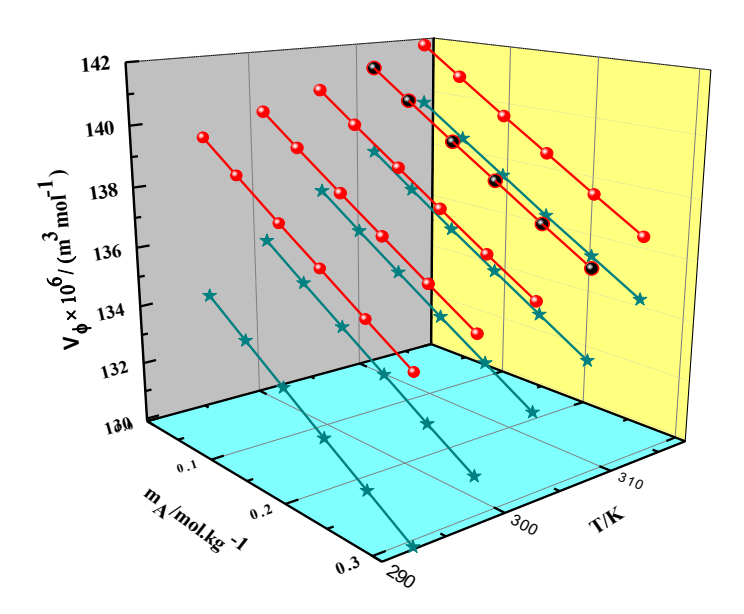


**Figure 4.4:** Plots of variation of apparent molar volume ( $V_{\phi}$ ) of, LiTFSI in 0.01 mol·kg<sup>-1</sup> (Red) and 0.05 mol·kg<sup>-1</sup> (cyan) of aqueous media of TEGDME at T = (293.15, 298.15, 303.15, 308.15 and 313.15) K.

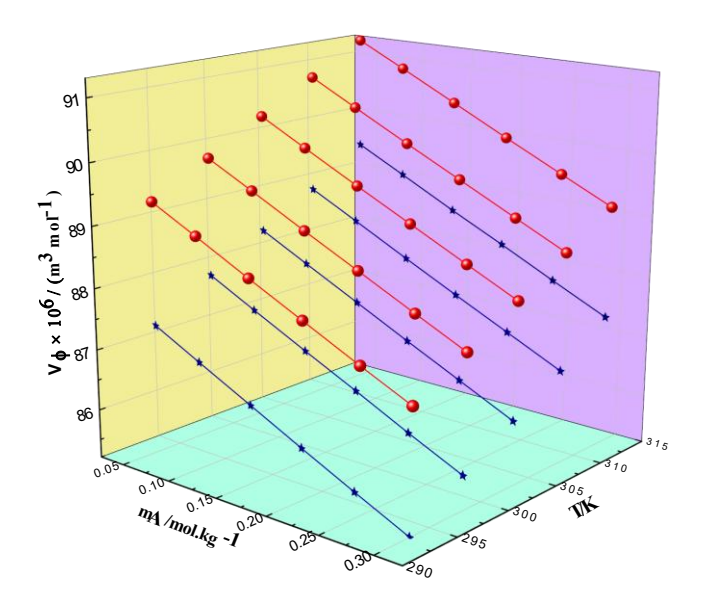


**Figure 4.5:**Plots of variation of apparent molar volume ( $V_{\phi}$ ) of, LiFSI in 0.01 mol·kg<sup>-1</sup> (Red) and 0.05 mol·kg<sup>-1</sup> (blue) of aqueous media of TEGDME at T = (293.15, 298.15, 303.15, 308.15 and 313.15) K

#### 4.3.4 Partial molar volume

The apparent molar volume at infinite dilution, also known as partial molar volume  $(V_{\phi}^{0})$ , was calculated utilizing Masson's least square fitting approach in equation 1.15. In this equation,  $V_{\phi}^{0}$  denotes partial molar volume. The slope of the graph represented as  $S_V^*$ .  $V_{\phi}^0$ , depicts the solute–solvent interactions, assuming that the solute molecules are apart at infinite dilution and hence no solute-solute interactions exist. **Table 4.22** shows the values of  $V_{\phi}^{0}$  and  $S_{V}^{*}$ . When the results are analysed, it becomes obvious that  $V_{\phi}^{0}$  has positive values that reduce as the molal concentration of TEGDME raises.  $V_{\phi}^{0}$  values also increase when the temperature rises. The positive  $V_{\phi}^{0}$  proves the occurrence of solute-solvent interactions in ternary systems (Borović et al., 2024). The electrostriction, which decreases as the temperature increases, could be responsible for the increasing of  $V_{\phi}^{0}$  values with temperature. Some solvation molecules emerge solute's loose solvation layers and penetrate the bulk solution sequentially. The water molecules that enclose LiTFSI and LiFSI are compressed by the electric field induced by their head groups. The negative values of the slope  $S_V^*$  clearly illustrate the prevalence of solute-solvent interactions and negligible solute-solute interactions. As a result, increased apparent molar volume values in the ternary (Li salts + H<sub>2</sub>O + TEGDME) solutions indicate the prevalence of solute-solvent interactions rather than solute-solute interactions. LiTFSI has higher values of  $V_\phi^0$  than LiFSI. There is no regular trend in the  $S_V^*$ , indicating there may be other variables that have a substantial influence on the solute–solvent interactions (Kumar & Behal, 2017).

**Table 4.22:** Partial molar volumes,  $(V_{\phi}^{0})$  and experimental slopes,  $(S_{v}^{*})$  of LiTFSI and LiFSI in aqueous media of TEGDME at various temperatures.

| <sup>a</sup> m <sub>B</sub> |          | $V_{\phi}^{0}$ × | 10 <sup>6</sup> /(m <sup>3</sup> ·n | nol <sup>-1</sup> ) |          | $S_v^* \times 10^6 / (\text{m}^3 \cdot \text{kg} \cdot \text{mol}^{-2})$ |          |          |          |          |  |
|-----------------------------|----------|------------------|-------------------------------------|---------------------|----------|--|----------|----------|----------|----------|--|
| (mol·kg <sup>-1</sup> )     | T=293.15 | T=298.15         | T=303.15                            | T=308.15            | T=313.15 | T=293.15   | T=298.15 | T=303.15 | T=308.15 | T=313.15 |  |
|                             | K        | K                | K                                   | K                   | K        | K  | K        | K        | K        | K        |  |
| -                           |          |                  |                                     |                     | LiTFSI   |  |          |          |          |          |  |
| 0.01                        | 140.71   | 141.30           | 141.80                              | 142.37              | 143.00   | -19.61   | -19.66   | -19.69   | -19.71   | -19.75   |  |
| 0.03                        | 138.01   | 138.99           | 139.99                              | 140.98              | 141.78   | -19.56   | -19.60   | -19.64   | -19.68   | -19.72   |  |
| 0.05                        | 135.91   | 137.00           | 138.38                              | 139.47              | 140.98   | -19.51   | -19.55   | -19.60   | -19.65   | -19.70   |  |
|                             |          |                  |                                     |                     | LiFSI    |  |          |          |          |          |  |
| 0.01                        | 87.73    | 88.30            | 88.81                               | 89.30               | 89.89    | -8.43  | -8.46    | -8.47    | -8.48    | -8.50    |  |
| 0.03                        | 88.54    | 89.06            | 89.52                               | 90.01               | 90.51    | -8.44  | -8.45    | -8.47    | -8.49    | -8.51    |  |
| 0.05                        | 89.75    | 90.24            | 90.73                               | 91.23               | 91.73    | -8.44  | -8.46    | -8.48    | -8.49    | -8.52    |  |

<sup>&</sup>lt;sup>a</sup>m<sub>B</sub> is molality of aqueous TEGDME medium.

# 4.3.5 Temperature dependence of partial molar volume

The effect of temperature on apparent molar volume at infinite dilution  $(V_{\phi}^{0})$  has been evaluated utilizing the polynomial equation (1.18). In this equation,  $T_{\text{ref}}$  is reference temperature (298.15 K), whereas the empirical constants are a, b and c. **Table 4.23** enlists the values of these empirical constants. Apart from c at  $m_{TEGDME} = 0.03 \text{ mol·kg}^{-1}$  for Li salts, wherein empirical constant c has minor negative values, all empirical constants are positive (Kumar & Behal, 2016b).

**Table 4.23:** Values of empirical parameters determined from Eq. (1.18) for LiTFSI and LiFSI in aqueous media of TEGDME.

| <sup>a</sup> m <sub>B</sub> / | a×10 <sup>6</sup> / b×10 <sup>6</sup> / |  | c×10 <sup>6</sup> /                                   | $\mathbb{R}^2$ | ARD(σ)  |  |  |  |  |  |  |  |
|-------------------------------|---|--|---|----------------|---------|--|--|--|--|--|--|--|
| (mol·kg <sup>-1</sup> )       | (mol·kg <sup>-1</sup> )                 | (m <sup>3</sup> ·mol <sup>-1</sup> ·K) | (m <sup>3</sup> ·mol <sup>-1</sup> ·K <sup>-2</sup> ) |                |         |  |  |  |  |  |  |  |
| LiTFSI                        |   |  |   |                |         |  |  |  |  |  |  |  |
| 0.01                          | 141.26                                  | 0.109                                  | 0.0004  | 0.9999         | 0.0007  |  |  |  |  |  |  |  |
| 0.03                          | 139.02                                  | 0.201                                  | -0.0011   | 0.9999         | 0.0008  |  |  |  |  |  |  |  |
| 0.05                          | 137.05                                  | 0.237                                  | 0.0015  | 0.9999         | 0.0027  |  |  |  |  |  |  |  |
|                               |   | Lil                                    | FSI   |                |         |  |  |  |  |  |  |  |
| 0.01                          | 88.27                                   | 0.1051                                 | 0.00010   | 0.9999         | 0.00101 |  |  |  |  |  |  |  |
| 0.03                          | 89.04                                   | 0.0978                                 | -0.00004  | 0.9999         | 0.00047 |  |  |  |  |  |  |  |
| 0.05                          | 90.24                                   | 0.0983                                 | 0.00004   | 0.9999         | 0.00001 |  |  |  |  |  |  |  |

<sup>&</sup>lt;sup>a</sup>m<sub>B</sub> is molality of aqueous TEGDME medium.

The experimental values of  $V_{\phi}^{0}$  deviate from the theoretical values. The ARD ( $\sigma$ ) deviations could be determined by employing the equation (1.20). **Table 4.23** summarizes the ARD data, demonstrating that polynomial equation fits significantly during the ternary compositions undergoing examination.

Furthermore, partial molar expansibilities,  $\phi_E^0$ , have been utilized to validate the significantly recurring solute—solvent interactions in the mixture by utilizing the equation (1.21). For all quantities of TEGDME and experimental temperatures, the partial molar expansibilities (given in **Table 4.24**) are positive, demonstrating that there are solute—solvent interactions in the ternary systems studied(Chen *et al.*, 2024). The packing effect phenomena verifies the occurrence of substantial interactions between LiTFSI/LiFSI and TEGDME with the reported positive values of,  $\phi_E^0$ .

**Table 4.24:** Limiting apparent molar expansibilities ( $\phi_E^0$ ) of LiTFSI and LiFSI in aqueous media of TEGDME at various temperatures.

| <sup>a</sup> m <sub>B</sub> / | $\phi_E^0 \times 10^6 / (\mathrm{m}^3 \cdot \mathrm{mol}^{-1} \cdot \mathrm{mol}^{-1} \cdot \mathrm{K}^{-1})$ |            |               |  |        |        |  |  |  |  |  |
|-------------------------------|---|------------|---------------|--|--------|--------|--|--|--|--|--|
| (mol·kg <sup>-1</sup> )       | T=293.15 K  | T=308.15 K | T=313.15<br>K | $(\partial \phi_E^0$ $/\partial \mathbf{T})$ |        |        |  |  |  |  |  |
|                               |   |            | LiTFSI        |  |        |        |  |  |  |  |  |
| 0.01                          | 0.105   | 0.109      | 0.113         | 0.117  | 0.121  | 0.001  |  |  |  |  |  |
| 0.03                          | 0.212   | 0.201      | 0.191         | 0.180  | 0.170  | -0.002 |  |  |  |  |  |
| 0.05                          | 0.222   | 0.237      | 0.253         | 0.268  | 0.284  | 0.003  |  |  |  |  |  |
| LiFSI                         |   |            |               |  |        |        |  |  |  |  |  |
| 0.01                          | 0.1041  | 0.1051     | 0.1061        | 0.1072                                       | 0.1082 | 0.0002 |  |  |  |  |  |

| 0.03 | 0.0982 | 0.0978 | 0.0974 | 0.0970 | 0.0967 | -0.0001 |
|------|--------|--------|--------|--------|--------|---------|
| 0.05 | 0.0979 | 0.0983 | 0.0987 | 0.0991 | 0.0995 | 0.0001  |

<sup>&</sup>lt;sup>a</sup>m<sub>B</sub> denotes molality of aqueous TEGDME media.

In a mixed solvent solution, the Hepler constant contributes in evaluating the solute's potential to function as a structure breaker/maker. Hepler's thermodynamic equation is found in equation (1.22) (Hepler, 1969). Positive & negative values of  $(\partial \phi_E^0/\partial T)_p$  have been reported for the ternary systems investigated for (LiTFSI/LiFSI + H<sub>2</sub>O + TEGDME (given in **Table 4.24**). The sign of  $(\partial \phi_E^0/\partial T)$  could be used to evaluate the function of a solute as a structure maker/breaker. Structure makers have positive values of  $(\partial \phi_E^0/\partial T)$  and minor negative values of  $(\partial \phi_E^0/\partial T)$ , while structure breakers solutes have negative values. In aqueous media of the glyme,  $m_{Glyme} = (0.01, 0.03, \text{ and } 0.05) \text{ molkg}^{-1}$ , LiTFSI and LiFSI operate as structure makers

# 4.3.6 Acoustic parameters derived from the speed of sound (acoustic) measurements

The acoustic values can reveal a lot concerning a solution's diverse characteristics. **Table 4.25** shows the sound speed of LiTFSI/LiFSI in  $m_{Glycol} = (0.01, 0.03 \text{ and } 0.05) \text{ mol·kg}^{-1}$  of aqueous TEGDME at above-specified temperatures. The molality of the LiTFSI and LiFSI, temperature and concentration of glyme affect the values attained for the acoustic values of LiTFSI/LiFSI.

**Table 4.25:** Values of ultrasonic speed, (*u*) and apparent molar isentropic compression, ( $K_{\phi,s}$ ) of LiTFSI and LiFSI in aqueous media of TEGDME at various temperatures, P = 0.1 MPa.

| <sup>a</sup> m <sub>A</sub> / |   |          | <i>u</i> / (r | n·s <sup>-1</sup> ) |          | $K_{\phi,S} \times 10^6  (\mathrm{m}^3 \cdot \mathrm{mol}^{-1} \cdot \mathrm{GPa}^{-1})$ |          |          |          |          |  |  |  |  |  |
|-------------------------------|---|----------|---------------|---------------------|----------|--|----------|----------|----------|----------|--|--|--|--|--|
| (mol·kg <sup>-1</sup> )       | T=293.15  | T=298.15 | T=303.15      | T=308.15            | T=313.15 | T=293.15   | T=298.15 | T=303.15 | T=308.15 | T=313.15 |  |  |  |  |  |
|                               | K   | K        | K             | K                   | K        | K  | K        | K        | K        | K        |  |  |  |  |  |
|                               | LiTFSI + aqueous 0.01 mol·kg <sup>-1</sup> TEGDME |          |               |                     |          |  |          |          |          |          |  |  |  |  |  |
| 0.00000                       | 1484.54   | 1497.38  | 1509.59       | 1521.13             | 1530.70  |  |          |          |          |          |  |  |  |  |  |
| 0.05015                       | 1484.84   | 1497.65  | 1509.84       | 1521.38             | 1530.90  | -6.76  | -5.93    | -5.24    | -4.61    | -4.02    |  |  |  |  |  |
| 0.09545                       | 1485.10   | 1497.89  | 1510.07       | 1521.61             | 1531.08  | -7.15  | -6.32    | -5.62    | -4.99    | -4.40    |  |  |  |  |  |
| 0.14966                       | 1485.42   | 1498.18  | 1510.34       | 1521.89             | 1531.29  | -7.60  | -6.76    | -6.07    | -5.44    | -4.84    |  |  |  |  |  |
| 0.19867                       | 1485.71   | 1498.44  | 1510.59       | 1522.14             | 1531.49  | -7.99  | -7.16    | -6.45    | -5.83    | -5.23    |  |  |  |  |  |
| 0.24995                       | 1486.02   | 1498.71  | 1510.84       | 1522.40             | 1531.69  | -8.39  | -7.55    | -6.85    | -6.22    | -5.62    |  |  |  |  |  |
| 0.30026                       | 1486.31   | 1498.98  | 1511.09       | 1522.65             | 1531.89  | -8.77  | -7.93    | -7.23    | -6.60    | -5.99    |  |  |  |  |  |

| LiTFSI + aqueous 0.03 mol·kg <sup>-1</sup> TEGDME |         |         |         |           |            |                        |             |        |        |        |  |  |
|---|---------|---------|---------|-----------|------------|------------------------|-------------|--------|--------|--------|--|--|
| 0.00000   | 1487.46 | 1499.90 | 1511.73 | 1522.89   | 1532.40    |                        |             |        |        |        |  |  |
| 0.04999   | 1487.90 | 1500.33 | 1512.15 | 1523.30   | 1532.80    | -10.82                 | -9.85       | -8.79  | -7.96  | -7.21  |  |  |
| 0.09845   | 1488.33 | 1500.76 | 1512.55 | 1523.70   | 1533.18    | -11.21                 | -10.24      | -9.18  | -8.36  | -7.60  |  |  |
| 0.14960   | 1488.78 | 1501.20 | 1512.97 | 1524.13   | 1533.59    | -11.61                 | -10.64      | -9.58  | -8.76  | -8.00  |  |  |
| 0.20012   | 1489.22 | 1501.64 | 1513.40 | 1524.54   | 1533.99    | -11.99                 | -11.02      | -9.97  | -9.14  | -8.38  |  |  |
| 0.25312   | 1489.69 | 1502.10 | 1513.84 | 1524.98   | 1534.42    | -12.37                 | -11.41      | -10.36 | -9.54  | -8.77  |  |  |
| 0.29913   | 1490.10 | 1502.50 | 1514.22 | 1525.36   | 1534.78    | -12.70                 | -11.73      | -10.68 | -9.86  | -9.10  |  |  |
|   |         |         | LiTFS   | I + aqueo | us 0.05 mo | l·kg <sup>-1</sup> TEC | <b>GDME</b> |        |        |        |  |  |
| 0.00000   | 1490.09 | 1502.85 | 1513.73 | 1524.89   | 1534.71    |                        |             |        |        |        |  |  |
| 0.05013   | 1490.51 | 1503.29 | 1514.17 | 1525.32   | 1534.83    | -12.24                 | -11.45      | -10.34 | -9.33  | -8.49  |  |  |
| 0.10014   | 1490.93 | 1503.72 | 1514.61 | 1525.75   | 1534.96    | -12.63                 | -11.84      | -10.73 | -9.73  | -8.84  |  |  |
| 0.14972   | 1491.34 | 1504.15 | 1515.05 | 1526.18   | 1535.08    | -13.00                 | -12.21      | -11.10 | -10.10 | -9.17  |  |  |
| 0.20031   | 1491.76 | 1504.59 | 1515.49 | 1526.62   | 1535.20    | -13.37                 | -12.57      | -11.47 | -10.48 | -9.50  |  |  |
| 0.24998   | 1492.18 | 1505.02 | 1515.93 | 1527.05   | 1535.32    | -13.71                 | -12.92      | -11.82 | -10.83 | -9.81  |  |  |
| 0.30014   | 1492.60 | 1505.46 | 1516.37 | 1527.48   | 1535.45    | -14.05                 | -13.26      | -12.17 | -11.18 | -10.12 |  |  |

| LiFSI + aqueous 0.01 mol·kg <sup>-1</sup> TEGDME |                               |                               |  |  |  |                            |                            |                |                |                |  |  |
|--|-------------------------------|-------------------------------|--|--|--|----------------------------|----------------------------|----------------|----------------|----------------|--|--|
| 0.00000  | 1484.54                       | 1497.38                       | 1509.59                                  | 1521.13                                  | 1530.70                                  |                            |                            |                |                |                |  |  |
| 0.05024  | 1485.25                       | 1497.98                       | 1510.14                                  | 1521.59                                  | 1531.05                                  | -14.21                     | -12.74                     | -11.11         | -9.56          | -7.87          |  |  |
| 0.09664  | 1485.91                       | 1498.54                       | 1510.65                                  | 1522.01                                  | 1531.38                                  | -14.36                     | -12.89                     | -11.26         | -9.71          | -8.02          |  |  |
| 0.14954  | 1486.66                       | 1499.17                       | 1511.23                                  | 1522.49                                  | 1531.75                                  | -14.52                     | -13.05                     | -11.42         | -9.87          | -8.19          |  |  |
| 0.19990  | 1487.37                       | 1499.77                       | 1511.78                                  | 1522.95                                  | 1532.10                                  | -14.67                     | -13.20                     | -11.57         | -10.03         | -8.35          |  |  |
| 0.25014  | 1488.08                       | 1500.37                       | 1512.33                                  | 1523.40                                  | 1532.46                                  | -14.81                     | -13.34                     | -11.72         | -10.18         | -8.50          |  |  |
| 0.30032  | 1488.80                       | 1500.97                       | 1512.88                                  | 1523.86                                  | 1532.81                                  | -14.95                     | -13.48                     | -11.86         | -10.32         | -8.65          |  |  |
|  |                               |                               |  |  |  |                            |                            |                |                |                |  |  |
| LiFSI + aqueous 0.03 mol·kg <sup>-1</sup> TEGDME |                               |                               |  |  |  |                            |                            |                |                |                |  |  |
|  |                               |                               | LiFSI                                    | + aqueou                                 | s 0.03 mol                               | kg <sup>-1</sup> TEG       | DME                        |                |                |                |  |  |
| 0.00000  | 1487.46                       | 1499.90                       | <b>LiFSI</b> 1511.73                     | + aqueou<br>1522.89                      | s 0.03 mol-                              | kg <sup>-1</sup> TEG       | DME                        |                |                |                |  |  |
| 0.00000<br>0.05021                               | 1487.46<br>1488.03            | 1499.90<br>1500.42            |  | -  |  | -11.62                     | <b>DME</b> -10.42          | -9.23          | -8.10          | -6.98          |  |  |
|  |                               |                               | 1511.73                                  | 1522.89                                  | 1532.40                                  | S                          |                            | -9.23<br>-9.40 | -8.10<br>-8.27 | -6.98<br>-7.14 |  |  |
| 0.05021  | 1488.03                       | 1500.42                       | 1511.73<br>1512.18                       | 1522.89<br>1523.28                       | 1532.40<br>1532.73                       | -11.62                     | -10.42                     |                |                |                |  |  |
| 0.05021<br>0.10042                               | 1488.03<br>1488.60            | 1500.42<br>1500.93            | 1511.73<br>1512.18<br>1512.63            | 1522.89<br>1523.28<br>1523.67            | 1532.40<br>1532.73<br>1533.05            | -11.62<br>-11.78           | -10.42<br>-10.58           | -9.40          | -8.27          | -7.14          |  |  |
| 0.05021<br>0.10042<br>0.14956                    | 1488.03<br>1488.60<br>1489.16 | 1500.42<br>1500.93<br>1501.43 | 1511.73<br>1512.18<br>1512.63<br>1513.08 | 1522.89<br>1523.28<br>1523.67<br>1524.06 | 1532.40<br>1532.73<br>1533.05<br>1533.37 | -11.62<br>-11.78<br>-11.93 | -10.42<br>-10.58<br>-10.74 | -9.40<br>-9.55 | -8.27<br>-8.42 | -7.14<br>-7.30 |  |  |

-10.01

-8.89

-7.76

0.30014 1490.86 1502.98 1514.43 1525.23 1534.35 -12.38 -11.20

LiFSI + aqueous 0.05 mol·kg<sup>-1</sup> TEGDME

| 0.00000 | 1490.09 | 1502.85 | 1513.73 | 1524.89 | 1534.71 |        |       |       |       |       |
|---------|---------|---------|---------|---------|---------|--------|-------|-------|-------|-------|
| 0.05022 | 1490.58 | 1503.31 | 1514.15 | 1525.28 | 1535.07 | -9.44  | -8.58 | -7.69 | -6.93 | -6.18 |
| 0.09617 | 1491.03 | 1503.73 | 1514.53 | 1525.64 | 1535.39 | -9.60  | -8.74 | -7.85 | -7.09 | -6.33 |
| 0.14965 | 1491.55 | 1504.22 | 1514.98 | 1526.05 | 1535.77 | -9.78  | -8.91 | -8.02 | -7.27 | -6.51 |
| 0.20191 | 1492.06 | 1504.69 | 1515.42 | 1526.46 | 1536.15 | -9.95  | -9.08 | -8.19 | -7.44 | -6.68 |
| 0.25538 | 1492.58 | 1505.18 | 1515.86 | 1526.87 | 1536.53 | -10.12 | -9.25 | -8.36 | -7.61 | -6.86 |
| 0.30218 | 1493.03 | 1505.61 | 1516.25 | 1527.24 | 1536.86 | -10.26 | -9.40 | -8.51 | -7.76 | -7.00 |

 $<sup>^{</sup>a}m_{A}$  denotes molality of LiTFSI and LiFSI in aqueous TEGDME medium. Standard uncertainties in molality of LiTFSI and LiFSI  $u_{r}(m_{A})$  and TEGDME  $u_{r}$  are 1% and 1.5% respectively. Standard uncertainty in acoustic,  $u(u) = 0.5 \text{m·s}^{-1}$ , u(T) = 0.001 K, and pressure, u(p) = 0.01 MPa.

## 4.3.7 Apparent molar isentropic compression:

The apparent molar isentropic compression  $(K_{\phi,s})$  can be determined by utilizing the equation (1.23). In this equation,  $\kappa_S$  denotes solution isentropic compressibility and  $\kappa_{S,\theta}$  denotes pure solvent isentropic compressibility. The molality of the solute is  $m_A$ , the molar mass of the LiTFSI (solute) is M, and the density values of the solute and solvent are  $\rho$  and  $\rho_\theta$  correspondingly.  $\kappa_S$  can be computed using Laplace Newton's equation (equation 1.24) where u and  $\rho$  refers to the density and acoustic values of the given solution.

The values of  $K_{\phi,s}$  determined employing (equation 8) have been indexed in **table 4.25** and plots for the same are provided in **figure 4.6** and **4.7**.

 $K_{\phi,s}$  is negative at all the aqueous TEGDME concentrations and temperatures. As the molality of the LiTFSI/ LiFSI and the temperature increases, the  $K_{\phi,s}$  values of Li salts ascent. Furthermore, as the concentration of solvent increased,  $K_{\phi,s}$  decreases. The occurrence of solute-solvent interactions is confirmed by negative values of  $K_{\phi,s}$  which indicate that H<sub>2</sub>O molecules in the bulk media are significantly more deformable than those nearby the solute (Kaur *et al.*, 2020). Because of the charge on ions, the electrostricted H<sub>2</sub>O molecules are mainly compacted. The electrostriction reduces with rising temperature, and some H<sub>2</sub>O molecules discharged from the hydration sphere and into the bulk media, resulting in less conformational distortion of the water and showing a reduced regulating influence by the solute on the solvent.  $V_{\phi}^{0}$  values have also determined that (solute–solvent) interactions predominate (Thakur Abhishek, Sharma Shashi Kant, 2022).

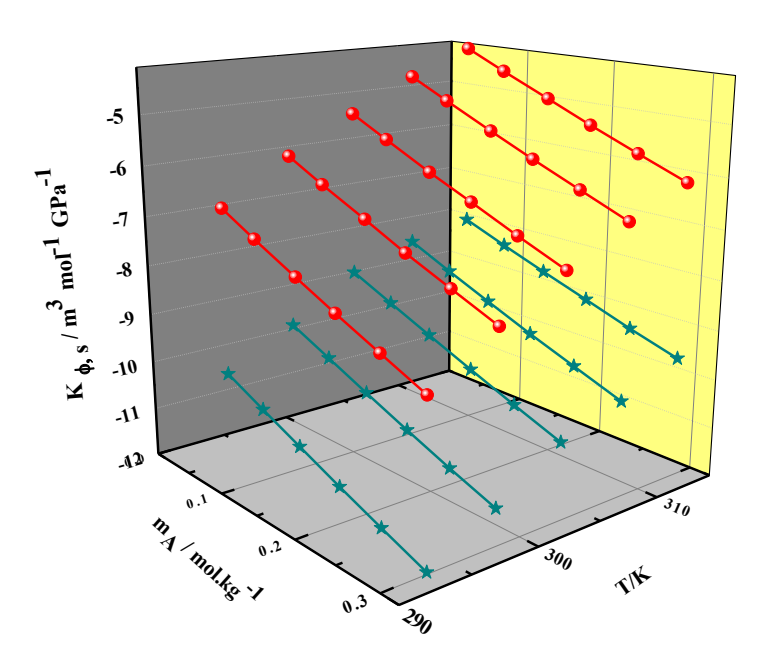


**Figure 4.6:** Plots of variation of apparent molar isentropic compression  $(K_{\phi,s})$  of, LiTFSI in 0.01 mol·kg<sup>-1</sup> (Red) and 0.05 mol·kg<sup>-1</sup> (cyan) of aqueous media of TEGDME at T = (293.15, 298.15, 303.15, 308.15 and 313.15) K.

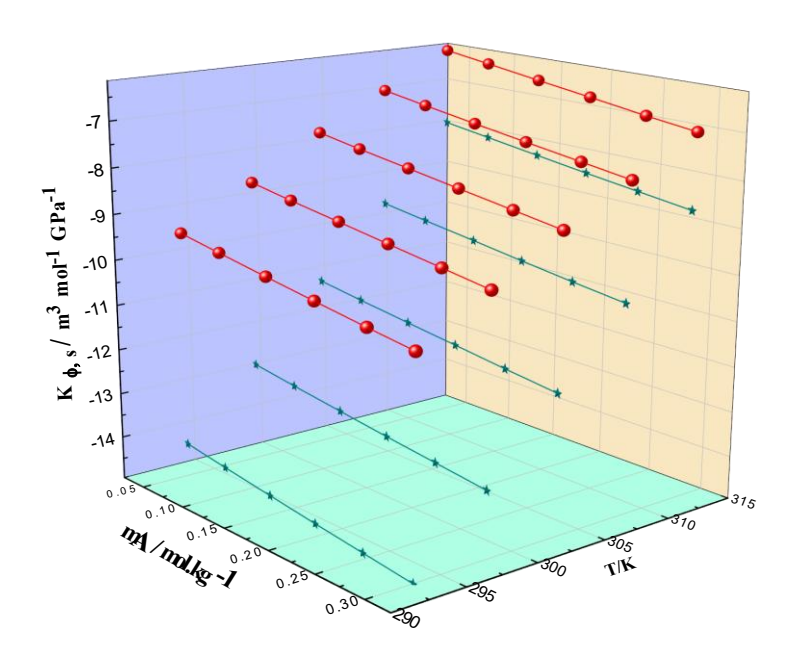


**Figure 4.7:** Plots of variation of apparent molar isentropic compression ( $K_{\phi,s}$ ) of LiFSI in 0.01 mol·kg<sup>-1</sup> (Red) and 0.05 mol·kg<sup>-1</sup> (cyan) of aqueous media of TEGDME at T = (293.15, 298.15, 303.15, 308.15 and 313.15) K.

### 4.3.8 Partial molar isentropic compression:

 $K_{\phi,s}^0$  (partial molar isentropic compression) referred to as limiting molar isentropic compression, indicates the existence of (solute-solvent) interactions whereas the solute–solute interactions in a particular solution are indicated by slope  $(S_K^*)$  values. Equation 1.25 calculates the variation of  $K_{\phi,s}^0$  with molality of solute. The molality of LiTFSI/ LiFSI utilised in an aqueous TEGDME media is denoted by m<sub>A</sub>. Table 4.26 shows the calculated values of  $K_{\phi,s}^0$  and,  $S_K^*$  of the ternary systems. In ternary systems (LiTFSI/ LiFSI +  $H_2O$  + TEGDME), lower value of the slope  $S_K^*$ . indicate that interactions between solute molecules are insignificant, while solute-solvent interactions are prominent (Kumar et al., 2021b). While raising the temperature,  $K_{\phi,s}^0$ lowers because water molecules are firmly bound to solute molecules at low temperatures, but as the temperature rises, the electrostriction between them reduces, and some H<sub>2</sub>O molecules are discharged into the bulk media (Bhakri et al., 2023). As a result, partial molar isentropic compression inference suggests that in this investigation, solute-solvent interactions exceed solute-solute interactions.  $K_{\phi,s}^0$  deduces that the solvent molecules are bounded to the solute molecules, which enhances the interactions between the ions.

**Table 4.26:** Partial molar isentropic compression,  $(K_{\phi,s}^0)$  and empirical slopes,  $(S_K^*)$  of LiTFSI and LiFSI in aqueous media of TEGDME at various temperatures.

| am <sub>B</sub> / (mol·kg <sup>-1</sup> ) |          | $K_{\phi,s}^0 	imes 1$ | 0 <sup>6</sup> /(m <sup>3</sup> ·mo | l <sup>-1</sup> ·GPa <sup>-1</sup> ) |          |          | $S_K^* \times 10^6 / (\text{kg} \cdot \text{m}^3 \cdot \text{mol}^{-2} \cdot \text{GPa}^{-1})$ |          |          |          |
|---|----------|------------------------|-------------------------------------|--------------------------------------|----------|----------|--|----------|----------|----------|
|   | T=293.15 | T=298.15               | T=303.15                            | T=308.15                             | T=313.15 | T=293.15 | T=298.15   | T=303.15 | T=308.15 | T=313.15 |
|   | K        | K                      | K                                   | K                                    | K        | K        | K  | K        | K        | K        |
|   |          |                        |                                     |                                      | LiTFSI   |          |  |          |          |          |
| 0.01                                      | -6.38    | -5.55                  | -4.86                               | -4.24                                | -3.64    | -8.04    | -8.01  | -7.94    | -7.93    | -7.88    |
| 0.03                                      | -10.46   | -9.49                  | -8.43                               | -7.56                                | -6.66    | -7.53    | -7.57  | -7.59    | -7.64    | -7.63    |
| 0.05                                      | -12.26   | -11.47                 | -10.35                              | -9.35                                | -8.50    | -7.28    | -7.27  | -7.38    | -7.44    | -6.56    |
|   |          |                        |                                     |                                      | LiFSI    |          |  |          |          |          |
| 0.01                                      | -14.07   | -12.60                 | -10.96                              | -9.41                                | -7.72    | -2.95    | -2.96  | -3.02    | -3.05    | -3.13    |
| 0.03                                      | -11.47   | -10.27                 | -9.08                               | -7.94                                | -6.82    | -3.07    | -3.11  | -3.12    | -3.17    | -3.16    |
| 0.05                                      | -9.29    | -8.43                  | -7.53                               | -6.78                                | -6.02    | -3.26    | -3.23  | -3.25    | -3.27    | -3.28    |

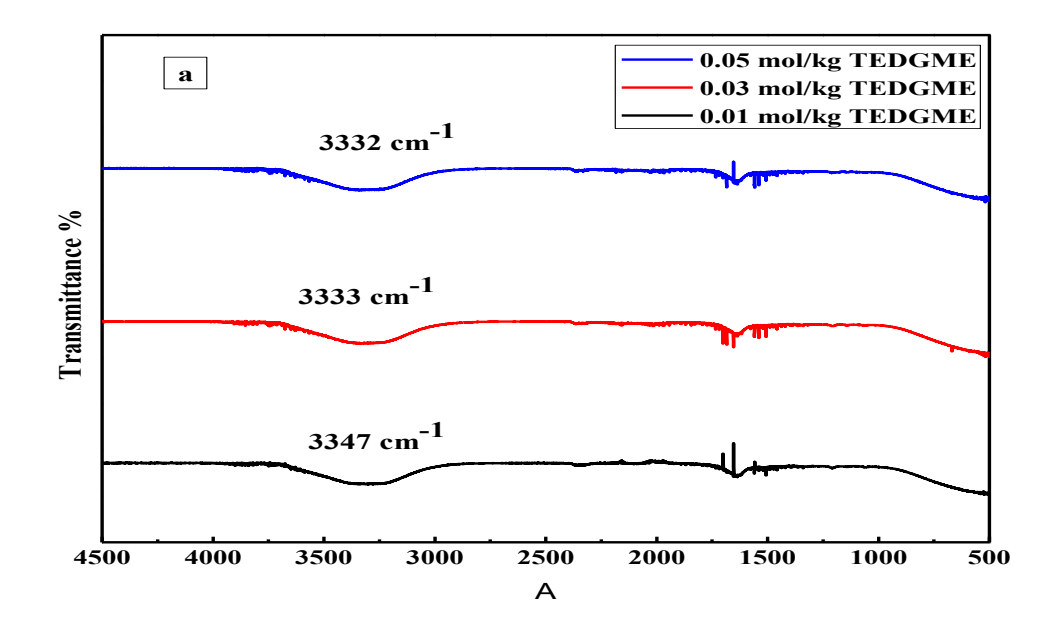
<sup>&</sup>lt;sup>a</sup>m<sub>B</sub> is molality of aqueous TEGDME solutions.

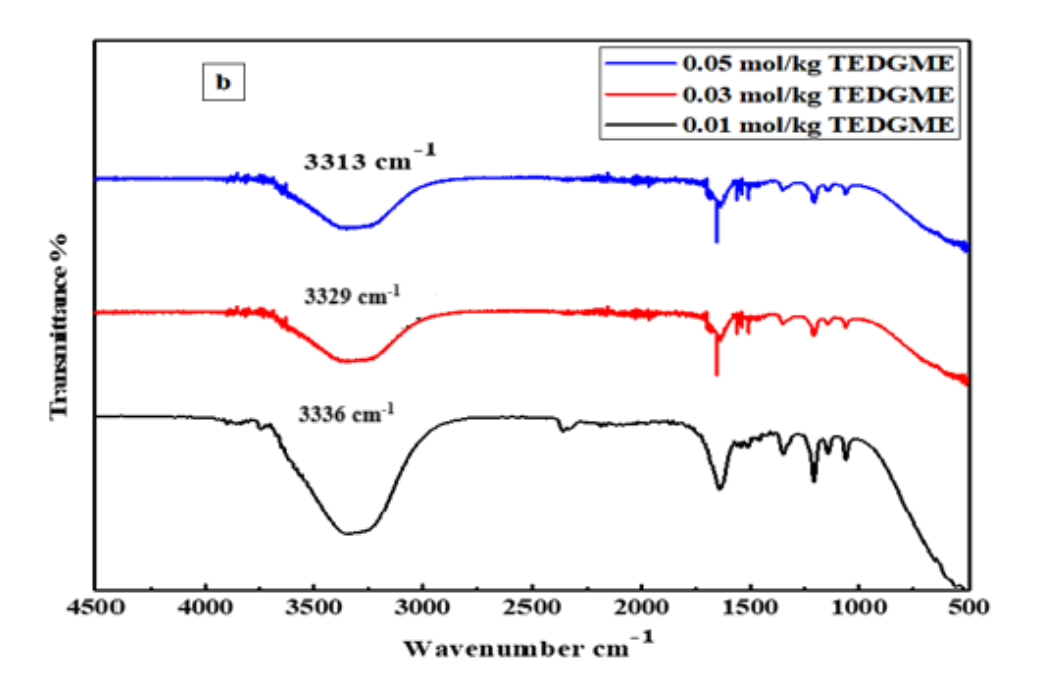
### 4.3.9 FT-IR spectral studies

The extent of intermolecular interactions in a specific solute and solvent mixture was investigated using infrared spectroscopy. The absorbance bands in the IR spectrum occur due to vibrations of various atoms when the sample is exposed to IR region of the electromagnetic spectrum. The vibrations cause the molecule's net dipole moment to shift. In addition, spectral investigations indicate bond length variation. To confirm the findings sourced from the thermodynamic parameters, FT-IR spectroscopy was performed for ternary systems at various concentration utilizing a Shimadzu FT-IR 8400S spectrophotometer within wavelength region of 4500 to 500 cm<sup>-1</sup>. Figures 4.8(a) and 4.8(b) show plots of FT-IR spectra for 0.05 mol/kg of LiTFSI and 0.30 mol/kg of LiTFSI in (0.01, 0.03 and 0.05) mol·kg<sup>-1</sup> of aqueous media of TEGDME respectively Similarly, Figures 4.9(a) and 4.9(b) show plots of FT-IR spectra for 0.05 mol/kg of LiFSI and 0.30 mol/kg of LiFSI in (0.01, 0.03 and 0.05) mol·kg<sup>-1</sup> of aqueous media of TEGDME respectively. A variation in the wavenumber arises while the concentration of LiTFSI/ LiFSI and TEGDME is changed, as seen in figure 4.8 and figure 4.9. The existence of intermolecular H-bonding between solute & solvent components is used to elucidate the shift in wavenumber. Because -OH stretching vibrations are unimpeded by hydrogen bonding, they could be utilized to determine the nature of interactions between the solute and the solvent.

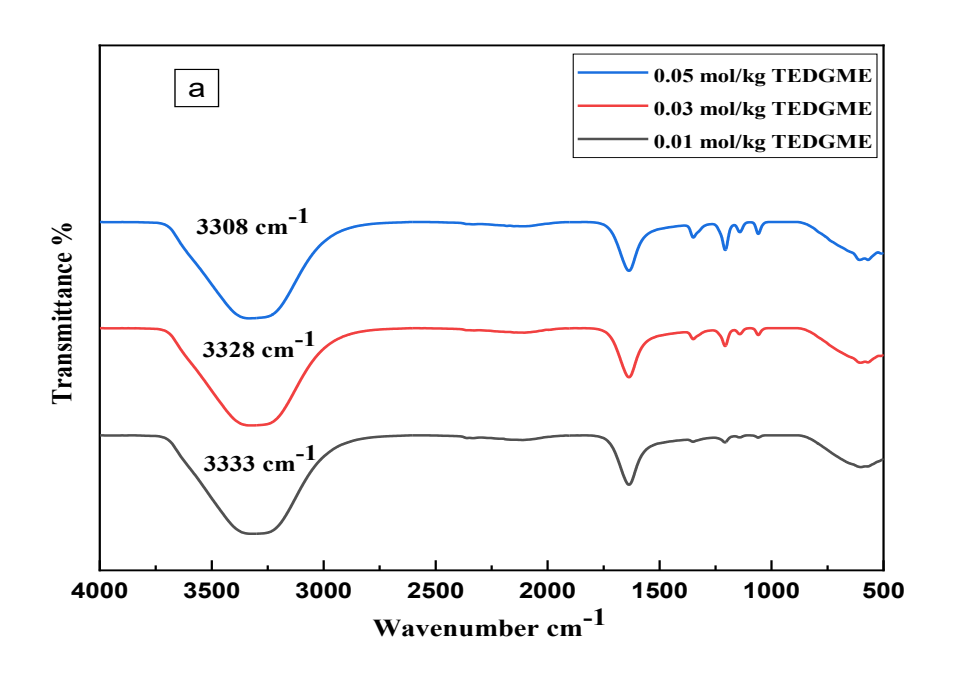
The anion orientation shifts because of the hydrogen bonds established between water and salt, causing the conformation to change. Above 3000cm<sup>-1</sup>, the hydrogen bond between the anionic and cationic regions breaks/weakens, causing less interaction between them, which, in turn interacts significantly with the ionic configuration of salt, as evidenced by the transition in wavenumber with various concentrations. FT-IR spectrum analyses can also identify the nature of contact (intermolecular or intramolecular). Intramolecular interactions are shown by an increase in the strength of the band reflecting hydrogen bonding, while intermolecular interactions are indicated by a drop in band intensity (T. Singh & Kumar, 2011) (Stangret & Gampe, 1999). Also, there is a band near (1635.69 cm<sup>-1</sup>) in such ternary systems which does not change (Chaudhary *et al.*, 2014). As a result, when the component of the constituents of ternary

combination was changed, the shift in wavenumber confirms intermolecular interactions and conformational modifications.





**Figure 4.8:** Plots of FT-IR spectra of (a) 0.05 mol/kg of LiTFSI and, (b) 0.30 mol/kg of LiTFSI in (0.01, 0.03 and 0.05) mol·kg<sup>-1</sup> of aqueous media of TEGDME.



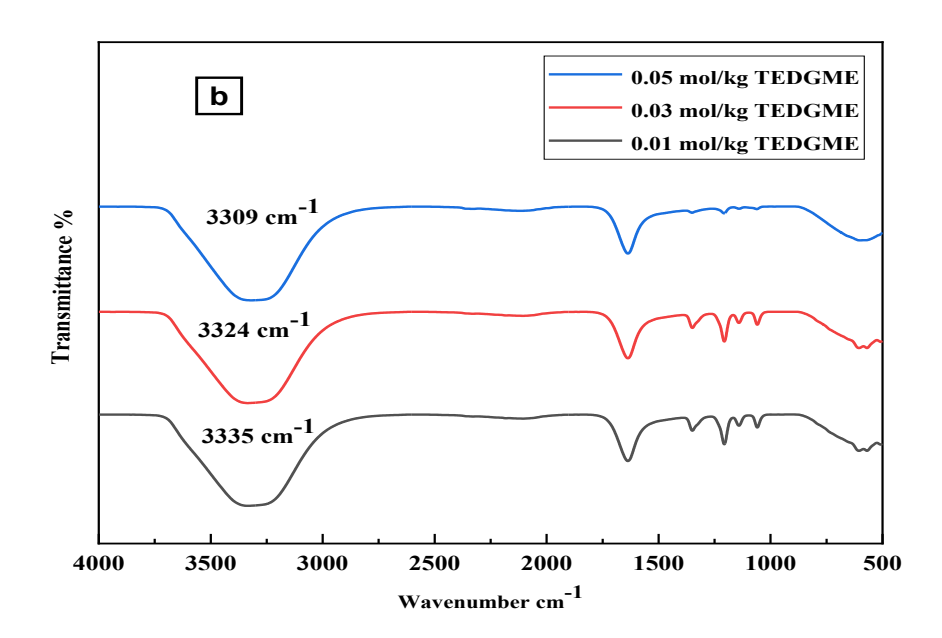


**Figure 4.9:** Plots of FT-IR spectra of (a) 0.05 mol/kg of LiFSI and, (b) 0.30 mol/kg of LiFSI in (0.01, 0.03 and 0.05) mol·kg<sup>-1</sup> of aqueous media of TEGDME.

#### 4.3.10 Conductance Studies

The specific conductivity (K) for LiTFSI and LiFSI in aqueous TEGDME solutions at different temperatures have been given in **Table 4.27**. The value of κ rises with both the solute concentration and the temperature. From κ values molar conductivity  $(\Lambda_m)$  have been calculated and presented in tabular form in **Table 4.27**. The resultant molar conductivity data has been analyzed to obtain limiting molar conductivity  $(\Lambda_m^0)$  values at infinite dilution using Onsager relation given in equation 1.32. The intercept of graph plot between  $\Lambda_m$  versus  $\sqrt{C}$  represents  $\Lambda_m^0$ . The values of  $\Lambda_m^0$  have been listed in **Table 4.28** (Kant *et al.*, 2009a). It has been demonstrated that the values of limiting molar conductivity elevated with temperature due to high ionic mobility at higher temperatures. Increase in temperature results in higher frequency and bond breaking as a consequence of the increase in translational & vibrational degrees of freedom and therefore the mobility of ions accelerates. The solvent molecules envelop the solute ions at infinite dilution, and no additional ions are present within a defined radius (Kant et al., 2009b). Further, positive activation energy of conductance values are obtained for LiFSI & LiTFSI in aqueous TEGDME solutions (given in Table **4.29**) which infers that ionic movement is thermally activated, and as the concentration increase, the values of activation energy of conductance increases due to the greater ion-ion interactions.

Table 4.27: Specific conductance ( $\kappa$ ), and molar conductance ( $\Lambda_m$ ) of LiTFSI and LiFSI in aqueous TEGDME solutions at different temperatures.

| κ/(μS cm <sup>-1</sup> )      |          |          |          |             |                         | $\Lambda_m/(\mathrm{S~cm^2~mol^{-1}})$ |        |        |        |        |  |
|-------------------------------|----------|----------|----------|-------------|-------------------------|--|--------|--------|--------|--------|--|
| <sup>a</sup> m <sub>A</sub> / | 293.15   | 298.15   | 303.15   | 308.15      | 313.15                  | 293.15                                 | 298.15 | 303.15 | 308.15 | 313.15 |  |
| (mol.kg-1)                    | K        | K        | K        | K           | K                       | K                                      | K      | K      | K      | K      |  |
|                               |          |          | LiTF     | SI + 0.01 m | ol·kg <sup>-1</sup> TEG | DME                                    |        |        |        |        |  |
| 0.05015                       | 2925.94  | 3163.93  | 3416.04  | 3933.96     | 4096.32                 | 58.83                                  | 63.71  | 68.90  | 79.48  | 82.89  |  |
| 0.09545                       | 5086.35  | 5468.87  | 5857.90  | 6649.67     | 7120.88                 | 54.07                                  | 58.22  | 62.46  | 71.03  | 76.18  |  |
| 0.14966                       | 7671.68  | 8227.16  | 8780.04  | 9899.53     | 10740.35                | 52.39                                  | 56.27  | 60.15  | 67.93  | 73.82  |  |
| 0.19867                       | 10009.01 | 10720.87 | 11421.89 | 12837.65    | 14012.62                | 51.82                                  | 55.59  | 59.32  | 66.80  | 73.02  |  |
| 0.24995                       | 12454.61 | 13330.08 | 14186.09 | 15911.85    | 17436.45                | 51.59                                  | 55.30  | 58.95  | 66.24  | 72.70  |  |
| 0.30026                       | 14853.94 | 15889.93 | 16898.02 | 18927.91    | 20795.52                | 51.54                                  | 55.22  | 58.83  | 66.02  | 72.64  |  |

#### LiTFSI + 0.03 mol·kg<sup>-1</sup> TEGDME 0.04999 3416.00 3654.04 3905.94 4452.09 4782.41 68.84 73.75 78.96 90.15 97.00 0.09845 5768.77 6170.24 6569.16 7403.98 8076.27 59.42 63.65 67.88 83.73 76.63 0.1496 8252.13 8826.11 9380.21 10519.73 11552.98 56.31 60.32 64.22 72.14 79.36 0.20012 10704.91 11449.27 12156.63 13597.11 14986.87 54.96 58.88 62.62 70.17 77.47 16825.55 58.13 0.25312 13278.09 14201.20 15069.36 18589.32 54.26 61.79 69.11 76.49 0.29913 15511.90 16590.19 17597.93 19628.20 21716.66 53.94 57.79 61.41 68.62 76.05 LiTFSI + 0.05 mol·kg<sup>-1</sup> TEGDME 0.05013 4004.09 4213.99 4465.90 5053.99 5605.72 80.41 84.74 89.96 101.97 113.30 0.10014 9008.87 65.12 69.16 6434.90 6824.05 7229.92 8120.46 73.39 82.57 91.77 0.14972 8844.82 9411.66 9970.16 11160.57 12382.75 60.25 64.21 68.14 84.92 76.40 0.20031 11303.83 12051.98 12766.23 14262.61 15825.36 57.92 61.85 65.63 73.46 81.66 0.24998 13718.12 14644.29 15511.45 17308.23 19205.37 56.67 60.59 64.30 71.88 79.91

22618.71

55.93

59.85

63.52

70.94

78.88

20383.90

18283.76

16156.22 17262.17

0.30014

|         |          |          | LiFS     | SI + 0.01 mo | l·kg <sup>-1</sup> TEGI | <b>ME</b> |        |        |        |        |
|---------|----------|----------|----------|--------------|-------------------------|-----------|--------|--------|--------|--------|
| 0.05024 | 4242.01  | 4465.94  | 4745.97  | 5250.01      | 5938.82                 | 84.92     | 89.53  | 95.31  | 105.60 | 119.64 |
| 0.09664 | 7140.92  | 7445.33  | 7839.69  | 8621.63      | 9997.29                 | 74.62     | 77.91  | 82.17  | 90.52  | 105.13 |
| 0.14954 | 10445.92 | 10842.09 | 11366.80 | 12465.56     | 14624.29                | 70.85     | 73.65  | 77.34  | 84.96  | 99.84  |
| 0.19990 | 13592.23 | 14075.76 | 14724.55 | 16124.93     | 19029.13                | 69.26     | 71.83  | 75.27  | 82.57  | 97.60  |
| 0.25014 | 16731.05 | 17301.72 | 18074.30 | 19775.58     | 23423.47                | 68.41     | 70.85  | 74.14  | 81.26  | 96.41  |
| 0.30032 | 19866.11 | 20523.83 | 21420.06 | 23421.87     | 27812.56                | 67.94     | 70.28  | 73.49  | 80.50  | 95.75  |
|         |          |          | LiFS     | SI + 0.03 mo | l·kg⁻¹ TEGI             | OME       |        |        |        |        |
| 0.05021 | 4802.06  | 5068.01  | 5376.04  | 5908.06      | 6722.89                 | 96.12     | 101.60 | 107.94 | 118.82 | 135.42 |
| 0.10042 | 8014.01  | 8367.12  | 8798.93  | 9620.64      | 11219.61                | 80.55     | 84.24  | 88.72  | 97.17  | 113.50 |
| 0.14956 | 11157.50 | 11595.92 | 12148.88 | 13254.10     | 15620.50                | 75.62     | 78.72  | 82.60  | 90.27  | 106.55 |
| 0.20302 | 14577.35 | 15108.57 | 15793.34 | 17206.98     | 20408.29                | 73.11     | 75.90  | 79.46  | 86.72  | 103.03 |
|         |          |          |          |              |                         |           |        |        |        |        |
| 0.25217 | 17721.49 | 18338.03 | 19143.97 | 20841.18     | 24810.08                | 71.85     | 74.47  | 77.87  | 84.92  | 101.25 |

LiFSI + 0.05 mol·kg<sup>-1</sup> TEGDME

| 0.05022 | 5487.98  | 5698.04  | 5963.97  | 6496.02  | 7683.17  | 113.97 | 114.12 | 119.64 | 130.52 | 154.63 |
|---------|----------|----------|----------|----------|----------|--------|--------|--------|--------|--------|
| 0.09617 | 8480.29  | 8761.88  | 9145.22  | 9935.16  | 11872.40 | 91.88  | 92.01  | 96.19  | 104.67 | 125.29 |
| 0.14965 | 11962.96 | 12327.81 | 12847.79 | 13937.89 | 16748.14 | 83.47  | 83.58  | 87.25  | 94.81  | 114.12 |
| 0.20191 | 15366.18 | 15812.39 | 16465.89 | 17849.31 | 21512.65 | 79.70  | 79.82  | 83.25  | 90.40  | 109.14 |
| 0.25538 | 18848.20 | 19377.66 | 20167.77 | 21851.30 | 26387.48 | 77.57  | 77.68  | 80.99  | 87.90  | 106.33 |
| 0.30218 | 21895.86 | 22498.18 | 23407.87 | 25354.06 | 30654.21 | 76.41  | 76.52  | 79.75  | 86.53  | 104.80 |

 $<sup>^</sup>a m_{\mbox{\scriptsize A}}$  is the molality of LiFSI and LiTFSI in aqueous TEGDME solutions.

**Table 4.28:** Limiting molar conductance  $(\Lambda_m^0)$  of LiTFSI and LiFSI in aqueous TEGDME solutions at different temperatures.

| Limiting molar conductance $(\Lambda_m^0)$ , |   |                                   |                                   |  |  |  |  |  |  |  |  |  |
|--|---|-----------------------------------|-----------------------------------|--|--|--|--|--|--|--|--|--|
| T (K)  | T (K) LiTFSI + 0.01 LiTFSI + 0.03 mol·kg <sup>-1</sup> LiTFSI + 0.05 mol·kg |                                   |                                   |  |  |  |  |  |  |  |  |  |
|  | mol·kg <sup>-1</sup> TEGDME   | TEGDME                            | TEGDME                            |  |  |  |  |  |  |  |  |  |
| 293.15K                                      | 61.95   | 75.63                             | 91.93                             |  |  |  |  |  |  |  |  |  |
| 298.15K                                      | 67.38   | 81.03                             | 96.43                             |  |  |  |  |  |  |  |  |  |
| 303.15K                                      | 73.31   | 86.98                             | 102.38                            |  |  |  |  |  |  |  |  |  |
| 308.15K                                      | 87.26   | 100.05                            | 116.58                            |  |  |  |  |  |  |  |  |  |
| 313.15K                                      | 65.03   | 106.54                            | 129.50                            |  |  |  |  |  |  |  |  |  |
| T (K)  | LiFSI + 0.01  | LiFSI + 0.03 mol·kg <sup>-1</sup> | LiFSI + 0.05 mol·kg <sup>-1</sup> |  |  |  |  |  |  |  |  |  |
|  | mol·kg <sup>-1</sup> TEGDME   | TEGDME                            | TEGDME                            |  |  |  |  |  |  |  |  |  |
| 293.15K                                      | 92.71   | 107.75                            | 126.07                            |  |  |  |  |  |  |  |  |  |
| 298.15K                                      | 98.40   | 114.64                            | 131.46                            |  |  |  |  |  |  |  |  |  |
| 303.15K                                      | 105.38  | 122.43                            | 138.04                            |  |  |  |  |  |  |  |  |  |
| 308.15K                                      | 117.22  | 135.17                            | 152.00                            |  |  |  |  |  |  |  |  |  |
| 313.15K                                      | 130.59  | 151.78                            | 177.59                            |  |  |  |  |  |  |  |  |  |

**Table 4.29:** Activation energy of conductance  $(E_{\lambda})$  of LiTFSI and LiFSI in aqueous TEGDME solutions.

|                               | E <sub>λ</sub> (kJ mol <sup>-1</sup> ) |                             |                                    |  |  |  |  |  |  |
|-------------------------------|--|-----------------------------|------------------------------------|--|--|--|--|--|--|
| a <sub>mA</sub> /             | LiTFSI + 0.01                          | LiTFSI + 0.03               | LiTFSI + 0.05 mol·kg <sup>-1</sup> |  |  |  |  |  |  |
| (mol.kg-1)                    | mol·kg <sup>-1</sup> TEGDME            | mol·kg <sup>-1</sup> TEGDME | TEGDME                             |  |  |  |  |  |  |
| 0.05                          | 0.00904                                | 0.00982                     | 0.01069                            |  |  |  |  |  |  |
| 0.10                          | 0.01010                                | 0.01070                     | 0.01125                            |  |  |  |  |  |  |
| 0.15                          | 0.01081                                | 0.01124                     | 0.01159                            |  |  |  |  |  |  |
| 0.2                           | 0.01124                                | 0.01161                     | 0.01185                            |  |  |  |  |  |  |
| 0.25                          | 0.01156                                | 0.01189                     | 0.01205                            |  |  |  |  |  |  |
| 0.3                           | 0.01182                                | 0.01209                     | 0.01214                            |  |  |  |  |  |  |
| <sup>a</sup> m <sub>A</sub> / | LiFSI + 0.01                           | LiFSI + 0.03                | LiFSI + 0.05 mol·kg <sup>-1</sup>  |  |  |  |  |  |  |
| (mol.kg-1)                    | mol·kg <sup>-1</sup> TEGDME            | mol·kg <sup>-1</sup> TEGDME | TEGDME                             |  |  |  |  |  |  |
| 0.05                          | 0.01155                                | 0.01194                     | 0.01401                            |  |  |  |  |  |  |
| 0.10                          | 0.01320                                | 0.01365                     | 0.01519                            |  |  |  |  |  |  |
| 0.15                          | 0.01430                                | 0.01466                     | 0.01602                            |  |  |  |  |  |  |
| 0.2                           | 0.01499                                | 0.01541                     | 0.01658                            |  |  |  |  |  |  |
| 0.25                          | 0.01551                                | 0.01592                     | 0.01701                            |  |  |  |  |  |  |
| 0.3                           | 0.01591                                | 0.01632                     | 0.01732                            |  |  |  |  |  |  |
|                               |  |                             |                                    |  |  |  |  |  |  |

#### References

Bhakri, K., Chakraborty, N., Harsh, K. C. J., & Ravinder, K. (2023). Thermodynamic behaviour and physicochemical characteristics of EG, DEG, TEG in aqueous gluconolactone solutions. *Journal of Thermal Analysis and Calorimetry*, *148*(14), 7185–7205. https://doi.org/10.1007/s10973-023-12223-z

Borović, T. T., Panić, J., Radović, I., Grozdanić, N., & Vraneš, M. (2024). Interactions of caffeine and 1-butyl-3-methylimidazolium salicylate ionic liquid in water – Solubility, volumetric, acoustic, viscometric and refractometric studies supported by MD simulation. *Journal of Molecular Liquids*, 397, 124058. https://doi.org/https://doi.org/10.1016/j.molliq.2024.124058

Chaudhary, G. R., Bansal, S., Mehta, S. K., & Ahluwalia, A. S. (2014). Thermophysical and spectroscopic studies of pure 1-butyl-3- methylimidazolium tetrafluoroborate and its aqueous mixtures. *Journal of Solution Chemistry*, *43*, 340–359. https://doi.org/10.1007/s10953-014-0137-8

Chen, W., Wei, Y., Ge, X., Li, S., Zhang, X., Wang, Z.-X., Xing, Z., Zhang, Q., & Liu, X. (2024). Insight of alkyl imidazolium tetrafluoroborate ionic gels as supercapacitors and motion sensors: Effects of alkyl chain length and intermolecular interactions. *Journal of Power Sources*, 599, 234224. https://doi.org/https://doi.org/10.1016/j.jpowsour.2024.234224

Gaba, R., Pal, A., Sharma, D., Kumar, H., & Kumar, A. (2019). Molecular interactions of some non-essential amino acids in aqueous solutions of 1-methylimidazolium chloride at different temperatures. *Journal of Molecular Liquids*, 279, 711–718. https://doi.org/10.1016/j.molliq.2019.01.094

Gerald R. Van Hecke, Oliver W. M. Baldwin, and B. C. W. (2022a). Density, Viscosity, Refractive Index, Isobaric Specific Heat Capacity, Ultrasonic Velocity, Molar Volume, Isentropic Compressibility, Isothermal Compressibility, and Heat Capacity Ratio for Binary Mixtures of the Organic Liquids Ethylbenzene, Ethylcyclohe. *J. Chem. Eng. Data*, 67, 1037–1053. https://doi.org/10.1021/acs.jced.9b00902

Gerald R. Van Hecke, Oliver W. M. Baldwin, and B. C. W. (2022b). Density, Viscosity, Refractive Index, Isobaric Specific Heat Capacity, Ultrasonic Velocity, Molar Volume, Isentropic Compressibility, Isothermal Compressibility, and Heat Capacity Ratio for Binary Mixtures of the Organic Liquids Ethylbenzene, Ethylcyclohe. *J. Chem. Eng. Data*, 67, 1037–1053. https://doi.org/10.1021/acs.iced.9b00902

Hepler, L. G. (1969). Thermal expansion and structure in water and aqueous solutions. *Canadian Journal of Chemistry*, 47, 4613–4617. https://doi.org/10.1139/v69-762

Kant, S., Kumar, A., & Kumar, S. (2009a). Molar volume, viscosity and conductance studies of some alkali metal chlorides in aqueous ascorbic acid. *Journal of Molecular Catalysis A: Chemical*, 150, 39–42. https://doi.org/10.1016/j.molliq.2009.09.010

Kant, S., Kumar, A., & Kumar, S. (2009b). Molar volume, viscosity and conductance studies of some alkali metal chlorides in aqueous ascorbic acid. *Journal of Molecular Catalysis A: Chemical*, 150, 39–42. https://doi.org/10.1016/j.molliq.2009.09.010

Kaur, H., Thakur, R. C., & Kumar, H. (2020). Effect of proteinogenic amino acids L-serine/L-threonine on volumetric and acoustic behavior of aqueous 1-butyl-3-propyl imidazolium bromide at T = (288.15, 298.15, 308.15, 318.15) K. *Journal of Chemical Thermodynamics*, 150, 106211. https://doi.org/10.1016/j.jct.2020.106211

Kaur, H., Thakur, R. C., Kumar, H., & Katal, A. (2021). Effect of α–amino acids (glycine, L-alanine, L-valine and L-leucine) on volumetric and acoustic properties of aqueous 1-Butyl-3-propylimidazolium bromide at T = (288.15, 298.15, 308.15, 318.15) K. *Journal of Chemical Thermodynamics*, *158*, 106433. https://doi.org/10.1016/j.jct.2021.106433

Kaur, H., Thakur, R. C., Pathania, V. S., & Sharma, S. (2022). Effect of Choline-based ionic liquid (Cholinium ethanoate) on volumetric and acoustic properties

of aliphatic amino acids (glycine and L-alanine). *Journal of Molecular Liquids*, 346, 118247. https://doi.org/10.1016/j.molliq.2021.118247

Khan, I. A., Wang, Y.-L., & Shah, F. U. (2022). Effect of structural variation in biomass-derived nonfluorinated ionic liquids electrolytes on the performance of supercapacitors. *Journal of Energy Chemistry*, 69, 174–184. https://doi.org/https://doi.org/10.1016/j.jechem.2021.12.041

Kumar, H. (2016). Densities and Speeds of Sound of D(+)-Glucose, D(-)-Fructose, D(+)-Xylose and D(-)-Ribose in Aqueous Tripotassium Citrate Solutions at Different Temperatures. https://doi.org/10.1021/acs.jced.5b00933

Kumar, H., & Behal, I. (2016a). Thermodynamics of (solute + solute) and (solute + solvent) interactions of homologous series of amino acids with thiamine hydrochloride in aqueous medium at T = (305.15, 310.15, 315.15) K: A volumetric and acoustic approach. *Journal of Chemical Thermodynamics*, 102, 48–62. https://doi.org/10.1016/j.jct.2016.06.026

Kumar, H., & Behal, I. (2016b). Volumetric and ultrasonic investigation of molecular interactions of 1-serine and 1-threonine in aqueous nicotinamide solutions at T = (288.15-318.15) K. *Journal of Molecular Liquids*, *219*, 756–764. https://doi.org/10.1016/j.molliq.2016.04.019

Kumar, H., & Behal, I. (2017). Volumetric and ultrasonic properties of α-amino acids (glycine, L-alanine and L-valine) in aqueous diammonium hydrogen phosphate at different temperatures and concentrations. *Journal of Molecular Liquids*, 241, 751–763. https://doi.org/10.1016/j.molliq.2017.06.044

Kumar, H., Behal, I., & Siraswar, S. (2019). Densities and Speeds of Sound for Sucrose in Aqueous Solutions of Ammonium Phosphate Salts at Different Temperatures through Density and Speed of Sound Measurements. *Journal of Chemical & Engineering Data*, 64(9), 3772–3780. https://doi.org/10.1021/acs.jced.8b01157

Kumar, H., Sharma, R., Kumar, V., & Alothman, A. A. (2021a). Exploration of the solvation behavior of the synthesized 1-hexyl-3-methylimidazolium bromide [C6mim][Br] ionic liquid with L-cysteine and N-acetyl L-cysteine) in aqueous medium at different temperatures. *Journal of Molecular Liquids*, 324, 114664. https://doi.org/10.1016/j.molliq.2020.114664

Kumar, H., Sharma, R., Kumar, V., & Alothman, A. A. (2021b). Exploration of the solvation behavior of the synthesized 1-hexyl-3-methylimidazolium bromide [C6mim][Br] ionic liquid with L-cysteine and N-acetyl L-cysteine) in aqueous medium at different temperatures. *Journal of Molecular Liquids*, *324*, 114664. https://doi.org/10.1016/j.molliq.2020.114664

Le Donne, A., Adenusi, H., Porcelli, F., & Bodo, E. (2018). Hydrogen Bonding as a Clustering Agent in Protic Ionic Liquids: Like-Charge vs Opposite-Charge Dimer Formation. *ACS Omega*, *3*(9), 10589–10600. https://doi.org/10.1021/acsomega.8b01615

Macchieraldo, R., Esser, L., Elfgen, R., Voepel, P., Zahn, S., Smarsly, B. M., & Kirchner, B. (2018). Hydrophilic Ionic Liquid Mixtures of Weakly and Strongly Coordinating Anions with and without Water. *ACS Omega*, *3*(8), 8567–8582. https://doi.org/10.1021/acsomega.8b00995

Millero, F. J., Surdo, A. Lo, & Shin, C. (1978). The apparent molal volumes and adiabatic compressibilities of aqueous amino acids at 25°C. *Journal of Physical Chemistry*, 82, 784–792.

Panduranga Rao, J., Narendra, K., Visalakshamma, V., Krishna, T. S., & Srinivasa Rao, G. (2024). Acoustic and volumetric study of binary mixtures containing Ethyl propionate with amides at various temperatures. *The Journal of Chemical Thermodynamics*, 190, 107222.

https://doi.org/https://doi.org/10.1016/j.jct.2023.107222

Pradhan, R. K., & Singh, S. (2024). Studies on interactions of L-glutamic acid with L-arabinose/D-xylose in aqueous medium: Ultrasonic velocity and acoustic parameter studies supported by FTIR spectroscopic investigation. *Journal of* 

*Molecular Liquids*, 412(May), 125790. https://doi.org/10.1016/j.molliq.2024.125790

Raheem, S., Richu, Kumar, A., Peerzada, G. M., & Rizvi, M. A. (2023). Molecular interactions of diphenyldiselenide in DMSO and varied weight % of ethanol in DMSO solvent media at different compositions and temperatures (288.15 to 318.15)K. *Journal of Molecular Liquids*, 390, 122941. https://doi.org/https://doi.org/10.1016/j.molliq.2023.122941

Rana, S., Thakur, R. C., Kaur, H., Sharma, A., Sharma, R., Thakur, V., Singh, H., & Fatma, I. (2023a). Investigating the Solvation Behavior of Some Lithium Salts in Binary Aqueous Mixtures of 1-Ethyl-3-methylimidazolium Tetrafluoroborate ([EMIM][BF4]) at Equidistant Temperatures (T = 298.15, 303.15, 308.15, 313.15, 318.15) K. *Journal of Chemical & Engineering Data*, 68(6), 1291–1304. https://doi.org/10.1021/acs.jced.3c00037

Rana, S., Thakur, R. C., Kaur, H., Sharma, A., Sharma, R., Thakur, V., Singh, H., & Fatma, I. (2023b). Investigating the Solvation Behavior of Some Lithium Salts in Binary Aqueous Mixtures of 1-Ethyl-3-methylimidazolium Tetrafluoroborate ([EMIM][BF4]) at Equidistant Temperatures (T = 298.15, 303.15, 308.15, 313.15, 318.15) K. *Journal of Chemical & Engineering Data*, 68(6), 1291–1304. https://doi.org/10.1021/acs.jced.3c00037

Ravinder Sharma, Harsh Kumar, Meenu Singla, Vaneet Kumar, Abdullah A. Al-Kahtani, S. P. (2022). Volumetric and acoustic properties of L-phenyl glycine and L-phenylalanine in aqueous solution of 1-dodecyl-3-methylimidazolium bromide [C12mim] [Br]. *Journal of Molecular Liquids*, *357*, 119014. https://doi.org/10.1134/S1023193517070035

Satheesh, A., & Kandasamy, E. (2024). Dibutyl benzotriazolium tetrafluoroborate doped PANI as an electrode material for energy storage. *Journal of Energy Storage*, 88, 111677. https://doi.org/https://doi.org/10.1016/j.est.2024.111677

Sharma, R., Athira, K. K., Gardas, R. L., Malek, N., & Ijardar, S. P. (2022). Physicochemical and acoustic characterization of binary mixtures of

tetraalkylammonium bromide: PEG based DES and water. *Journal of Molecular Liquids*, 367, 120386.

https://doi.org/https://doi.org/10.1016/j.molliq.2022.120386

Singh, J., Singh, M., Sharma, S., Sharma, S., & Sharma, M. (2021). Molecular Interactions of Diphenhydramine-hydrochloride with Some Imidazolium-Based Ionic Liquids in Aqueous Media at T =. *ACS Omega*, *35*, 22655–22671. https://doi.org/10.1021/acsomega.1c02733

Singh Thakur, Y., Deep Acharya, A., Sharma, S., Bisoyi, S., & Bhawna. (2024). Enhanced electrochemical performance of in situ polymerized V2O5-PANI nanocomposites and its practical application confirmation by assembling ionic liquid as well as solid state-based supercapacitor device. *Results in Chemistry*, 7, 101259. https://doi.org/https://doi.org/10.1016/j.rechem.2023.101259

Singh, T., & Kumar, A. (2011). Vibrational Spectroscopy Cation – anion – water interactions in aqueous mixtures of imidazolium based ionic liquids. *Vib Spectrosc*, *55*, 119–125. https://doi.org/10.1016/j.vibspec.2010.09.009

Srinivasa Reddy, M., Nayeem, S. M., Raju, K. T. S. S., & Hari Babu, B. (2016). The study of solute–solvent interactions in 1-ethyl-3-methylimidazolium tetrafluoroborate + 2-ethoxyethanol from density, speed of sound, and refractive index measurements. *Journal of Thermal Analysis and Calorimetry*, *124*(2), 959–971. https://doi.org/10.1007/s10973-015-5205-9

Stangret, J., & Gampe, T. (1999). Hydration Sphere of Tetrabutylammonium Cation. FTIR Studies of HDO Spectra. *J. Phys. Chem*, *103*, 3778–3783.

Thakur Abhishek, Sharma Shashi Kant, K. M. (2022). Limiting apparent molar volumes, limiting apparent molar isentropic compressions, transfer parameters and transition state theory for ternary mixtures of Gly-Gly-Gly in aqueous solutions of ascorbic acid at temperatures between (298.15 and 318.15) K (p. 118653).

Widegren, J. A., & Magee, J. W. (2007). Density, viscosity, speed of sound, and electrolytic conductivity for the ionic liquid 1-hexyl-3-methylimidazolium bis(trifluoromethylsulfonyl)imide and its mixtures with water. *Journal of Chemical and Engineering Data*, 52, 2331–2338. https://doi.org/10.1021/je700329a

Wu, X., & Si, P. (2023). Electrochemical detection of lignin from dietary fiber by laccases immobilized on nanocomposite of CNTs and ionic liquid. *International Journal of Electrochemical Science*, 18(3), 100065. https://doi.org/https://doi.org/10.1016/j.ijoes.2023.100065

Zahra, T., Alanazi, M. M., Alahmari, S. D., Abdelmohsen, S. A. M., Abdullah, M., Aman, S., Al-Sehemi, A. G., Henaish, A. M. A., Ahmad, Z., & Tahir Farid, H. M. (2024). Hydrothermally synthesized ZnSe@FeSe nanocomposite: A promising candidate for energy storage devices. *International Journal of Hydrogen Energy*, 59, 97–106. https://doi.org/https://doi.org/10.1016/j.ijhydene.2024.01.293

Zhang, Y., He, H., Zhang, S., & Fan, M. (2018). Hydrogen-Bonding Interactions in Pyridinium-Based Ionic Liquids and Dimethyl Sulfoxide Binary Systems: A Combined Experimental and Computational Study. *ACS Omega*, *3*(2), 1823–1833. https://doi.org/10.1021/acsomega.7b01805

Zheng, A., Guo, T., Guan, F., Chen, X., Shu, Y., & Wang, J. (2019). Ionic liquid mediated carbon dots: Preparations, properties and applications. *TrAC - Trends in Analytical Chemistry*, 119, 115638. https://doi.org/10.1016/j.trac.2019.115638

# Chapter 5 Conclusion

#### Conclusion

Section I determines the density and acoustic parameters for LiOTf in aqueous solutions of DME and TEGDME. When the results for  $V_{\phi}$  and  $V_{\phi}^{0}$  are compared, it could be inferred that intermolecular interactions are significant in the ternary mixtures studied. The positive values of  $V_{\phi}^{0}$  indicated the presence of solute-solvent interactions in the ternary systems studied (LiOTf+ H<sub>2</sub>O+ DME/TEGDME). Further, the values of  $V_{\phi}^{0}$  suggests that the (solute-solvent) interactions are more in LiOTf in DME and decrease with the concentration of DME whereas these interactions increase as the concentration of the TEGDME rises. Moreover, the positive and small negative values of Hepler's constant confirm the structure-making tendency of the studied Li salt in the DME/ TEGDME. The negative values of  $K_{\phi,s}$  and  $K_{\phi,s}^0$  confirms the existence of the solute-solvent interactions in the systems under investigation. Furthermore, as the result attained from the CV analysis, TEGDME was found to have a higher EW of 1.36 V in 0.01 TEGDME and 1.40 V in 0.05 TEGDME compared to that of 1.25 V in 0.01 DME and 1.38 V in 0.05 DME. The EW was also found to be increasing with the increasing concentration of LiOTf, as EW of 0.01 TEGDME system with 0.05 LiOTf is 2.23 V and with 0.30 LiOTf is 2.30 V. This data suggests promising outcomes of these studied systems, yielding a favourable and comparable working electrochemical window. The values of k increases with the concentration and temperature. With increase in temperature the values of limiting molar conductance rises as a result of high ionic mobility. The positive activation energy of conductance indicates greater ion-ion interactions. The ternary systems (LiOTf+H2O+DME/TEGDME) exhibit strong solutesolvent interactions (favourable for stability of ions), larger electrochemical windows (important for energy storage applications), and excellent conductance. In Section II, the density and acoustic parameters for LiBF4 and LiPF6 have been evaluated in aqueous TEGDME media. From transfer volumes, it has been affirmed that the solutesolvent interactions are more prominent in ternary mixtures containing LiPF<sub>6</sub> in aqueous TEGDME. Also, values of the Hepler constant state that LiBF4 and LiPF6 act as structure makers in the aqueous TEGDME. This makes these systems very promising electrolyte systems for energy storage applications. In Section III, the density and acoustic parameters for LiFSI and LiTFSI have been evaluated in aqueous TEGDME media. To have a better understanding of the interactions in ternary mixtures, several thermophysical parameters like partial molar volume, apparent molar volume, partial molar isentropic compression and apparent molar isentropic compression has been calculated using the obtained density and acoustic values. Also, values of Hepler constant states that LiFSI and LiTFSI acts as structure maker in the aqueous TEGDME. A shift in wavelengths confirms the structural and interactions changes in the molecules. The positive activation energy of conductance specifies greater ion-ion interactions. Hence, LiFSI and LiTFSI in aqueous TEGDME are potential electrolyte choices for energy storage owing to their strong solute-solvent interactions, advantageous conductivity, structural stability, and excellent thermal responsiveness.

### **Future scope of work**

There is a vast potential for future work on both fundamental science and practical implementation from this study, as high-performance energy storage becomes more important in many applications (electric vehicles and grid-level storage) and electrolyte materials must continue to advance. Beneath are the suggested future scope:

- **Solvent innovations:** The future work can be devoted to testing new aprotic solvents with higher thermal stability and safety profiles. Future studies can explore screening and synthesizing new aprotic organic solvents with enhanced thermal and electrochemical stability, low viscosity, high dielectric constant, reduced toxicity, low volatility and improved safety profiles, which could further improve the safety and performance of lithium-based batteries, especially at elevated temperatures.
- Concentration and Temperature effects: Investigation of electrolytes with higher salt concentrations. The range of temperatures can be widened to include extreme cold and heat should be tested to assess the stability of these electrolytes for practical energy storage systems such as electric vehicles.
- Additives: The use of functional additives with the ability to improve ion transport or stabilize interphases can be an effective way to tailor the electrolyte behavior. They enhance interfacial stability, prevent dendrite formation, or increase ionic mobility, which offer an opportunity to develop a new class of additive that can dramatically change the solvation structure and electrochemical behavior of lithium ions.
- electrolyte Compatibility: Investigating these electrolytes with novel electrode materials would assist in the development of safer and more durable batteries. Understanding the electrolyte-electrode interactions would enable us to design next-generation batteries with higher cycle life, energy density, and safety by means of compatible electrolytes with next-generation electrode materials (e.g., high-voltage cathodes or lithium-metal anodes).

- **Simulation:** Greater aid in computer tools/molecular simulations as well as other computational methods can be helpful to obtain the interaction of Lithium ions with solvents to determine good formulations. This can improve experimental efforts to predict solvation structures, ion transport mechanisms, and ideal solvent-salt combinations that hasten the formulation of effective electrolytes.
- **Practical translation:** Extending laboratory-scale research to practical testing in order to transform these materials into marketable commercial battery solutions. Making more electrolyte, fitting it into complete battery setups, and testing it under standard industry conditions will help turn research findings into real-world products. Further cooperative research involving chemistry, materials science, computer modelling, and practical testing has promise to change lithium-based energy storage systems using aprotic electrolytes.

#### **LIST OF PUBLICATIONS**

#### **Research Article Published**

- **Chitra Sharma**, and Ramesh Chand Thakur. "Potential solvents and electrolytes for energy storage applications: A Review." In *Journal of Physics: Conference Series*, vol. 2267, no. 1, p. 012051. IOP Publishing, 2022.
- Chitra Sharma, Harpreet Kaur, Abhinay Thakur, Akshay Sharma, Ramesh Chand Thakur, Harmanjit Singh Dosanjh, and Vivek Pathania. "Investigating Molecular Interactions through Computational Modelling, Thermodynamic Analysis, and Acoustic Measurements of LiOTf in Aqueous TEGDME and DME Solutions at Different Temperatures. "ACS omega10, no. 1 (2024): 754-768.
- Chitra Sharma, Harpreet Kaur, Abhinay Thakur, Ramesh Chand Thakur, Harmanjit Dosanjh "Hybrid lithium electrolytes as potential electrolytes for Energy storage devices: A Pathway to Sustainable and High-Efficiency Solutions" In Journal of Topics in Catalysis, Springer.

#### **Book Chapter published**

- **Sharma, Chitra**, Ramesh Chand Thakur, and Harmanjit Singh. "Microbial vitamins in dairy products." In *Microbial Vitamins and Carotenoids in Food Biotechnology*, pp. 299-325. Academic Press, 2024.
- Challenges and Future Perspectives of Nano-Technologically Derived Foods by Ramesh Chand Thakur, Abhinay Thakur, Harpreet Kaur, Chitra Sharma, Akshay, Renuka, and Ashish Kumar (In Process).

#### LIST OF CONFERENCES/WEBINARS/WORKSHOPS ATTENDED

- 1. Participated and presented a Poster on "Potential solvents and electrolytes for energy storage applications: A Review" in the International Conference on "Recent Advances in Fundamental and Applied Sciences" (RAFAS 2021) held on June 25-26, 2021, organized by Lovely Professional University, Punjab.
- 2. Attended online 1 week Faculty Development Programme on "Tools and Techniques for Effective Research", organized by I.K. Gujral Punjab Technical University from 14 December to 18 December 2020.
- 3. Attended online workshop on **analytical instrumentation** for students and teachers of Himachal Pradesh organized by Sophisticate Analytical Instrumentation facilities Panjab University, Chandigarh.
- 4. Participated in the International Conference on "Recent Advances in Fundamental and Applied Sciences" (RAFAS 2023) held on March 24-25, 2023, organized by Lovely Professional University, Punjab

Journal of Physics: Conference Series

2267 (2022) 012051 doi:10.1088/1742-6596/2267/1/012051

# Potential solvents and electrolytes for energy storage applications: A Review

Chitra Sharma1 and Ramesh Chand Thakur1\*

<sub>1</sub>Department of Chemistry, Lovely Professional University, Phagwara, 144411, Punjab, India.

1-Department of Chemistry, Himachal Pradesh University, Summer Hill Shimla,171005, Himachal Pradesh, India.

·Corresponding author: drthakurchem@gmail.com

Abstract. Since the industrial sector leans more on fossil fuels to pace up with the required energy needs. To overcome increasing demand for electricity, it is important to store the energy generated from natural resources so that energy can be used as and when required. Energy storage devices are one such means used worldwide for conserving different forms of energies and need of the hour is to discover and explore strong and secure electrical energy storage technologies. In this review an effort is made to do a comparative analysis of various types of materials and solvents used for energy storage applications during last two decades. Attempt has also been made to explore and discover different class of solvents and electrolytes that are environment friendly and have minimal impact on living organisms. As salts and the solvents are significant ingredients in the energy storage devices, so this analysis will also provide a first-hand perspective of many solvent candidates for energy storage applications. From the analysis and detailed review, it has been observed that the solvents exhibiting large electrochemical window, high thermal and chemical stability, low toxicity, and volatility are the important features which makes them important constituent of different energy storage devices like flow batteries, supercapacitors, and rechargeable batteries. Advancement of cutting-edge battery innovation is important in view of various applications like hybrid cars, smartphones, laptops etc.

Keywords: Lithium-ion batteries, energy storage devices, Aprotic Lithium salts, Glymes.

#### Investigating Molecular Interactions through Computational Modeling, Thermodynamic Analysis, and Acoustic Measurements of LIOTf in Aqueous TEGDME and DME Solutions at Different Temperatures

Chitra Sharma, Harpreet Kaur,\* Abhinay Thakur, Akshay Sharma, Ramesh Chand Thakur,\* Harmanjit Singh Dosanjh, and Vivek Pathania



Cita This: http://doi.org/10.1021/accomega.4c01708

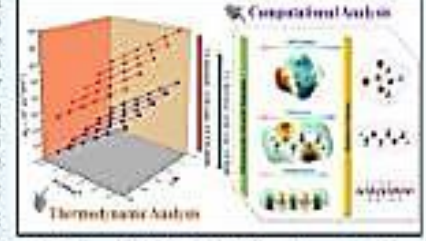


ACCESS I

M Metrics & More

(C) Article Recommendations

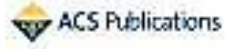
ABSTRACT: This study investigates solute-solvent interactions in ABSTRACT: Has study investigates solute—screen enteractions in ternary systems consisting of lafatura triflacementhaneualforate (LiOTr) as the solute and tetrathylene glycol directly) either (TEGDME) and 1,2-directly objections (DME) as solvents over a range of temperatures (293.15–313.15 K). A multidisciplinary approach involving computational modeling, freemodynamic analysis, and acoustic measurements was used to electricis molecular-level dynamics. The positive V<sub>2</sub> values in the thermodynamic analysis revealed the positive V<sub>2</sub> values in the thermodynamic analysis revealed the positive V<sub>2</sub> values in the transfer of the properties of the structure in the investigated termany (LiOTF + R<sub>2</sub>O + DME/TEGDME) solutions. Hopker's constant was determined to predict the structure maker/breaker behavior. Cyclic volumentry studyes showed that TEGDME contained the transfer of the structure inside the contained and the structure of the structur approach involving computational modeling, thermodynamic as



#### 1. INTRODUCTION

Energy storage devices play a proctal role in modern energy systems, particularly in integrating renewable energy sources and the power grid.<sup>1-1</sup> For example, in grid-scale applications, large battery storage systems such as lithium-ten batteries are etilized to store excess energy generated from renewable sources such as wind and solar during periods of low demand. This stored energy can then be discharged during peak demand periods or when renovable energy generation is low, helping in stabilize the grid and ensure a reliable power supply. \*\*\* Moreover, in transportation, electric vehicles (EVs) supply. Moreover, in transportation, each to betterior to mittee energy etorage in the form of bibliomion betterior to store electrical energy for propulsion. The development of advanced leatery technologies with higher energy density and faster charging capabilities in driving the adoption of EVs, reducing greenbouse gas emissions and dependence on fossil fads in the transportation sector. \*\*-11 Their shility to respond rapally to factuations in sapply and demand helps mitigate gral metabulty, encuring reliable and realisms electricity delivery. Furthermore, energy storage devices facilitate load shifting, allowing electricity to be stored during off-peak hours buckep power neuron during times of grid instability or outages, providing an uninterrupted electricity supply to smeetial services such as hospitals, emergency response systems, and telecommunications networks. Among the various energy storage options, electrochemical energy storage devices, such as batteries and expercupaction, have genered agraficant attention due to their high efficiency, scalability, and versulfity. Electrolyte, a key component that facilitates son transport between the electrodes, is majorly responsible for the performance and efficiency of electrochemical energy storage

Becarred: August 20, 2024 Bartand: November 18, 2014 Accepted: December 3, 2014



# 2020 The Surings Published by American Discount Security

AT Design \$330, 300, 300 - 619

170

#### SPRINGER NATURE Link

Find a journal Publish with us Track your research Q Search

Home > Topics in Catalysis > Article

# Hybrid Lithium Electrolytes as Potential Electrolytes for Energy Storage Devices: A Pathway to Sustainable and High-Efficiency Solutions

Review Paper | Published: 29 July 2025 (2025) Cite this article

<u>Chitra Sharma, Harpreet Kaur</u> <u>M, Abhinay Thakur, Ramesh Chand Thakur</u> <u>M & Harmanjit Singh</u> Dosanjh

124 Accesses Explore all metrics →

#### Abstract

The urgent demand for high-performance and sustainable energy storage solutions necessitates the development of advanced electrolytes with superior electrochemical properties. Hybrid lithium electrolytes, which integrate the advantages of inorganic and organic ionic conductors, have emerged as promising candidates for next-generation energy storage devices. This review presents a comprehensive bibliometric analysis of 1569 research articles from 2019 to 2024, sourced from Scopus and Web of Science (WOS) databases, highlighting the rising research focus on hybrid electrolytes. Key material properties such as wide electrochemical windows, thermal and chemical stability, low toxicity, and reduced volatility are critical for enhancing battery performance. The discussion encompasses recent advancements in solid-state, polymer, and hybrid electrolytes, emphasizing their role in improving energy density, cycling stability, and safety. Furthermore, this study examines the challenges associated with hybrid electrolytes, including ionic conductivity limitations, interfacial compatibility, and scalability for industrial applications. The integration of novel materials such as NASICONtype ceramics, perovskites, sulfides, and garnet-based electrolytes is explored for their potential to revolutionize lithium-ion battery technologies. By bridging the gap between fundamental research and practical implementation, this review provides insights into the future directions of hybrid electrolytes, paving the way for more efficient and sustainable energy storage systems.



#### Microbial Vitamins and Carotenoids in Food Biotechnology



Novel Source and Potential Applications

2024, Peges 299-325

## Chapter eleven - Microbial vitamins in dairy products

Chitro Sharma 1, Ramesh Chand Thokur 2, Harmanjit Singh 1

Show more 

+ Add to Mendeley 40 Share 55 Cite

Imps://doi.org/10.1616/8978-0-440-15525-4.0001-6 A Ge rights and contact A

#### Abstract

This chapter gives a brief overview of the process of producing vitamins, with primary attention being placed on the microbial fermentation techniques that are presently being used in the synthesis of vitamins in dairy products. Milk and the products derived from milk are an outstanding source of several vital vitamins. Dairy products like milk, cheese, butter, etc. contain a significant quantity of vitamins. A and B, including thiamine, riboflavin, and nicotinic acid. Additionally, dairy products contain vitamin B12 in them. Organic chemical synthesis has traditionally been used to manufacture such vitamins; however, this process typically involves many reactions, numerous solvents, and a variety of costly equipment. The biological production of vitamins has evolved by identifying natural producer organisms, determining the most productive growth conditions, scaling up production, and optimizing downstream procedures to extract pure products. The synthesis of vitamins by microbes offers several benefits since microbes have a rapid growth rate, they are not subject to the effects of climate or the passage of time, they are simple to scale up, and they do not compete with the requirements of humans for food. In conclusion, an examination of emerging patterns in the microbial synthesis of vitamins and a discussion of current developments in the process of microbial vitamin synthesis are presented in this chapter.



Certificate No. 225468

## **Certificate of Participation**

| This is to certify that Prof./Dr./Mr./M | s. Ms. Chitra Sharma  |
|---|---|
| of                                      | Lovely Professional University  |
| has given poster presentation on        | Potential solvents and electrolytes for energy storage applications; A Review     |
| in the International Conference o       | n "Recent Advances in Fundamental and Applied Sciences" (RAFAS 2021) held on      |
| June 25-26, 2021, organized by So       | chool of Chemical Engineering and Physical Sciences, Lovely Faculty of Technology |
| and Sciences, Lovely Profession         | nal University, Punjab.   |
| Date of Issue: 15-07-2021               |   |

Prepared by

Organizing Secretary (RAFAS 2021)

Convener (RAFAS 2021

#### I.K. GUJRAL PUNJAB TECHNICAL UNIVERSITY AMRITSAR CAMPUS

# ONE WEEK FACULTY DEVELOPMENT PROGRAMME ON TOOLS & TECHNIQUES FOR EFFECTIVE RESEARCH

CERTIFICATE NUMBER
IKGPTU/FDP/TTR-040



DATED

18 December 2020

# Certificate of Participation

This is to certify that

## Ms. Chitra Sharma

from Lovely Professional University

has attended online One Week Faculty Development Programme on Tools and Techniques for Effective Research organised by I.K. Gujral Punjab Technical University Amritsar Campus from 14 December 2020 to 18 December 2020.

Dr. Prabhkiran Kaur

COURSE COORDINATOR

Dr. Vipul Sharma

COURSE COORDINATOR



## Workshop

# Analytical Instrumentation

Students And Teachers of Himachal Pradesh

(Online mode) 01-02 July, 2021 Organized by

Sophisticated Analytical Instrumentation Facilities Panjab University, Chandigarh

Maharaja Lakshman Sen Memorial College Sundernagar, Mandi, (H.P.)

Certificate of Participation

This is to certify that Chitra Sharma of Panjab University, Chandigarh has attended two day online Workshop on Analytical Instrumentation organized by Sophisticated Analytical Instrumentation Facility,

Panjab University, Chandigarh and Maharaja Lakshman Sen Memorial College Sundernagar, Mandi,

H.P. on July 1 & 2, 2021

Dr. Naresh Kumar Dept. of Chemistry MI SM College Sundernagar (H.P.) Organizing Secretary

Sudhi Dr. Sudhir Kumar

Head, Dept. of Chemistr MLSM College, Sundernagar (H.P.)

Dr. Ramesh K Sharma

SAIF/CIL Chandigarh Convene

Dr. C.P Kaushal

MLSM College, Sundernagar (H.P.)

Prof. G.R. Chaudhary Director, SAIF, CIL, UCIM Panjab University, Chandigarh Patron



Transforming Education Transforming India



Certificate No. 263556

This is to certify that Dr./Mr./Ms. Chitra Sharma of Lovely Professional University has given oral presentation on Comparative analysis of thermophysical and acoustic properties of Lithium tetrafluoroborate(LiBF 4) and Lithium hexafluorophosphate(LiPF 6) in binary aqueous mixtures of tetra ethylene glycol dimethyl ether(TEGDME) at different temperatures in the 4th International Conference on "Recent Advances in Fundamental and Applied Sciences" (RAFAS 2023) held on March 24-25, 2023, organized by School of Chemical Engineering and Physical Sciences, Lovely Faculty of Technology and Sciences, Lovely Professional University, Punjab. UNIVERSITY

Date of Issue: 12-04-2023 Place: Phagwara (Puniab), India SIONAL UNIVERSITY

(Administrative Officer-Records)

Organizing Secretary (RAFAS 2023)

(RAFAS 2023)